

**EXAMINING NANOPARTICLE BASED SYSTEMS FOR  
APPLICATIONS IN MATERNAL/FETAL HEALTH**

by

N'Dea Irvin-Choy

A dissertation submitted to the Faculty of the University of Delaware in partial fulfillment of the requirements for the degree of Doctor of Philosophy in Biomedical Engineering

Summer 2023

© 2023 N'Dea Irvin-Choy  
All Rights Reserved

**EXAMINING NANOPARTICLE BASED SYSTEMS FOR  
APPLICATIONS IN MATERNAL/FETAL HEALTH**

by

N'Dea Irvin-Choy

Approved: \_\_\_\_\_

Kristi Kiick, Ph.D.  
Chair of the Department of Biomedical Engineering

Approved: \_\_\_\_\_

Levi Thompson, Ph.D.  
Dean of the College of College of Engineering

Approved: \_\_\_\_\_

Lou Rossi, Ph.D.  
Vice Provost for Graduate and Professional Education and  
Dean of the Graduate College

I certify that I have read this dissertation and that in my opinion it meets the academic and professional standard required by the University as a dissertation for the degree of Doctor of Philosophy.

Signed:

---

Emily Day, Ph.D.  
Professor in charge of dissertation

I certify that I have read this dissertation and that in my opinion it meets the academic and professional standard required by the University as a dissertation for the degree of Doctor of Philosophy.

Signed:

---

Jason Gleghorn, Ph.D.  
Member of dissertation committee

I certify that I have read this dissertation and that in my opinion it meets the academic and professional standard required by the University as a dissertation for the degree of Doctor of Philosophy.

Signed:

---

Catherine Fromen, Ph.D.  
Member of dissertation committee

I certify that I have read this dissertation and that in my opinion it meets the academic and professional standard required by the University as a dissertation for the degree of Doctor of Philosophy.

Signed:

---

LaShanda Korley, Ph.D.  
Member of dissertation committee

I certify that I have read this dissertation and that in my opinion it meets the academic and professional standard required by the University as a dissertation for the degree of Doctor of Philosophy.

Signed:

---

Curtis Johnson, Ph.D.  
Member of dissertation committee

## ACKNOWLEDGMENTS

I would first like to thank my advisor, Emily. You have allowed me to take this work in my own direction and gave me great feedback along the way. I would also like to thank my secondary advisor, Jason, for pushing me to think critically about my work. The support from both of you has helped me learn so much about conducting research, how the science industry works, and about life.

Next, I would like to thank the Day and Gleghorn Lab members, both alum and current, that helped me throughout this journey. Thank you to Katie, who took me under her wing when I was just a first year and has worked alongside me ever since. You showed me the ropes of science and helped me transition into graduate school life. Thank you, Megan, and Jenna, for being great moral support and providing encouragement for me when lab days were tough. Thank you, Mackenzie, who started this journey with me as a first year. Our endless conversations about pop-culture, social media, and everything else under the sun kept me going throughout the years. Thank you to the graduate students I am leaving behind: Elise, Eric, Sara, and George. I will miss you all and our lab social gatherings. Thank you for going along with my constant shenanigans and participating in the many events I've hosted over the years.

I would also like to thank the undergraduate students that worked with me during their time at UD. First, thank you to Violet for joining me early on in my graduate school career. You've taught me much about UD and the Day Lab when I first joined and continue to still teach me about how to be a good mentor to this day. I

also want to thank Casey for joining me in this work and teaching me how to guide younger students through mentorship.

I could not have completed this work without the gracious and kind staff members at UD. I would like to acknowledge Debbie Powell in DBI for training me on cryo-sectioning and always being available when I needed help. I would also like to thank Shannon Modla for your imaging expertise throughout this work and Andrew Jenner for being so patient with me while helping me with the instruments in DBI. You were all an incredible help to me and I really appreciate you for your help when the instruments were having bad days.

The moral support of my friends and family is what has pushed me to get up every day and go to lab to complete this work and I could not have survived without you all. Thank you to my friends UD friends, A'maya, Roxy, Liz, and Alyssa for being supportive friends to vent to. Thank you to my long-time friends, Meghan, Megan, and Kiara, for keeping me sane throughout this program and providing me a place for escape when I needed it most. Thank you to my online friends, Nettie, Lora, Jervaughn, Korie, Simone, and so many others that constantly and consistently encouraged me. Also thank you to my online community for being a safe place for me to create, vent, and remember about my life outside of research.

Last, but not least, thank you to my family for your support throughout this process. This has been a long road and I appreciate you all for reminding me about life after a PhD and pushing me to be my best. You have reminded me to rest and take breaks, when I forgot to do it myself, and always welcomed me home with a plate full of home-cooked food. This degree is a culmination of all of our hard work, and I'm honored to represent you with it.

## TABLE OF CONTENTS

FIGURES .....	xi
ABSTRACT .....	xviii

### Chapter

1	INTRODUCTION.....	1
1.1	Nanoparticle Design Characteristics Influence Function .....	3
1.1.1	The Significance of Nanoparticle Size .....	3
1.1.2	The Impact of Nanoparticle Shape .....	3
1.1.3	Nanoparticle Surface Chemistry Impact on Delivery .....	4
1.2	Applications of Nanotechnology in Maternal/Fetal Health.....	4
1.2.1	Pregnancy Conditions that Primarily Impact the Fetus .....	6
1.2.1.1	Preeclampsia.....	6
1.2.1.2	Fetal Growth Restriction .....	8
1.2.1.3	Preterm Birth .....	11
1.2.1.4	Preterm Premature Rupture of Membranes .....	13
1.2.2	Preexisting Maternal Health Conditions Exacerbated During Pregnancy .....	15
1.2.2.1	Endometriosis .....	15
1.2.2.2	Gestational Diabetes Mellitus.....	17
1.2.2.3	Hypertension.....	19
1.2.2.4	Bacterial Vaginosis.....	21
1.3	Biological Barriers to Targeting Reproductive Organs.....	23
1.3.1	Challenges with Intravenous Delivery .....	24
1.3.2	Barriers Associated with the Vaginal Delivery .....	26
1.3.3	Nanoparticle Design for Vaginal Delivery .....	30
1.3.4	Physiologic Changes in Human Anatomy During Pregnancy ....	32

1.4	Unanswered Questions for Nanomedicine in Maternal/Fetal Health .....	36
2	<b>GOLD NANOPARTICLE BIODISTRIBUTION IN PREGNANT MICE FOLLOWING INTRAVENOUS ADMINISTRATION VARIES WITH GESTATIONAL AGE .....</b>	<b>38</b>
2.1	Introduction .....	38
2.2	Materials and Methods .....	41
2.2.1	Synthesis of 15 nm Diameter Gold Nanoparticles .....	41
2.2.2	Synthesis of 150 nm Diameter Nanoshells.....	42
2.2.3	Nanoparticle Characterization .....	42
2.2.4	In Vivo Pregnancy Murine Model.....	43
2.2.5	Quantification of Gold Content in Tissues by ICP-MS.....	44
2.2.6	Qualitative Evaluation of NP Presence in Tissues by Silver Staining.....	44
2.3	Results .....	45
2.3.1	Nanoparticle Characterization .....	45
2.3.2	PEG-Coated 15 nm AuNPs 150 nm NSs Exhibit More Accumulation in Placentas and Embryos When Administered at E9.5 than at E14.5.....	47
2.3.3	15 nm AuNPs and 150 NSs Both Have Minimal Effect on Fetal Growth.....	54
2.4	Nanoparticle Distribution to Maternal Non-Reproductive Organs in Not Gestation Dependent .....	55
2.5	Discussion.....	59
3	<b>DELIVERY AND SHORT TERM MATERNAL AND FETAL SAFETY OF VAGINALLY ADMINISTERED PEG-PLGA NANOPARTICLES .....</b>	<b>63</b>
3.1	Introduction .....	63
3.2	Materials and Methods .....	66
3.2.1	Synthesis of DiD-Loaded PEG-PLGA NPs .....	66
3.2.2	Synthesis of Cy5-PEG-PLGA NPs .....	67
3.2.3	Nanoparticle Characterization .....	68
3.2.4	Evaluation of DiD Encapsulation and Release from PEG-PLGA NPs.....	68
3.2.5	In Vivo Pregnancy Murine Model and IVIS Imaging.....	69
3.2.6	Qualitative Evaluation of DiD Cargo Presence in Cryosections.	71

3.3	Results .....	71
3.3.1	Nanoparticle Characterization .....	71
3.3.2	DiD-PEG-PLGA NPs Administered Vaginally at E14.5 and \$17.5 Show Localized Fluorescence in Vagina Twnty-Four Hours Post-Injection .....	74
3.3.3	Cy5-PEG-PLGA NPs Administered Vaginally at E17.5 Exhibit Fluorescence in Vaginas, Placentas, and Embryos Twenty-Four Hours Post-Injection .....	82
3.3.4	DiD-PEG-PLGA NPs Do Not Directly Affect in utero Fetal and Maternal Growth over Twenty-Four Hours of Exposure .....	83
3.4	Discussion.....	85
4	CLINDAMYCIN-LOADED PEG-PLGA NPs INHIBIT GARDNERELLA VAGINAL GROWTH IN VITRO .....	89
4.1	Introduction .....	89
4.2	Methods .....	92
4.2.1	Synthesis of CLN-PEG-PLGA NPs .....	92
4.2.2	Synthesis of DiD-PEG-PLGA NPs .....	93
4.2.3	Nanoparticle Characterization .....	94
4.2.4	CLN-PEG-PLGA NPs Loading Efficiency and Drug Release Profile .....	95
4.2.5	DiD-PEG-PLGA NP Microscopy Tracking .....	96
4.2.6	<i>Gardnerella Vaginalis</i> Culture .....	97
4.2.7	<i>G. Vaginalis</i> Growth Following Free Clindamycin and CLN-PEG-PLGA NP Treatment .....	97
4.2.8	CLN-PEG-PLGA NP Treatment of Adhered <i>G. Vaginalis</i> .....	98
4.3	Results .....	100
4.3.1	Nanoparticle Characterization .....	100
4.3.2	DiD-PEG-PLGA NP Velocity is Decreased in the Presence of Reconstituted Mucus .....	103
4.3.3	CLN-PEG-PLGA NPs Inhibit <i>G. Vaginalis</i> Growth in Suspension.....	104
4.3.4	CLN-PEG-PLGA NPs Inhibit Adhered <i>G. Vaginalis</i> Growth in the Presence of a Mucus Barrier.....	106
4.4	Discussion.....	108
5	CONCLUSIONS AND FUTURE WORK.....	112

5.1	Introduction .....	112
5.2	Overview of the Work Presented .....	112
5.3	Significance, Innovation, and Impact of the Research .....	115
5.4	Future Directions .....	118
5.4.1	Understanding Long-Term Effects of NP Delivery on Fetal Growth and Maternal Safety .....	118
5.4.2	Demonstrating the Need for NP Carriers for Treating BV.....	120
5.4.3	Traditional Considerations .....	123
REFERENCES .....		126
Appendix		
A	PERMISSIONS FOR USE.....	139
A.1	Nanomedicine: Nanotechnology, Biology, and Medicine Journal Permissions.....	139
A.2	Drug Delivery Translational Research Journal Permissions.....	140

## FIGURES

- Figure 1.1: Maternal and fetal conditions that would benefit from nanomedicine treatments. Pregnancy conditions that are exacerbated during pregnancy or that are induced by pregnancy are indicated by \*. Diabetes can be pre-existing or induced by pregnancy is indicated by #. Parts of the figure were created using modified graphics from BioRender..... 6
- Figure 1.2: The potential routes of bacterial infection in pregnant women with preterm premature rupture of membranes (PPROM). Parts of the figure were created using modified graphics from Servier Medical Art, provided by Servier, licensed under a Creative Commons Attribution 3.0 Unported License..... 14
- Figure 1.3: The potential routes of bacterial infection in pregnant women with preterm premature rupture of membranes (PPROM). Parts of the figure were created using modified graphics from Servier Medical Art, provided by Servier, licensed under a Creative Commons Attribution 3.0 Unported License..... 22
- Figure 1.4: NPs that are delivered via intravenous injections enter the circulation and are immediately coated in protein corona. Coated NPs are marked by macrophages for removal from the circulation and accumulate in the liver. Parts of the figure were created using modified graphics from Servier Medical Art, provided by Servier, licensed under a Creative Commons Attribution 3.0 Unported License..... 25
- Figure 1.5: (A) Schematic of cervicovaginal mucus layer on epithelium and mucin glycoprotein structure. Parts of the figure were created using modified graphics from Servier Medical Art, provided by Servier, licensed under a Creative Commons Attribution 3.0 Unported License. (B) Cervicovaginal mucus at (i) 20<sup>th</sup> day of pregnancy (ii) 2.5 months of pregnancy and (iii) last week of pregnancy. Figure Reproduced with permission from *N. Becher, et al. Acta Obstet Gynecol Scand.* 2009; 88: 502-513 under a Creative Commons Attribution License. .... 28

Figure 1.6: The human reproductive anatomy experiences many changes throughout pregnancy, including narrowing of the cervix to protect the fetus, thickening of the uterine walls to prepare for delivery, and the development of the placenta to provide nutrients to the fetus during the second and third trimesters. Parts of the figure were created using modified graphics from Servier Medical Art, provided by Servier, licensed under a Creative Commons Attribution 3.0 Unported License.....	33
Figure 2.1: Nanoparticle characterization. (A) Hydrodynamic diameter and (B) zeta potential of AuNPs before and after PEGylation. (C) Electron micrograph of AuNPs. (D) Hydrodynamic diameter and (E) zeta potential of NSs before and after PEGylation. (F) Electron micrograph of NSs. Data in (A,B,D,E) are mean +/- standard deviation. ....	47
Figure 2.2: Nanoparticle distribution to placentas and embryos determined by ICP-MS. Analysis of gold content in placentas and embryos of dams that received intravenous injections of (A) 15 nm diameter AuNPs or (B) 150 nm diameter NSs on E9.5 or E14.5. Gold content in tissues was measured one day post-NP administration. ....	48
Figure 2.3: Histological examination of NP distribution to placentas and embryos one day post administration to dams at E9.5 or E14.5. Tissues were silver stained to enable visualization of AuNPs and NSs. (A) Images of placentas from dams treated with saline, AuNPs, or NSs. White arrows indicate representative NPs along the maternal or fetal sides of the placenta. Scale bars = 20 $\mu$ m. (B) Images of embryos from dams treated with saline or NPs at E9.5 or E14.5. Insets depict lower abdomen area. Scale bars = 20 $\mu$ m. ....	50
Figure 2.4: Nanoparticle biodistribution to maternal non-reproductive organs. (A,B) Number of NPs in non-reproductive organs of pregnant mice that were injected with AuNPs (A) or NSs (B) at E9.5 or E14.5, based on ICP-MS analysis of gold content measured one-day post intravenous administration of the NPs. Graphs in (A) and (B) are mean +/- standard error, with individual data points shown as circles. (C) Silver stained sections of liver and spleen from dams treated with saline, AuNPs, or NSs. White arrows point to representative NP locations. Scale bars = 20 $\mu$ m. ....	52

Figure 2.5: NP distribution to placentas and embryos by location in uterus. (A) Schematic of pregnant mouse uterus. Image reproduced with permission from <i>Raz T, et al. PLoS ONE. 2012; 7(12): e52273</i> under a Creative Commons Attribution License. Number of (B) 15 nm AuNPs and (C) 150 nm NSs in proximal and distal embryos and placentas at E9.5 and E14.5 as determined by ICP-MS analysis of gold content in tissues. ....	53
Figure 2.6: Analysis of embryo and placenta weight as a measure of NP safety. (A) Ratio of embryo weight to placenta weight in dams administered 15 nm AuNPs. (B) Embryo weights 24 hours post 15 nm AuNP injection in pregnant mice. (C) Ratio of embryo weight to placenta weight in dams one day after 150 nm NS administration. (D) Embryo weights in NS-treated mice 24 hours post injection. Data are mean +/- standard deviation. No significant differences were found between saline or NP-treated mice when analyzing E:P ratio or embryo weight by t-test. .	55
Figure 2.7: Nanoparticle biodistribution to maternal non-reproductive organs. (A,B) Number of NPs in non-reproductive organs of pregnant mice that were injected with AuNPs (A) or NSs (B) at E9.5 or E14.5, based on ICP-MS analysis of gold content measured one-day post intravenous administration of the NPs. Graphs in (A) and (B) are mean +/- standard error, with individual data points shown as circles. (C) Silver stained sections of liver and spleen from dams treated with saline, AuNPs, or NSs. White arrows point to representative NP locations. Scale bars = 20 $\mu$ m. ....	58
Figure 2.8: Silver-stained sections of livers and spleens from pregnant mice treated with AuNPs or NSs. White boxes indicate area of interest that is shown in magnified view to the right. White arrows point to representative AuNPs or NSs. These images provide additional fields of view and magnifications to supplement the data presented in Figure 5. Scale bar = 20 $\mu$ m. ....	59

- Figure 3.1: Synthesis and characterization of DiD-PEG-PLGA NPs and Cy5-PEG-PLGA NPs. **A.** Schematic of DiD-PEG-PLGA NP synthesis. **B.** Transmission electron micrograph of NPs. **C.** Hydrodynamic diameter, zeta potential, encapsulation efficiency, and DiD loading of NPs after synthesis and removal of excess dye by suspension in Triton X-100 and centrifugal filtration. Data indicate mean  $\pm$  standard deviation. n=4 **D.** DiD release profile over 24 hours under storage (pH 7.0, 4°C) and physiologic (pH 3.5, 37°C) conditions. Data are mean  $\pm$  standard deviation of n=3 experiments. **E.** Schematic of Cy5-PEG-PLGA NP synthesis. **F.** Hydrodynamic diameter and zeta potential of Cy5-PEG-PLGA NPs following synthesis and purification. Data show mean  $\pm$  standard deviation of n=4 experiments..... 73
- Figure 3.2: NP characteristics as a function of DiD volume added during synthesis. **A.** Hydrodynamic diameter, **B.** Zeta potential, **C.** Fluorescence intensity measured in a plate reader at excitation/emission of 640 nm/670nm, and **D.** the encapsulation and DiD loading efficiency of synthesized PEG-PLGA NPs. NP characterization was performed without the Triton X-100 purification method. Data show mean  $\pm$  standard deviation. n = 3 ..... 74
- Figure 3.3: Vaginal delivery method. **A.** Experimental timeline, from vaginal injection at t=0 hours through tissue collection and imaging at t=24 hours. **B.** Whole body IVIS imaging of E14.5 mice at t=0 hours after DiD-PEG-PLGA NP or saline injection..... 76
- Figure 3.4: Assessment of DiD cargo accumulation in maternal organs. **A.** IVIS imaging of maternal non-reproductive and reproductive organs taken 24 hours post-DiD-PEG-PLGA NP or saline administration at E14.5 or E17.5. **B.** Average radiant efficiency of vaginas excised from mice 24 hours after DiD-PEG-PLGA NP or saline administration at E14.5 or E17.5. \*indicates p<0.05 by t-test. There were no significant differences in vaginal radiant efficiency between gestational ages (i.e., between E14.5 and E17.5 mice exposed to NPs) as confirmed by a t-test. n=6 mice per group ..... 76

- Figure 3.5: NP delivery to E14.5 mice following additional purification by Triton-X washing to remove any unencapsulated DiD. **A.** IVIS of three mouse vaginas injected with purified NP samples. **B.** Overlay of average radiant efficiency of Triton X-washed NPs (yellow circles) compared to signal from NPs washed by standard methods and injected into vaginas of mice at E14.5. There is no statistical difference between NPs washed by standard methods or Triton X purification ( $\alpha = 0.24$ ). n =3 ..... 77
- Figure 3.6: Fluorescence microscopy of cryo-sectioned vaginas that were excised from mice 24 hours post NP or saline administration. **A.** Tile images (5x magnification) of excised vaginas. Arrows indicate vaginal opening where NPs were injected. Brackets indicate region of the vaginal canal and the dotted line denotes cervix separation. \*indicates full vaginal opening is not visible in image. Boxes in blue and red indicate areas shown in magnified images in B. **B.** Magnified images (20x) of vaginal regions indicated by blue or red boxes in A. In A and B, red indicates DiD fluorescence. .... 79
- Figure 3.7: Evaluation of spleen and liver cryosections. The spleens and livers of pregnant mice that received vaginal NP or saline injection at gestational age E14.5 or E17.5 were excised 24 hours post injection, cryo-sectioned, and examined by fluorescence microscopy for DiD fluorescence. Minimal/no signal was observed in these tissues. Scale bars = 50  $\mu$ m..... 80
- Figure 3.8: Examination of maternal reproductive organs. The ovaries, placentas, and embryos from pregnant mice treated with NPs or saline at both gestational ages were cryo-sectioned and observed by fluorescence microscopy for DiD presence. Minimal/no signal was observed in these tissues. Scale bars = 50  $\mu$ m. .... 81
- Figure 3.9: Evaluation of NP distribution to placentas and embryos and NP effects on short-term embryo and placenta growth. **A.** IVIS imaging of representative embryos and placentas excised from pregnant mice 24 hours after saline or NPs were injected on E14.5 and E17.5. **B.** Embryo-to-placenta weight ratio (E:P ratio) from mice treated with NPs or saline at each gestational age. Data show mean  $\pm$  standard deviation. n = 6 litters of 307 embryos and 307 placentas total. A student's t-test determined no significant differences between the NP and saline-treated mice. .... 82

Figure 3.10: Assessment of Cy5-PEG-PLGA NP accumulation in maternal organs and embryonic tissues. **A.** IVIS imaging of maternal non-reproductive and reproductive organs taken 24 hours post-NP or saline administration at E17.5. **B.** Average radiant efficiency of vaginas, placentas, and embryos excised from mice 24 hours after administration of NPs or saline at E17.5. \*indicates  $p < 0.05$ , \*\*\*\* indicates  $p < 0.0001$  by t-test.  $n = 1$  saline mouse with 9 placentas and embryos,  $n = 3$  NP injected mice with a combined total of 41 placentas and embryos. .... 83

Figure 3.11: Short-term effects of NPs on maternal and fetal growth. **A.** Maternal weight gain from embryonic day 0 to the end of the study. **B.** Maternal weight change over the 24 hours after NP or saline injection. **C.** The number of embryonic resorptions per litter in each treatment group. **D.** Number of embryos in utero per liter. There were no significant differences between the treatment groups across any of these metrics, as confirmed by a t-test comparing saline to NP-exposed mice. Data show mean  $\pm$  standard deviation.  $n = 6$  pregnant mice per group, with a total of 307 embryos. .... 85

Figure 4.1: Schematic of NP Treatment on *G. Vaginalis* Culture in Suspension ..... 98

Figure 4.2: Schematic of NP Treatment on Adhered *G. Vaginalis*. **A.** Method for *G. Vaginalis* cultures adhered on chocolate agar plates without, and **B.** with porcine gut mucus reconstituted in NaOH. .... 99

Figure 4.3: Nanoparticle Characterization. **A.** Schematic of NP synthesis procedure. **B-D.** CLN-PEG-PLGA NPs **B.** hydrodynamic diameter, **C.** Zeta potential, and **D.** drug loading content. **E-F.** CLN release profile from the NPs over 24 hours under **E.** storage (Water, pH 7.0, 4°C) and **F.** physiologic (NaCl, pH 5.0, 37°C) conditions. **G-H.** The **G.** hydrodynamic diameter and **H.** zeta potential of DiD-PEG-PLGA NPs. Data are mean  $\pm$  standard deviation of  $n = 3$  experiments. .... 102

Figure 4.4: Analysis of DiD-PEG-PLGA NPs movement when placed in different media. Root mean square (RMS) displacement of DiD-PEG-PLGA NPs in water and reconstituted mucus. \*indicated  $p < 0.05$  by t-test. Data are mean  $\pm$  standard deviation of  $n = 200$  nanoparticles. .... 104

Figure 4.5: *G. vaginalis* Growth Following Free CLN and CLN-PEG-PLGA NPs Treatment in Suspension **A.** *G. vaginalis* growth after 12 hours of free CLN treatments only. **B.** *G. vaginalis* growth following CLN-PEG-PLGA NPs dosed with 4 µg/ml of loaded CLN over 12 hours **C.** MIC50 values of Free CLN and CLN-PEG-PLGA NP treatments. Data are mean ± standard deviation of n=3 experiments. .... 106

Figure 4.6: Growth of adherent *G. vaginalis* cultures following CLN-PEG-PLGA NP treatment in the absence of presence of mucus. **A.** Representative images of *G. vaginalis* grown on chocolate agar plates following CLN-PEG-PLGA NP or free CLN treatments with and without mucus. **B.** Quantification of bacterial colonies within the ROI of sample without and **C.** with mucus present. Data are mean ± standard deviation of n=3 experiments. .... 108

## **ABSTRACT**

The presence of pregnancy complications poses significant challenges for both the mother and the developing fetus, as available treatment options are limited due to safety and ethical considerations. Conditions like preeclampsia, fetal growth restriction (FGR), and placenta accreta exemplify pregnancy-induced disorders that lack effective remedies. As pregnancy progresses, these conditions worsen, leading to adverse consequences on the health of both the mother and the fetus. Consequently, emergency cesarean section delivery is often necessary, resulting in additional complications associated with premature birth for the newborns. Addressing the pressing need for enhanced maternal and fetal health during pregnancy, it is imperative to develop therapeutic advancements that can effectively treat pregnancy-related conditions while ensuring the well-being of the developing baby.

In recent years, significant progress has been made in engineering nanocarrier systems for targeting various diseases, including cancers. The behavior of these nanocarriers in the body following systemic delivery is known to depend on factors such as size, shape, and surface chemistry. While researchers have harnessed this knowledge to develop powerful systems for treating ailments like cervical cancer, endometriosis, and HIV, the exploration of nanomedicine for pregnancy complications remains limited. The unique state of pregnancy introduces additional variables that influence NP distribution and design, including the dynamic physiology of the maternal reproductive system, the transport of nutrients and drugs through the placenta, and the development of the fetus. It is crucial to comprehend the impact of

these factors on NP distribution to develop effective treatments that can support full-term pregnancies and improve the health of both mother and fetus.

First, the biodistribution of gold-based nanoparticles (NPs) in pregnant mice was investigated following systemic delivery. Two different sizes of NPs, namely 15 nm gold nanoparticles and 150 nm diameter silica core/gold nanoshells coated with poly(ethylene) glycol (PEG), were intravenously administered to pregnant mice at gestational days (E)9.5 or 14.5. After twenty-four hours, the distribution of NPs in tissues was analyzed using inductively coupled plasma-mass spectrometry and silver staining of histological samples. The findings revealed a higher accumulation of NPs in the placentas compared to the embryos, with a greater delivery to these tissues observed at E9.5 than E14.5. Additionally, no adverse effects on fetal or placental weight were observed, indicating minimal short-term toxicity during early to mid-stage pregnancy. These results underscore the potential of further developing NPs as safe tools for targeted therapeutics delivery to reproductive tissues.

The following study delved into the distribution of PEG-coated poly(lactic-co-glycolic) acid nanoparticles (PEG-PLGA NPs) in pregnant mice through vaginal delivery, as well as their short-term toxicity. Two types of NPs were employed: DiD-PEG-PLGA NPs loaded with fluorophores for cargo tracking, and Cy5-PEG-PLGA NPs incorporating tagged polymer for distribution analysis. DiD-PEG-PLGA NPs were administered on either gestational day (E)14.5 or 17.5, and after 24 hours, the distribution of cargo was examined in excised tissues and histological sections using

fluorescence imaging. Interestingly, no variations in DiD distribution were found between the gestational periods. Therefore, Cy5-PEG-PLGA NPs were exclusively administered on E17.5 to assess polymer distribution in reproductive organs. The results showed the presence of Cy5-PEG-PLGA NPs in the vagina, placentas, and embryos, while DiD cargo was limited to the vagina. Furthermore, maternal, fetal, and placental weights remained unaffected by the NPs, indicating no immediate adverse effects on maternal or fetal growth. These findings suggest the potential of exploring vaginally delivered NP therapies for managing vaginal conditions during pregnancy.

Lastly, the effectiveness of clindamycin-loaded PEG-PLGA nanoparticles (CLN-PEG-PLGA NPs) with different L:G ratios (50:50, 75:25, and 85:15) in inhibiting the growth of *G. vaginalis*, a pathogenic bacteria associated with bacterial vaginosis (BV) infections, was examined. *G. vaginalis* was cultured in suspension and on agar plates and treated with CLN-PEG-PLGA NPs of each L:G ratio. The growth of *G. vaginalis* was monitored using spectrophotometry or imaging at regular intervals over a 12-hour treatment period. The experiments demonstrated the effective inhibition of *G. vaginalis* growth in both suspension and on surfaces by CLN-PEG-PLGA NPs, irrespective of the L:G ratio. Interestingly, the bacterial growth inhibition did not significantly differ among the three L:G ratios, indicating that the ratio had minimal impact on short-term antibacterial treatment, likely due to similar total drug release from each formulation within the 12-hour period. While freely delivered clindamycin exhibited greater potency against *G. vaginalis*, it is important to note that CLN-PEG-PLGA NPs were able to decrease *G. vaginalis* growth *in vitro*.

The foundational knowledge provided in this thesis holds utmost importance for the initial advancement of nanomedicines designed to address maternal-fetal health conditions. By incorporating the additional experiments mentioned earlier, researchers can assess the prolonged impacts of NP injections on pup development and growth. This comprehensive understanding will guide researchers in optimizing NP delivery and treatment efficacy while safeguarding the well-being of both the mother and the fetus. Such insights can aid in determining the most suitable administration routes, be it systemic or vaginal, to enhance NP delivery and promote successful treatment outcomes without compromising maternal or fetal health.

## **Chapter 1**

### **INTRODUCTION**

The field of nanomedicine is a rapidly growing area of research focused on the development of nanoparticle-based systems for prophylactic, diagnostic, and therapeutic applications. The prefix “nano” is derived from the Greek word “nanos,” meaning extremely small, however the National Nanotechnology Initiative (NNI) in the United States formally defines nanotechnology as “a science, engineering, and technology conducted at the nanoscale (1 to 100 nm), where unique phenomena enable novel applications in a wide range of fields, from chemistry, physics, and biology, to medicine, engineering, and electronics”<sup>1</sup>. Although the term “nanomedicine” only started to appear in research publications at the start of this century, its roots can be traced back to the use of colloidal gold in the late 1700s<sup>2</sup>. Metchnikov and Ehrlich, the 1908 winners of the Nobel Prize for Medicine, are publicly recognized as the pioneers of nanomedicine for their works on phagocytosis and respiratory cell-specific diagnostics and therapy<sup>2</sup>. Since then, the field of nanomedicine has flourished in providing therapies for many applications, with the most popular being cancer, cardiovascular diseases, and now the COVID-19 vaccines. In addition to providing a treatment platform for a variety of diseases, there are additional medical applications for NPs including magnetic resonance imaging (MRI), contrast agents, tissue engineering, drug and gene delivery agents, and the separation of biological molecules and cells. Today, there are many FDA approved nanomedicines that are on the market or are currently in clinical trials.

While nanotherapeutics have been developed for many applications and diseases, few researchers have investigated nanoparticle-based platforms for the treatment of maternal-fetal conditions during pregnancy, which are in dire need of new management and treatment strategies. In 2020, the maternal mortality rate was 23.8 deaths per 100,000 live births in the United States, compared to 20.1 in 2019<sup>3</sup>. Additionally, the maternal mortality rate for non-Hispanic Black women was 2.9 times the rate of non-Hispanic White women, at 55.3 deaths per 100,00 live births<sup>3</sup>. The most common causes of maternal mortality are pregnancy complications including postpartum hemorrhage, eclampsia, obstructed labor, and sepsis; however, close observation and medical attention can greatly improve the chance of survival<sup>4</sup>. Despite the advancements in technology and medical care overall, the United States holds the highest mortality rate of industrialized countries, nearly tripling the mortality rate of the second highest country, France<sup>5</sup>. Considering the urgent need for maternal treatment during pregnancy, this dissertation examines the use of nanoparticle-based systems to manage and treat maternal-fetal health during pregnancy. The administration methods and NP platforms investigated in this work provide fundamental knowledge that is necessary for designing targeted nanoparticle-based therapies that are safe and more efficient than traditional treatment strategies. In this chapter, the maternal-fetal health conditions that could benefit from nanomedicine are discussed along with the design criteria that are necessary when engineering a nanomedicine for pregnancy-related applications. This chapter contains sections adapted from: adapted from a manuscript published by Irvin-Choy NS, Nelson KM, Dang MN, Gleghorn JP, Day ES.

## **1.1 Nanoparticle Design Characteristics Influence Function**

The physical characteristics of nanoparticles (NPs), such as the size, shape, and surface charge, can greatly influence its function and biological applications.

Together, these characteristics play a significant role in adsorption, cellular uptake, biodistribution, and clearance mechanisms.

### **1.1.1 The Significance of Nanoparticle Size**

A nanoparticle is a structure with at least one dimension in the range of 1-100 nm. Unlike bulk materials, nanoparticles have a high surface area to volume ratio<sup>6</sup>, which impact their optical, electronic, magnetic, and mechanical properties<sup>7</sup>. One of the properties impacted by NP size is the NP circulation time. Specifically, NPs that are less than 200 nm improve the blood half-life due to their ability to evade spleen and liver detection<sup>8</sup>. Another key benefit related to NP size is the improved solubility. In traditional therapies, insoluble or poorly soluble drugs require the use of toxic organic solvents in bulk materials or larger molecules. The use of small NPs allows for previously insoluble drugs to be converted into soluble aqueous solutions without the need of organic solvents, thus improving the bioavailability<sup>8,9</sup>.

### **1.1.2 The Impact of Nanoparticle Shape**

Another physical characteristic that can impact the performance of a NP is its shape. NPs can be made into spheres, hemispheres, cylinders, rods, cones, and wires and be hollow, porous, or solid<sup>8</sup>. NP geometry largely impacts its cellular uptake and residence time inside the cell<sup>10</sup>. Specifically, rods with a diameter of less than 100 nm have displayed the highest uptake, followed by spheres, cylinders, and cubes<sup>11</sup>. Further, decreasing the aspect ratio of NPs (that are less than 100 nm in diameter) has been shown to decrease total cell uptake<sup>12,13</sup>. In terms of blood half-life, rod-shaped

micelles have displayed circulation times that are ten times longer than that of spheres<sup>10</sup>. NP shape can also determine the loading capacity, as hollow NPs are typically used for drug carriers or image contrast agents<sup>8</sup>.

### **1.1.3 Nanoparticle Surface Chemistry Impact on Delivery**

The surface chemistry of NPs plays a significant role in determining the fate of the NP. In nanoparticle systems where passive targeting is used, the NPs nonspecifically accumulate in tissues or tumors. However, NP systems can be designed to actively target specific cells. In these systems, targeting moieties, such as antibodies and small molecules, are conjugated to the NP surface, which can alter the NP surface charge. The surface charge of a NP system influences cellular interactions, one of them being cellular uptake. Neutral or negatively charged nanoparticles exhibit lower cellular uptake compared to positively charged NPs<sup>10</sup>. It is believed that the electrostatic interactions occurring between the slightly negatively charged cellular membrane and the positively charged NP favors NP adhesion to the cell surface, which leads to cellular uptake<sup>12</sup>. The NP circulation time is also affected by the surface charge. NP circulation is highest for neutral nanoparticles, whereas positively charged nanoparticles are cleared the fastest and have been known to cause complications such as hemolysis and platelet aggregation<sup>10</sup>.

## **1.2 Applications of Nanotechnology in Maternal/Fetal Health**

Given the success of nanomedicine in various diseases and cancers, there are many maternal and fetal conditions during pregnancy that could benefit from nanotechnology, specifically nanoparticle-based treatment systems. For many pregnancy-related conditions, there are minimal treatment strategies and management

methods available due to safety and ethical concerns regarding fetal development. Due to these concerns, a cesarean section is often recommended if the condition poses safety risks to either the mother or fetus during pregnancy. Additionally, people with pre-existing conditions that are being managed or treated by a physician face heightened risks at the onset of pregnancy. In these scenarios, patients are urged to end their treatments, terminate their pregnancy, or are constantly observed during the pregnancy term in the interest of their own health. The development of nanoparticle-based treatment systems for maternal-fetal conditions would provide alternative treatment strategies for various maternal and fetal conditions (**Figure 1.1**). In the following sections, we describe how each condition impacts either the pregnant mother or fetus and the current strategies that have been used to manage or treat each condition.

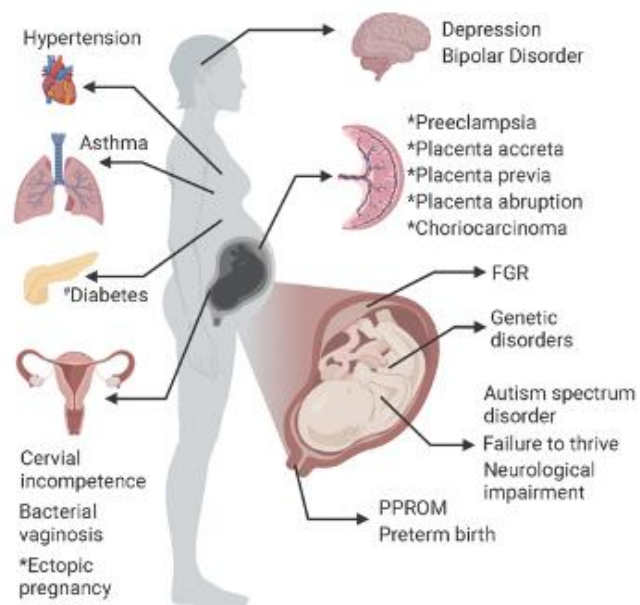


Figure 1.1: Maternal and fetal conditions that would benefit from nanomedicine treatments. Pregnancy conditions that are exacerbated during pregnancy or that are induced by pregnancy are indicated by \*. Diabetes can be pre-existing or induced by pregnancy is indicated by #. Parts of the figure were created using modified graphics from BioRender.

## 1.2.1 Pregnancy Conditions that Primarily Impact the Fetus

### 1.2.1.1 Preeclampsia

The pregnancy condition, preeclampsia (PE), complicates 5-7% of all pregnancies. It is the development of severe hypertension and proteinuria or other maternal organ dysfunction as 20 weeks' gestation<sup>14</sup>. This common condition can lead to severe maternal and fetal consequences such as seizures and death of the parent and fetus<sup>14,15</sup>. The etiology of PE is unknown, however it is thought to stem from a dysfunctional placenta. Because there is limited knowledge regarding the exact cause

of PE, it is difficult to treat this condition and the symptoms are typically the focus for management methods. However, recent studies have investigated a new potential target, sFlt-1, for treating PE<sup>16</sup>. Maynard et al. demonstrated increased levels of sFlt-1 are associated with decreased maternal free VEGF and placental growth factor (PlGF). This discovery led to the hypothesis that the excess sFlt-1 could bind and sequester free VEGF and PlGF in the maternal blood and consequently reduce the pro-angiogenic function of these growth factors, leading to endothelial dysfunction, hypertension, and proteinuria<sup>16</sup>. Following this study, many researchers have shown the delivery of recombinant VEGF, or the VEGF gene can reduce symptoms of PE in multiple rat and mouse models<sup>17-21</sup>. This effect could be a result of either the delivered VEGF acting physiologically in its pro-angiogenic function or by the delivered VEGF binding to excess sFlt-1, allowing endogenous VEGF to act on downstream targets. Another recent study used an elastin like peptide (ELP)-VEGF conjugate to sequester excess sFlt-1 from the maternal circulation while ensuring VEGF cannot cross the placenta and potentially disrupt fetal development<sup>22</sup>. The total sFlt-1 amount increased in the presence of the ELP-VEGF conjugate, but the free sFlt-1 levels decreased indicating the conjugate was able to successfully bind excess free sFlt-1 and decreased maternal blood pressure and nitric oxide levels<sup>22</sup>. The study to follow demonstrated that changing the molecular weight of the ELP can provide control over the biodistribution and clearance times of the ELP conjugates<sup>23</sup>. Further, increasing ELP size increases organ deposition but yields slower plasma clearance<sup>23</sup>.

Other work regarding the expression of sFlt-1 in PE animal models incorporated small interfering RNA (siRNA) in different delivery vehicles. One delivery system used self-assembled poly(amidoamine) (PAMAM) dendrimers to

reduce hypertension, proteinuria, and circulating sFlt-1 in a tumor necrosis factor- $\alpha$  (TNF- $\alpha$ )<sup>24</sup> in an induced PE rat model<sup>25</sup>. PAMAM dendrimers have been shown to be biocompatible and have low transport rates across the placenta, making them promising carriers for treating pregnancy complications<sup>26</sup>. The siRNA delivery system was able to increase fetal weight without any detected maternal tissue damage or fetal resorptions<sup>24</sup>. Another study used hydrophobically modified asymmetric siRNAs conjugated to cholesterol (hsiRNAs) to target specific isoforms of sFlt-1, specifically sFlt1-i13 and sFlt-1e15a, which are expressed in mice and non-human primates respectively. When delivered to healthy pregnant mice, hsiRNA<sup>sFLT1i13</sup> reduced mRNA levels in the placenta by 40% but did not accumulate in maternal liver and kidney<sup>27</sup>. The treatment did not affect the number of pups or the weight of pups. In a baboon uteroplacental ischemia (UPI) PE model, hsiRNA<sup>sFLT1i13/e15a</sup> successfully reduced serum sFlt-1 levels by 50% 2 weeks post UPI surgery and treatment. Further, the treated animals had decreased blood pressure and proteinuria, and newborn weights were not statistically significantly different between control groups and PE groups<sup>27</sup>. Lastly, placenta targeted lipid polymer nanoparticles carrying sFlt1 siRNA have been used to decrease placental sFlt1 mRNA levels and circulating sFlt-1 levels in a healthy pregnant mouse model. After NP treatment, it was determined maternal liver function, fetal weight, and fetal number were unchanged<sup>28</sup>. In totality, these studies demonstrate engineering nanocarriers could be used to treat PE.

### **1.2.1.2 Fetal Growth Restriction**

Fetal growth restriction (FGR) is one of the most common fetal development complications, effecting up to 15% of all pregnancies<sup>29</sup>. This condition, which is thought to be caused by a dysfunctional placenta, can negatively influence childhood

and adult life. In fact, adults who have experience FGR have a higher lifetime incidence of hypertension, obesity, metabolic syndrome, and diabetes<sup>30</sup>. Further, maternal disorders such as hypertension, diabetes, preeclampsia, inflammation, thrombosis, and Lupus, increase the likelihood of FGR. When comparing placental weight, it was determined placentas of FGR babies are approximately 24% lighter than those of healthy babies, suggesting there is a lack of nutrients and oxygen necessary for fetal growth<sup>30</sup>.

Although the exact cause of FGR is not known, the growth of the placenta has been compared to malignant cells, showing similar characteristics such as high cell proliferation, migratory and invasive properties, and the ability to evade the immune system<sup>31</sup>. Because of the similarities between the placenta and malignant cells, targeting moieties, such as insulin growth factor-2 (IGF-2), have been shown to be an important growth factor for placental development and growth and may be helpful for treating FGR<sup>32,33</sup>. The targeting peptide, iRGD (CRGKGPDC), which has been shown to target tumor vessels, was conjugated to liposomes loaded with IGF-2 and delivered to healthy pregnant mice. In this placenta-specific *Igf-2* knockout mouse model, researchers observed an increase in fetal weight and fetal weight distribution, but no changes in litter size or number of resorptions following liposome delivery<sup>34</sup>. IGF-1, a related growth factor necessary for placental development, was used to treat FGR in mice<sup>35</sup>. In this study, a diblock-copolymer polyplex system and a placenta specific promoter, PLAC1, was directly injected into the placenta of mice with FGR induced by uterine artery branch ligation<sup>36</sup>. After treatment, it was determined the placenta labyrinth thickness increased to baseline, indicating the IGF-1 assisted in placenta

development in this model. There were no differences in the litter size, but the pup weight significantly increased after polyplex treatment<sup>36</sup>.

Other peptides that are known to bind tumor associated vasculature and have been used to target the placenta are CCGKRK and CNKGLRNK<sup>37,38</sup>. CCGKRK-miRNA inhibitor conjugates were synthesized against miRNAs known to be native regulators of placental growth then delivered to healthy pregnant mice at three time points during pregnancy<sup>37</sup>. The miR-675 inhibitors significantly increased placental weight compared to saline injected controls and the miR-145 inhibitors significantly reduced the variability in placental weight. Both miRNA inhibitors increased fetal weight without decreasing mean litter size or increasing number of resorptions. The CNKGLRNK peptides were used to target the placenta in a liposome system loaded with nitric oxide donor (SE175)<sup>38</sup>. In FGR, nitric oxide (NO) which is produced by endothelial nitric oxide synthase (eNOS) are both upregulated<sup>39,40</sup>. Therefore, it was hypothesized that delivering a NO donor via the peptide target liposomes would increase vasodilation in the placenta and reduce resistance<sup>38</sup>. The liposomes were injected in a health and eNOS knockout pregnant mice as a FGR model and it was determined the treatments did not alter litter size or number of resorptions in healthy mice. However, the liposome treatment did increase fetal weight in eNOS knockout mice and maintained placental weight similar to the control group. The treatment also increased spiral artery diameter by 33%, indicating a physiological mechanism for NO<sup>38</sup>. Collectively, these studies suggest engineered nanomedicines can be tailored to treat FGR.

### **1.2.1.3 Preterm Birth**

Preterm Birth (PTB) is the most common pregnancy condition effecting 400,000 newborns in the United States annually <sup>41</sup>. There are many underlying causes of PTB that arise from other complications, such as PPRM (approximately 30% of PTB cases), maternal or fetal infections, or other pregnancy conditions, but PTB can also be a result of spontaneous preterm labor (approximately 45% of all cases), multiple pregnancies and cervical incompetence. Additionally, there are many other risk factors that include short cervical length, multiple births, and genetic predisposition. While PTB is traditionally defined as a birth occurring before 37 weeks of gestation, there are different levels of severity for preterm infants including moderate prematurity (32-33 weeks), severe prematurity (28-31) and extreme prematurity (less than 28 weeks) <sup>42</sup>. The prematurity level often results in extensive complications for the newborn and infants born extremely premature face a decreased survival rate due to the underdevelopment of fetal lungs and cardiac system. Due to the varied underlying causes and pregnancy complications that are often associated with PTB, this condition is very difficult to treat, yet several researchers have begun to develop drug delivery vehicles to reduce prostaglandin production and subsequently delay the onset of labor.

Refuerzo et al. developed a liposomal drug delivery vehicle that was loaded with indomethacin and decorated with oxytocin receptor antagonists (LIP-IND-ORA) <sup>43</sup>. Indomethacin is a non-steroidal inflammatory drug that reduces prostaglandin production by the uterus. However, due to the side effects of indomethacin, such as premature closure of the ductus arteriosus and potential increase of intraventricular hemorrhage, the use of free indomethacin is limited to protect the fetus. Using a targeted drug carrier system to deliver indomethacin would allow for its use in treating

PTB. ORA, an FDA approved receptor antagonist, was used to target the overexpressed oxytocin receptors in the uterus to reduce uterine contractions during preterm labor. In this study, the LIP-IND-ORA was administered daily via i.v. injections to pregnant mice at E15 and evaluated for liposome distribution and effects on PTB. LIP-IND-ORA displayed 3x higher accumulation in the uterus, liver, placenta, and fetus compared to freely delivered ORA. In terms of PTB, the LIP-IND-ORA prolonged pregnancy by 31% and decreased PTB cases (defined as delivery on or before E19) by 15%. Interestingly, the LIP-IND, LIP-ORA, and LIP-IND-ORA treatment systems all displayed statistically similar inhibition of murine uterine contraction, indicating there is no synergistic effect of ORA and IND. Another study confirmed the need of targeted drug loaded liposomes for reducing PTB rates by comparing ORA-targeted liposomes to non-targeted liposomes <sup>44</sup>. In this work, the targeted liposomes reduced PTB rates more than the untargeted liposomes, confirming the results from the previous study.

Researchers have explored other drug delivery vehicles to decrease PTB in pregnant mice using the vaginal administration of a progesterone nanosuspension (NS) <sup>45</sup>. In this work, RU486, a progesterone antagonist, was subcutaneously administered to pregnant mice daily starting at E15 to induce PTB. The mice received daily doses of either RU486 only, RU486 and vaginally administered progesterone gel (Crinone®) or RU486 and vaginally administered progesterone NS. The biodistribution analyses indicated the NS were retained in the uterus and cervix up to 6 h post-administration. Additionally, the oxytocin receptor levels in the cervix were reduced in the mice treated with NS or with progesterone gel. When comparing the delivery ages, it was determined that 55% of the mice treated with NS reached full term (median parturition

day 19.5), whereas 32% of mice treated with the progesterone gel reached full term (median parturition day 16)<sup>45</sup>. Overall, the results of this study concluded NS delivery of progesterone is more effective in preventing PTB compared to progesterone gel. The results of this work in combination with the studies previously described suggest engineered drug delivery vehicles have the potential to be used to prevent PTB.

#### **1.2.1.4 Preterm Premature Rupture of Membranes**

Another pregnancy condition that could largely benefit from the use of nanoparticle-based systems is Preterm Premature Rupture of Membranes (PPROM), as it is responsible for approximately one-third of preterm births<sup>46</sup>. PPRM occurs when the amniotic sac is ruptured either through the vagina or amniocentesis (**Figure 1.2**). During this condition, bacteria enter the uterus and early labor is initiated. The fetus is also exposed to bacteria, which initiates fetal inflammatory syndrome (FIRS). *Ureaplasma urealyticum*, *Ureaplasma parvum*, and *Mycoplasma hominus* are the bacterial species that are mostly commonly present in amniotic infections that are associated with 70% of PPRM cases<sup>46-48</sup>. However, there are other behavioral factors (e.g., smoking, poor nutrition), obstetric complications (e.g., multiple pregnancies, incompetent cervix), and genetic predispositions that can increase the risk of PPRM. Additionally, some cases of PPRM have been recently associated with sterile inflammation, a condition that presents as an inflammatory response in the absence of bacteria<sup>46</sup>.

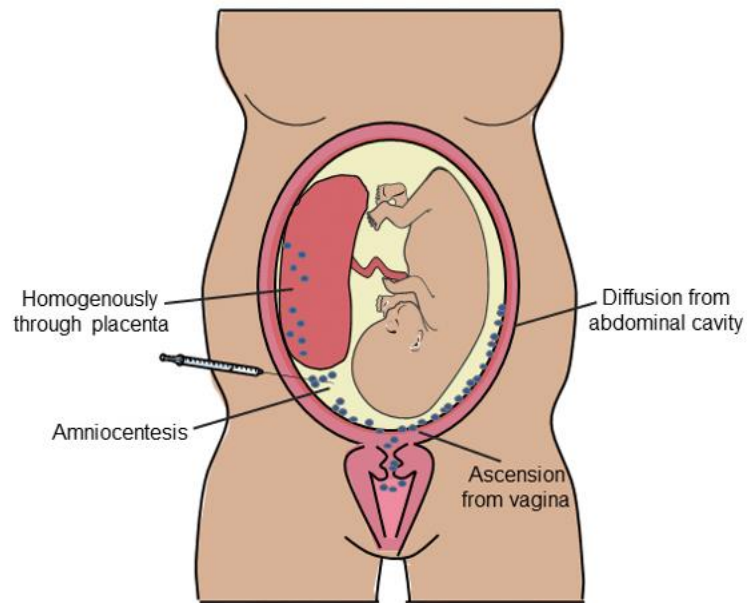


Figure 1.2: The potential routes of bacterial infection in pregnant women with preterm premature rupture of membranes (PPROM). Parts of the figure were created using modified graphics from Servier Medical Art, provided by Servier, licensed under a Creative Commons Attribution 3.0 Unported License.

Due to the increased risk of FIRS for the fetus and sepsis for the pregnant person, steroids or antibiotics are quickly administered either orally or intravenously to decrease the bacterial infection. The most used antibiotics for this condition, erythromycin, amoxicillin, and clavulanic acid, have been tested alone and in combination in previous clinical trials. Despite their success in limiting bacterial infection and delaying preterm labor, these treatment strategies have shown conflicting data pertaining to fetal risk of cerebral palsy<sup>46,49</sup>.

While there aren't any studies that have used nanoparticle-based systems to treat PPRM, one study evaluated the use of freely delivered azithromycin (AZ) treatments during pregnancy. The goal of the study was to determine which delivery route, intra-amniotic or intravenous, displayed the least undesirable fetal effects if administered at the 2<sup>nd</sup> trimester <sup>47</sup>. To compare the delivery routes, pregnant sheep were either given a single intra-amniotic (i.a.) dose of AZ or multiple intravenous (i.v.) AZ doses every 12 h at the 80<sup>th</sup> gestation day (of 150 days). The sheep were euthanized 120 h after the single i.a. dose or the initial i.v. and the drug distribution, fetal weight, and development effects were evaluated <sup>47</sup>. The drug distribution analysis revealed AZ was present in the amniotic fluid and fetal lungs following the i.a. administration method, but the i.v. administration method showed drug accumulated in the fetal lung, liver, and plasma <sup>47</sup>. There were no distinct toxic responses or exposure to the fetus using either administration method, however the i.v. method was preferred for the accumulation and administration ease. The knowledge obtained from this study can be used to develop a targeted nanoparticle system loaded with antibiotics for the treatment of PPRM *in vivo*.

## **1.2.2 Preexisting Maternal Health Conditions Exacerbated During Pregnancy**

### **1.2.2.1 Endometriosis**

Endometriosis is a gynecological disorder in which endometrial tissue and stroma is present outside of the uterus <sup>50-52</sup>. This condition is prevalent in 5% and 10% in premenopausal people and is a major cause of infertility <sup>52</sup>. Patients diagnosed with endometriosis often experience chronic pelvic pain and severely painful menstruation, however endometriosis can often present without symptoms, resulting in frequently

missed diagnoses. One of the main physical symptoms of endometriosis is the growth of lesions in the pelvic region. While there are many hypotheses regarding the pathogenesis of endometriosis, the theory that is most widely accepted suggests the establishment of an early lesion in the uterus occurs during implantation and serves as a nidus for endometrial tissue proliferation<sup>52</sup>. It is believed the endometrial tissue spreads to other pelvic regions through retrograde menstruation, a menstruation in which blood flows backwards to the pelvis instead of the vagina<sup>50</sup>. The spreading of endometrial tissue then leads to the establishment of ectopic endometrial tissues and lesions outside of the uterus. The growth of lesions and improper implantation often results in increased infertility in women that are less than 35 years old<sup>52</sup>. Additionally, researchers observed an increase in macrophages and cytokines in the peritoneal fluid in women with endometriosis compared to healthy women. Scientists have suggested the high infertility rates in women with endometriosis are possibly due to the increased presence of macrophages and scarring impacts sperm motility and ciliary function of the fallopian tubes. Another possible explanation for high infertility rates with this condition is that the development of adhesions could obstruct egg transport in the fallopian tubes. Considering the impact of endometriosis on women's fertility rates, there is an urgent need for treatment methods for women with this condition.

To treat endometriosis, a vaginal ring system loaded with 1500 mg of danazol was evaluated in 56 patients and observed for 7 months for changes in pain levels during menstruation and infertility<sup>53</sup>. In terms of menstruation pain, 88% of patients experienced less pain within 2 months of the vaginal ring insertion. Within 1 month of ring insertion, 4 patients achieved successful conception. As the study continued, more patients achieved conception (2 patients within 3 months, 5 patients within 10

months), indicating the danazol rings improved fertility. Endometriosis mass was also compared using transvaginal ultrasonography to determine the infiltration depth of the lesions. Here it was determined the endometriosis mass disappeared in 36 out of 42 patients and was reduced in 6 out of 42 patients with deeply infiltrating cases. From this study, it was suggested the danazol was absorbed through the vaginal mucosa, thus infiltrating the endometriosis via diffusion to successfully alleviate menstruation pain <sup>53</sup>.

#### **1.2.2.2 Gestational Diabetes Mellitus**

The hormonal changes that occur during pregnancy cause changes in pregnant people's insulin sensitivity<sup>54</sup>. During the early stages of pregnancy, higher levels of estrogen increase insulin sensitivity, whereas lactogen and progesterone production in the placenta that occurs in later gestations of pregnancy decrease insulin sensitivity. As a result of these physiologic changes, diabetes mellitus is a risk factor for pregnancy complications, including fetal hyperinsulinemia which results in excess fetal growth that can increase complications during delivery or cause late-term death <sup>55</sup>. Pregnant patients with type 1 diabetes have increased rates of preeclampsia, premature delivery, mortality, and birth of a child with congenital malformations<sup>56</sup>. With the increasing rates of type 2 diabetic patients and risk factors, such as obesity, there has been an increase in pregnancy induced diabetes, gestational diabetes mellitus (GDM) <sup>57</sup>. GDM affects 14% of pregnancies in the United States and is responsible for nearly 90% of pregnancies complicated by diabetes<sup>58</sup>. People with GDM are at an increased risk of remaining diabetic after their pregnancy and being diagnosed with type 2 diabetes in the future<sup>59</sup>. Further, their children have an increased risk of obesity and impairs intellectual achievement<sup>60,61</sup>.

GDM is currently managed in pregnant women with either diet changes or medication. People with GDM that are a low risk for additional pregnancy complications are advised to limit carbohydrate intake and increase aerobic exercise<sup>62</sup>. However, GDM patients with high risk factors are given incremental oral metformin or glyburide prescriptions, of increasing doses to combat rising blood sugars<sup>62</sup>. Despite the lack of FDA approval of these hypoglycemic agents, there has been minimal evidence of perinatal complications in comparison to insulin<sup>57,62,63</sup>. Recent treatment advancements have explored the use of antioxidants, such as vitamin D and E or zinc to alleviate oxidative stress caused by GDM. However, these studies have no evaluated effects on fetal development and growth following treatment<sup>57,64</sup>.

While few researchers have explored nanoparticle-based therapies for the treatment of GDM, one study developed a nanoparticle-based treatment system of cerium oxide NPs (nanoceria) for pregnant diabetic mice<sup>65</sup>. The synthesis of nanoceria formed a crystalline structure with antioxidant properties like vitamin E and was shown to protect against reactive oxygen species (ROS) that cause oxidative stress by shifting between oxidation states. Single doses of the nanoceria formulation or vitamin E were administered to pregnant diabetic mice every day for 16 days and the weight changes, blood glucose levels, ROS formation, and embryonic effects were evaluated<sup>65</sup>. In terms of embryonic effects, nanoceria increased embryonic weight and decreased morphological embryonic. The nanoceria treatment also decreased ROS formation and displayed a stronger antioxidant effect than the vitamin E treatment. Despite the success in antioxidant effects, nanoceria did not significantly alter maternal blood glucose levels as the authors expected. The goal of lowering blood glucose levels was not achieved in this pregnancy model; however, glucose responsive

insulin delivery systems have decreased glucose in non-pregnant animal models<sup>66-69</sup>. Examples of these delivery systems that have been used to deliver insulin subcutaneously or trans dermally in non-pregnant and swine models of diabetes<sup>67,70-72</sup> include glucose-sensitive polymeric nanogels<sup>71</sup>, pH-sensitive polymeric and metal-organic framework (MOF) NPs<sup>70,72</sup>, and charge-switchable polymer conjugates<sup>73</sup>. The use of glucose-responsive delivery systems is especially attractive for maternal-fetal health applications because they only release insulin when there is excess glucose and reduce the risk of a common side effect, hypoglycemia, that is dangerous for the fetus<sup>74</sup>. These strategies should be explored in the future to include GDM as an application.

### **1.2.2.3 Hypertension**

A common disease effecting 5-10% of pregnant women in chronic hypertension<sup>75</sup>. Pregnant patients with hypertension face increased risks such as maternal pulmonary edema, acute renal failure, stillbirth, premature delivery, and infants that are small for their gestational age<sup>76</sup>. Another high-risk factor for chronic hypertensive patients is preeclampsia, which is complicated by the potential effects of a therapeutics on the fetus<sup>76,77</sup>. Due to the risks associated with therapeutics on fetal development, clinical management methods such as diet and lifestyle changes are encouraged and most often implemented. However, in the case of high maternal blood pressure levels, pharmacological treatments are needed. As a result of the limited information and knowledge regarding fetal toxicity, patients undergoing hypertensive therapies are carefully monitored.

To manage GDM through targeted nanomedicine-based systems, it is essential we understand the pathology of hypertension and how it impacts the onset of

additional pregnancy complications. While it is known that pre-existing hypertension can cause a variety of different complications, the exact pathways in which complications develop during pregnancy due to hypertension is unknown. Thus, a BPH/5, mildly hypertensive mouse was used as a model of human pregnancy, as these mice have fetal growth restriction, abnormal placentation, and defects in maternal decidual arteries like humans<sup>78,79</sup>. Consequently, these issues lead to inflammation and activation of the complement pathway, which has been shown to be associated with adverse pregnancy outcomes<sup>80-82</sup>. In this work, a fusion protein (CR1-Crry) was synthesized from a pan-C3 convertase inhibitor, Crry, and a targeting protein that binds to C3 degradation products, CR2, to inhibit the complement pathway. The delivery of CR1-Crry in the hypertensive mouse model increased placental weight, normalized junctional zone and spiral artery morphology, increased placental vascular endothelial growth factor (VEGF) concentration, and decreased neutrophil recruitment to the placenta without altering the numbers of uterine natural killer cells or macrophages<sup>83</sup>. From this work, it is apparent the complement pathway plays a role in the pathology of adverse outcomes during pregnancy due to hypertension. Considering hypertension is a risk factor for preeclampsia, it is also suggested the complement pathway is a part of this condition's pathology<sup>81,82,84</sup>. In delivering CR2-Crry to a CBA/J x DBA/2 mouse model of preeclampsia, it was determined the CR2-Crry treatment prevented oxidative stress, lowered circulating soluble fms-like tyrosine kinase-1 (sFlt-1) levels, reduced fetal resorption, and improved kidney function<sup>85</sup>. The success of this fusion protein in both a hypertensive and preeclamptic mouse model provides insight to the disease pathologies and gives promise to the use of target nano therapies to treat either hypertension or preeclampsia.

#### 1.2.2.4 Bacterial Vaginosis

In bacterial vaginosis (BV), a common condition occurring in pregnant and non-pregnant people, the vaginal microbiome is disrupted which poses several challenges for the patient. In the healthy vaginal microbiome, the *Lactobacillus* species secrete lactic acid and other anti-microbial molecules to maintain the vaginal pH at 3.5-4.5<sup>86</sup>. In BV conditions, the *Lactobacillus* species is decreased and replaced by a variety of pathogenic bacteria, primarily *Gardnerella vaginalis* (**Figure 1.3**)<sup>87</sup>. The most observed symptoms in BV are abnormal vaginal discharge, pain, infertility, other infections such as HIV and urinary tract infections in non-pregnant patients<sup>88,89</sup>. However, BV symptoms can be mild and undetected and only 37% of pregnant people with BV are symptomatic and exhibit changes in vaginal discharge or odor<sup>87</sup>. Due to the limited symptom detection, pregnant patients with BV face additional risks, often leading to spontaneous abortion, PTB, and PPRM<sup>88,90,91</sup>. Although BV is not a life-threatening condition, babies delivered by patients with BV have an increased risk of assisted ventilation or respiratory distress at birth and sepsis<sup>92</sup>.

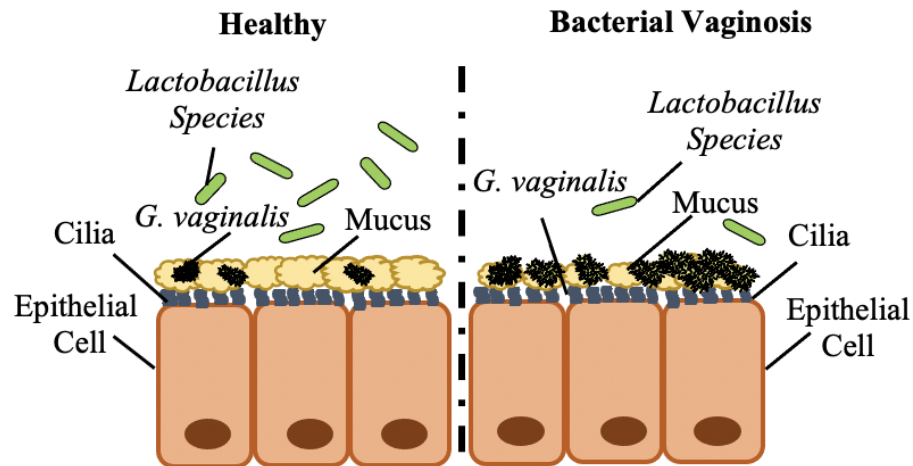


Figure 1.3: The potential routes of bacterial infection in pregnant women with preterm premature rupture of membranes (PPROM). Parts of the figure were created using modified graphics from Servier Medical Art, provided by Servier, licensed under a Creative Commons Attribution 3.0 Unported License.

The most common treatments available for BV patients are non-specific antibiotics that are delivered orally or in vaginal creams. Unfortunately, recurrence is significant within 6 months of treatment<sup>93</sup> and 10-15% of patients do not improve after the first course of antibiotics<sup>87</sup>. One of the reasons why the recurrence of BV in patients is so common is because the regrowth of the *Lactobacilli* is slowed following antibiotic treatments. As a result of the diminished *Lactobacilli*, patients with BV also face an increased risk of acquiring sexually transmitted diseases<sup>87</sup>.

To combat BV in non-pregnant people researchers have developed a probiotic treatment system which addresses the lack of *Lactobacilli* regrowth and inflammatory responses in mice following BV infection<sup>94</sup>. In this study, estrogen-treated mice were infected with *E. coli* for 5 days prior to treatment and a *Clostridium butyricum* was

vaginally administered in either high or low doses once per day for 6 days. The probiotic treatment, *C. butyricum*, was compared to an antibiotic treatment, kanamycin. Of the treatment groups administered, the neutrophil presence and bacteria count was the lowest for the high dose of *C. butyricum* and was the only treatment group to restore lactobacillus growth<sup>94</sup>. This work demonstrated *E. coli* growth is inhibited in the presence of *C. butyricum* and promotes lactobacillus growth.

While few studies have investigated the use of nanoparticle-based systems for the treatment of BV, nanocarrier systems have been developed for the treatment of HIV. One study loaded a PLGA nanoparticle with an HIV antiviral drug and embedded the particles in a dissolvable film made from polyvinyl alcohol PVC and hydroxypropyl methyl (HPMC) cellulose<sup>95</sup>. The drug release profiles in vitro data revealed 80% drug release occurred within 5-10 mins and 90% release occurred within the first 2h. The films were placed in the vagina once daily for 14 days in diestrus phase mice and mice cytokine production, toxicity levels, and morphological changes were evaluated. While there were no histological changes in the cervix or uterine horns between the treatment groups, the mice treated with the vaginal films experience a mild thinning of the vaginal epithelium and slightly raised IL- $\beta$  levels. Further, minimal toxicity levels were observed in the film treatment group *in vivo*<sup>95</sup>. Overall, this study suggests there is potential of nanoparticle-base therapies for treating vaginal infections.

### **1.3 Biological Barriers to Targeting Reproductive Organs**

The administration method used to deliver NPs to the female reproductive organs is critical to determine the biological barriers the NPs will encounter. Intravenous administration and vaginal administration are systemic and local delivery

methods, respectively, that present different advantages and biological barriers when targeting the reproductive organs. In each section below, we discuss the challenges associated with each administration method and present maternal/fetal health applications that have utilized each delivery route.

### **1.3.1 Challenges with Intravenous Delivery**

The major challenge with intravenously delivering nanoparticles to the reproductive organs is the removal of the nanoparticles from the bloodstream by the mononuclear phagocytotic system (MPS). When nanoparticles are delivered intravenously, they immediately enter the bloodstream and circulate throughout the body. Once in the bloodstream, nanoparticles are opsonized, a process in which they are coated in a protein corona. The protein corona is immediately recognized and marked by macrophages circulating in the bloodstream (**Figure 1.4**) to be phagocytosed later. The nanoparticles are then removed from the circulation and accumulate in the liver.

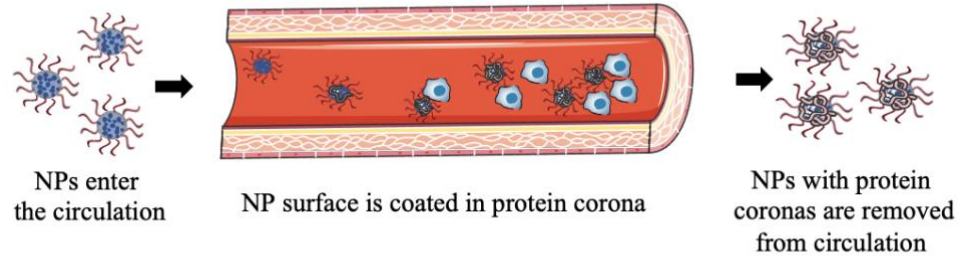


Figure 1.4: NPs that are delivered via intravenous injections enter the circulation and are immediately coated in protein corona. Coated NPs are marked by macrophages for removal from the circulation and accumulate in the liver. Parts of the figure were created using modified graphics from Servier Medical Art, provided by Servier, licensed under a Creative Commons Attribution 3.0 Unported License.

To bypass the MPS, nanoparticles are coated in a “stealth” agent. One of the most common stealth agents is polyethylene glycol (PEG), which has been extensively studied by researchers and has been shown to increase circulation *in vivo*<sup>96</sup>. PEG also reduces particle aggregation by blocking interactions between nanoparticle surfaces, thereby reducing cellular uptake<sup>97</sup>. PEG surface coatings also inhibit direct interactions between nanoparticles and proteins which decreases opsonization. One factor that has been shown to increase the blood half-life is the length of the PEG nanoparticle surface<sup>98</sup>. Researchers have suggested the longer PEG lengths reduce protein adsorption and delay phagocytosis. The delay in phagocytosis allows the nanoparticles to better evade macrophages in the bloodstream, which leads to increased blood half-life.

Another factor that should be considered when delivering nanoparticles to the reproductive organs in females is the menstrual cycle. One study evaluated the impact

of the menstrual cycle in mice, the estrus cycle, on nanoparticle biodistribution<sup>99</sup>. Gold PEGylated nanoparticles (AuNPs) with sizes of 20 nm, 50 nm, 100 nm, and 200 nm were delivered to mice via IV injections at the estrus, proestrus, diestrus, and metestrus phases of the estrus cycle. AuNPs of <100 nm accumulated in the ovaries at each stage. However, the ovarian accumulation during the estrus phase was significantly higher than the proestrus, metestrus, and diestrus phases. In the same study, lipid nanoparticles of 80 nm were delivered intravenously to mice during either the estrus or diestrus phases to mice with orthotopic triple negative breast (4T1) tumors or epithelial cervical cancer. Here, it was determined nanoparticles delivered at the estrus phase accumulated more in the reproductive organs. However, nanoparticles delivered at the diestrus phase displayed more accumulation in the 4T1 tumors than in the reproductive organs. From this work, it is evident the menstrual cycle plays a role in nanoparticle accumulation in the reproductive organs following intravenous delivery.

### **1.3.2 Barriers Associated with the Vaginal Delivery**

While the intravenous delivery method is useful for specific targets, there are many challenges with delivering nanoparticles to the reproductive organs. Local delivery methods are alternative administration method that can be utilized to limit the off-target effects that are often observed with IV delivery and increase nanoparticle accumulation at the desired sites. For targeting the reproductive organs, vaginal delivery is an attractive administration method because of its proximity to the reproductive organs and elimination of MPS removal.

One of the main barriers to using vaginal administration for the delivery of nanoparticles is cervicovaginal mucus (CVM). CVM is a gel-like fluid that lines the

cervical and vaginal epithelium and serves as a protective barrier to prevent foreign antigens and bacteria from entering the uterus <sup>100,101</sup>. The structural unit of CVM are glycoproteins, which are arranged in porous fibrous networks (**Figure 1.5**). These fibrous networks help to remove pathogens by trapping the pathogens then clearing them from the system in the form of discharge in both pregnant and non-pregnant people <sup>102-104</sup>. The rheological properties of CVM are non-linear and dependent on the length scale and shear stress. Under low shear stress and at the nanoscale, CVM acts as a low-viscous fluid. However, under high shear stress conditions, CVM has a high viscosity. Additionally, CVM viscosity changes can result from external chemical signals, with gradual changes induced by estradiol (within days), immediate changes induced by spermatozoa presence (within minutes) <sup>103,105</sup>, or with gestational age during pregnancy (**Figure 1.5**).

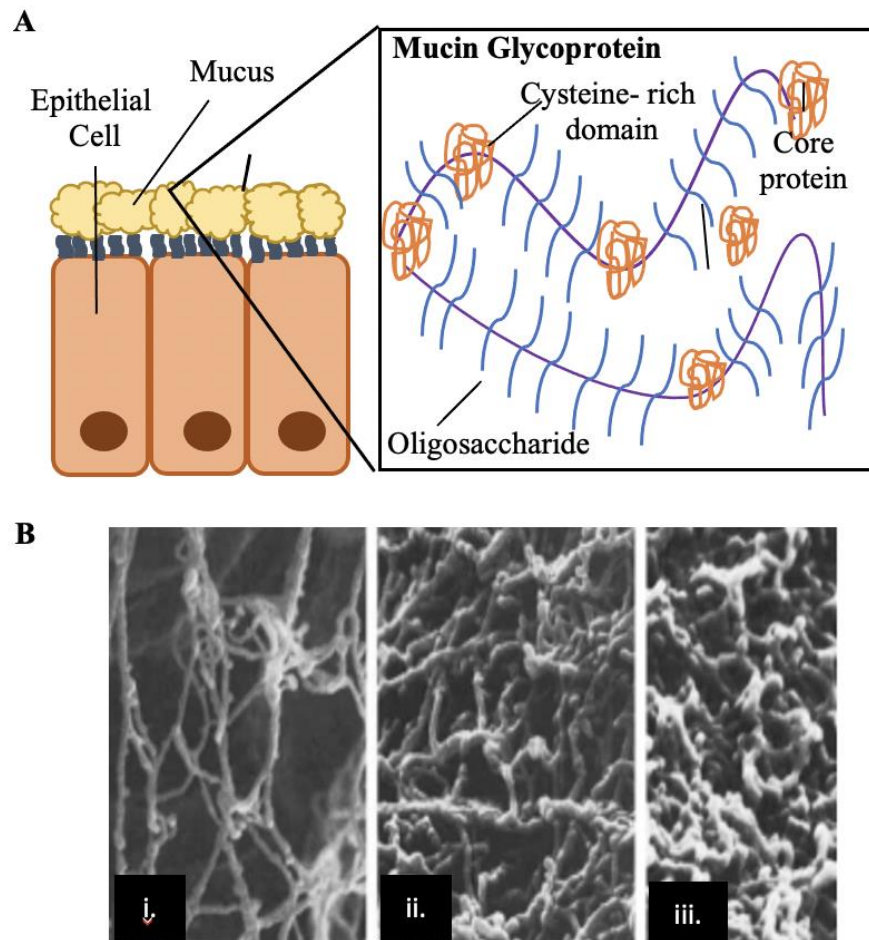


Figure 1.5: (A) Schematic of cervicovaginal mucus layer on epithelium and mucin glycoprotein structure. Parts of the figure were created using modified graphics from Servier Medical Art, provided by Servier, licensed under a Creative Commons Attribution 3.0 Unported License. (B) Cervicovaginal mucus at (i) 20<sup>th</sup> day of pregnancy (ii) 2.5 months of pregnancy and (iii) last week of pregnancy. Figure Reproduced with permission from *N. Becher, et al. Acta Obstet Gynecol Scand.* 2009; 88: 502-513 under a Creative Commons Attribution License.

In addition to the increased presence of CVM during pregnancy, the properties of CVM change with the hormonal fluctuations that occur during pregnancy. After conception, estradiol levels are low and CVM viscosity increases to discourage sperm and bacteria transport to the uterus. As pregnancy progresses and the placenta develops, estradiol levels increase, and mucin production is initiated. Next, progesterone levels decrease to initiate epithelial proliferation and cervical remodeling, resulting in increased CVM production and immune protection for the fetus <sup>106</sup>. In the third trimester, estradiol and CVM production is increased and maintained for the rest of the pregnancy. Immediately before labor, progesterone levels decrease rapidly to end oxytocin production and initiate labor. The significant drop in progesterone levels results in the release of the CMP from the uterus and the onset of labor. The fluctuations in CVM viscosity that occur throughout pregnancy can also serve as a barrier to targeting the female reproductive organs using the vaginal delivery method.

Another biological barrier that is present during pregnancy is the cervical mucus plug (CMP). The CMP is a collection of immune cells, shed cells, and secretory that is formed in the cervical canal during the first trimester <sup>106,107</sup>. The physical barrier structure of the CMP serves to prevent large foreign pathogens and bacteria from entering the uterus (**Figure 1.5B**) <sup>106-108</sup>. The presence of the CMP is critical for maintaining the safety of the fetus, as bacteria in the uterus can result in the initiation of preterm labor and subsequent preterm birth. Like CVM, the viscosity of the CMP depend on the shear stress conditions. Under low shear stress, the CMP acts as an elastic solid but under high shear stress, the CMP experiences very little

deformity. Understanding the properties of the CMP is necessary for designing nanoparticles for the treatment of women's health conditions during pregnancy.

### **1.3.3 Nanoparticle Design for Vaginal Delivery**

To deliver targeted nanoparticles to effectively treat maternal/fetal health conditions during pregnancy, it is necessary to understand how the design properties of the nanoparticles can be affected by the biological barriers that accompany the use of vaginal delivery. Previous literature regarding nanoparticle design has shown nanoparticle size, shape, and surface charge effect the drug delivery properties and must be tailored for the desired target<sup>10</sup>. In terms of vaginal delivery, researchers have determined specific guidelines for each nanoparticle design property that will be discussed below.

Nanoparticle size plays a significant role in evading the CVM barrier for vaginal administration methods. In previous work, PEG-coated polystyrene NPs of 100 nm, 200 nm, and 500 nm, were examined for their mean displacement values (MSD) in *ex vivo* CVM samples of from non-pregnant patients<sup>109</sup>. The MSD values from this study determined 100 nm and 200 nm NPs diffused much faster in CVM compared to 500 nm NPs. The measured diffusion rates of the NPs were estimated using Amsden's obstruction-scaling model to determine the approximate size of the porous networks. Researchers determined the average diameter of CVM in non-pregnant people was 340 nm+- 70 nm. From this data, researchers suggested smaller NPs (100 nm and 200 nm) diffused faster through the CVM samples because they were smaller than the average diameter of the pores within the fibrous networks of the mucosal structure<sup>109</sup>. Using the knowledge gained from these studies, it is essential

that vaginally delivered NPs be less than 200 nm to minimize NPs entrapment in the CVM barrier.

The NP surface charge should also be optimized to overcome the CVM barrier. To determine the impact of NP surface charge on mucosal escape, PEG coated polystyrene NPs and uncoated polystyrene were tested in non-pregnant *ex vivo* CVM samples for their mean squared displacement values. The PEG-coated NPs outperformed the uncoated NPs, with the PEG NPs displaying mucus penetration rates 400 to 6,000 fold faster than the bare NPs <sup>109</sup>. The authors attributed the PEG NPs diffusivity success to the neutralized surface charge and suggested electrostatic interactions between the NPs and CVM were minimized by the PEG coating. Further, the PEG density was evaluated on polystyrene NPs to analyze how coating density effect NP diffusion in *ex vivo* human CVM samples <sup>110</sup>. NPs coated with 5 kDa PEG, 10 kDa PEG, 20 kDa PEG and 40 kDa PEG were analyzed for their diffusivity in undiluted human CVM. The results from this study revealed densely coated NPs diffuse faster in mucus compared to less dense coatings.

Another avenue to enhance the nanoparticle mucus penetration is the use of muco-inert biomaterials for nanoparticle synthesis. Khutoryanskiy evaluated muco-inert biomaterials for the development of mucus-penetrating nanoparticles, including poly (2-alkyl-2-oxazolines), polysarcosine and poly (vinyl alcohol) as an alternative to PEGylation <sup>111</sup>. The conclusions from these studies have highlighted and confirmed a near-neutral surface charge from either “stealth” agents or muco-inert biomaterials is imperative for nanoparticle escape from the CVM barrier.

Taken together, NPs must be designed strategically to successfully overcome the CVM barrier for vaginal administration methods. Smaller NPs and NPs with a

near-neutral surface charge have shown great success in minimizing mucosal interactions and NP entrapment in the CVM. In treating maternal/fetal conditions during pregnancy, these NP design characteristics must be considered to maximize NP delivery.

#### **1.3.4 Physiologic Changes in Human Anatomy During Pregnancy**

The female reproductive anatomy undergoes many changes over the course of pregnancy. The reproductive organs that are primarily involved in pregnancy complications are the cervix, uterus, and placenta, which all contribute to the growth and development of the fetus (**Figure 1.6**). It is essential that engineered nanoparticle-based systems for the treatment of pregnancy conditions consider the gestational changes that occur during pregnancy when targeting the female reproductive organs. Without proper consideration of the dynamic reproductive anatomy, the safety of the parent and fetus could be at risk.

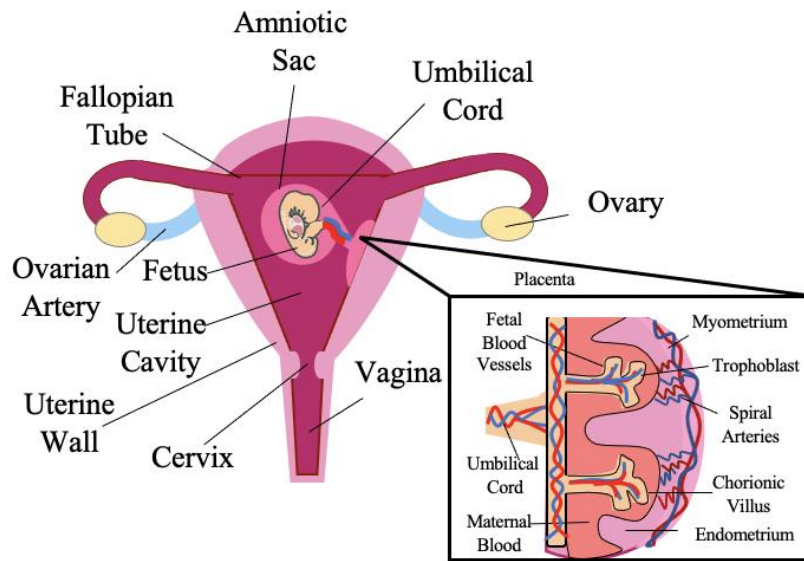


Figure 1.6: The human reproductive anatomy experiences many changes throughout pregnancy, including narrowing of the cervix to protect the fetus, thickening of the uterine walls to prepare for delivery, and the development of the placenta to provide nutrients to the fetus during the second and third trimesters. Parts of the figure were created using modified graphics from Servier Medical Art, provided by Servier, licensed under a Creative Commons Attribution 3.0 Unported License.

The cervix is a narrow canal that connects the lumen on the vagina to the uterine cavity. This structure is made of dense, connective tissue and is approximately 3cm long and 3.5 cm in diameter in non-pregnant people. However, during pregnancy, the cervix remodels itself to prepare for delivery by shortening, softening, and dilating. The remodeling of the cervical extracellular matrix (ECM) is induced by fetal growth to decrease the cervical length and increase cervical tissue volume. During this remodeling process, fibroblasts, smooth muscle cells, and collagen networks are reorganized to decrease tensile strength, increase compliance, and expand the cervix.

Additionally, the epithelial cells that line the cervix help to protect the fetus. These epithelial cells secrete cytokines to activate immune cells and produce mucus to eliminate foreign pathogens. Cervical remodeling plays a significant role in maintain the health of the parent and fetus during pregnancy. If too little cervical remodeling occurs, cervical incompetence can result, often leading to pregnancy loss. Conversely, too much cervical shortening could lead to preterm birth.

The uterus is a hollow, muscular reproductive organ that protects the fetus during development. After conception, the fertilized egg undergoes cell divisions to form a zygote. The zygote undergoes additional cell division to form a blastocyst, which implants on the uterine wall to initiate placental and fetal development. Following implantation, VEGF and angiopoietins induce angiogenesis to facilitate growth of the small uterine arteries during the first trimester. As pregnancy progresses, these proteins support the remodeling of the uterine and placental vessels to increase blood flow to the placenta and nutrient transport to the fetus. Hormones, specifically estrogen and progesterone, also contribute to uterine blood vessel maturation through cellular processes involving vascular contractility, growth, and matrix deposition, although the specific mechanisms are unknown. As the placenta and fetus grow, the uterus increases in size, by approximately 1 cm in diameter per week, and the uterine wall thickens to provide structural support to the fetus. At the time of delivery, the uterus artery diameter has doubled and blood flow to the uterus has increased exponentially in that most of the blood flow (>90%) is directed to the placenta. If the uterine vasculature is not adequately formed or remodeled, pregnancy complications can occur, including preeclampsia and intrauterine growth restriction (IUGR). Additionally, improper uterine formation during pregnancy increases the risk of

fibroids, which are abnormal benign tumors. Fibroid overgrowth is often a result of the increased estrogen levels that enhance the growth of fibroids that were present prior to the onset of pregnancy. Ultimately, fibroid overgrowth can be painful and lead to pregnancy loss in the second trimester.

The placenta is a new organ that develops as the interface between the parent and fetus and its purpose is to facilitate nutrient transport and gas exchange during pregnancy. The placenta is approximately 15-20 cm in diameter, 2-3 cm thick, and has a surface area of almost 15 m<sup>2</sup> at 40 weeks gestation. The basic structural unit of the placenta is the chorionic villus, which differentiates into several layers as pregnancy progresses. The extravillous trophoblasts infiltrate the maternal spiral arteries during the uterine remodeling processes in the first trimester. These cells essentially replace smooth muscle cells to prevent arterial contraction in the uterus. Further, in the first trimester, the extravillous trophoblasts plug the spiral arteries and prevent blood flow, creating a hypoxic environment for the fetus. During this 12-week period, the fetus receives nutrients from the uterine glands. Meanwhile, the villous trophoblasts differentiate into syncytiotrophoblasts, which create a tight barrier between the maternal and fetal circulation and are in direct contact with the maternal blood. At the beginning of the second trimester, the spiral arteries are remodeled and the trophoblasts that initially plugged the spiral arteries are released, allowing maternal blood to enter the placenta. The remodeling of the spiral arteries alters transport of nutrients, cytokines, immune cells, and drugs from the maternal blood to enter the placenta. Although transport of factors is not well understood, it is known that drug concentration, molecular weight, and mechanism contribute to its transport across the placenta.

#### 1.4 Unanswered Questions for Nanomedicine in Maternal/Fetal Health

Researchers in the emerging field of women's health are now investigating new treatment strategies to treat pregnancy conditions. However, there are many physiologic changes occurring during pregnancy, including changes in the uterine anatomy, the growth of a new organ, the placenta, and fetal growth. Together, these changes can impact nanoparticle delivery to the reproductive organs and drug efficacy in treatment and management strategies for pregnancy-related conditions.

Nanoparticle distribution following intravenous administration is largely impacted by the remodeling of the uterus and cervix and growth of the placenta. Considering the gaps in knowledge of drug transport across the placenta, the potential effects of nanoparticle-based therapies on fetal development is also a major ethical concern. In Chapter 2, we synthesize gold nanoparticles and nanoshells and intravenously administer them to pregnant mice at two gestational ages to evaluate nanoparticle biodistribution to the reproductive organs as a function of gestational age and potential short-term effects on fetal growth. To eliminate potential off-target effects from systemic delivery methods, we analyze polymer-based nanoparticle distribution to the maternal organs, placenta, and fetus following vaginal administration in Chapter 3 and evaluate changes in maternal and fetal growth after nanoparticle delivery. In Chapter 4, we demonstrate nanomedicine-based therapies are useful for pregnancy related conditions, specifically BV, by engineering a PLGA nanoparticle system to overcome the CVM barrier and successfully eradicate the most prevalent bacteria in BV, *G. vaginalis*. The work from this thesis will contribute to the field of nanomedicine by providing a fundamental understanding of how to overcome biological barriers to successfully deliver nanoparticles for treating maternal-fetal conditions. Chapter 6

summarizes the implications of these findings and describes future directions to continue the advancement of nanomedicine therapies in maternal-fetal applications.

## Chapter 2

### **GOLD NANOPARTICLE BIODISTRIBUTION IN PREGNANT MICE FOLLOWING INTRAVENOUS ADMINISTRATION VARIES WITH GESTATIONAL AGE**

The work presented in this chapter is adapted from a manuscript published by Irvin-Choy NS\*, Nelson KM\*, Gleghorn JP#, Day ES#. Delivery and short-term maternal and fetal safety of vaginally administered PEG-PLGA nanoparticles. *Drug Delivery and Translational Research*. 2023; <https://doi.org/10.1007/s13346-023-01369-w>. \*co-first authors; #co-corresponding authors.

#### **2.1 Introduction**

Pregnancy complications pose several challenges to the mother and developing fetus as treatments are limited due to many safety and ethical concerns. Preeclampsia<sup>112-114</sup>, fetal growth restriction (FGR)<sup>115-117</sup> and placenta accreta<sup>118,119</sup> are examples of pregnancy-induced conditions that have limited treatments. As pregnancy progresses, symptoms of these diseases worsen leading to detrimental effects for maternal and fetal health. As a result, mothers often need to undergo emergency delivery *via* cesarean section and the newborns face additional morbidities related to their resultant premature birth. These pregnancy-related conditions warrant a dire need for therapeutic advances that can treat conditions that negatively affect maternal and fetal health during pregnancy without harm to the developing baby.

Over the last decade, various nanoparticle (NP)-based carrier systems have been engineered to target a variety of diseases and cancers. It is well established that the ultimate fate of nanocarriers in the body following systemic delivery varies as a function of size, shape, and surface chemistry<sup>10,120</sup>. While researchers have harnessed this knowledge to create powerful systems for the treatment of diseases such as cervical cancer<sup>121,122</sup>, endometriosis<sup>123,124</sup>, and HIV<sup>125,126</sup>, few have explored the potential of nanomedicine to treat pregnancy complications<sup>120,127</sup>. The state of pregnancy introduces additional factors that will influence NP distribution and hence, NP design<sup>120,127</sup>. These factors include the dynamic physiology of the maternal reproductive system<sup>115,128–130</sup>, the transport of nutrients and drugs through the placenta<sup>131,132</sup>, and the development of the fetus<sup>116,133</sup>. Understanding how these variables impact NP distribution is necessary to develop effective treatments that can extend pregnancies to term and advance maternal and fetal health.

To date, many studies examining the distribution of NPs in pregnant mice or rats have utilized gold-based NPs as model carriers due to the ease of controlling their size and surface chemistry, as well as the ability to quantify gold content in tissues with high sensitivity using inductively coupled plasma mass spectrometry (ICP-MS). These studies have indicated that gold NP accumulation in reproductive tissues is size-dependent. For example, when gold nanoparticles (AuNPs) of varying sizes (1.5 nm – 70 nm) were intravenously delivered to pregnant mice, it was determined that only particles less than 10 nm could readily cross the placental barrier and enter the fetal circulation<sup>134</sup>. Another study evaluated AuNPs of 1.4 nm, 18 nm, and 80 nm diameter

in pregnant rats and observed 1.4 nm and 18 nm AuNPs in embryos despite all sizes of AuNPs being present in pooled tissues samples consisting of the placenta, umbilical cord, and amniotic membranes<sup>135</sup>. Together, these findings demonstrate that size plays a critical role in NPs' ability to reach placentas and fetuses following systemic administration<sup>134–137</sup>.

Given that maternal and fetal physiology undergo dynamic changes throughout pregnancy, we wanted to determine whether the biodistribution of gold NPs in pregnant mice is gestation dependent. To investigate this question, we intravenously administered either 15 nm diameter spherical gold NPs (15 nm AuNPs) or 150 nm diameter silica core/gold shell nanoshells (150 nm NSs) to pregnant mice at gestational day (E) 9.5 or 14.5. These gestational ages were selected to represent approximately the second and third trimesters of human pregnancies based on placental development<sup>138</sup>. We did not choose to explore distribution at earlier timepoints because many pregnancy complications are not detected prior to the end of the first trimester, and consequently, nanomedicine-based treatment strategies would likely not be administered until the second or third trimesters. Twenty-four hours after the AuNPs or NSs were delivered *via* tail vein injections, mice were humanely euthanized and the maternal reproductive and non-reproductive tissues collected for both histological analysis and quantitative measurement of gold content by ICP-MS. These assays revealed that the accumulation of both 15 nm AuNPs and 150 nm NSs in placentas and embryos is gestation dependent, with more NPs found in these tissues at E9.5 than E14.5. We also found that both 15 nm AuNPs and 150 nm NSs can

accumulate in these reproductive tissues without altering fetal or placental weight, and they also do not impact the histological appearance of maternal non-reproductive organs. These findings indicate that 15 nm AuNPs and 150 nm NSs have minimal short-term fetal or maternal toxicity, although the safety of these and other nanocarriers should be fully vetted in future studies that include relevant therapeutic cargo in the formulation. Overall, the results obtained from this fundamental study will guide the development of new nanomedicines to improve the treatment of pregnancy complications.

## **2.2 Materials and Methods**

### **2.2.1 Synthesis of 15 nm Diameter Gold Nanoparticles**

AuNPs of 15 nm diameter were synthesized using the Frens method as previously described<sup>139</sup>. Briefly, gold chloride dissolved in deionized water was stirred and heated until boiling. Sodium citrate was added, and the reaction observed for ~15 minutes until the solution became a deep red color. The resultant AuNPs were filtered to remove aggregates then resuspended in water. The AuNPs were passivated by adding 10  $\mu$ M of 5 kDa methoxy-poly (ethylene glycol)-thiol (mPEG-SH) to the AuNP solution while stirring. After stirring for 1 hour, the PEG-coated AuNPs were purified by centrifuging (21,000g x 30 min) the sample to form a pellet and removing unbound mPEG-SH with the supernatant. The purified PEGylated AuNPs were dispersed in sterile phosphate buffered saline (PBS).

### **2.2.2 Synthesis of 150 nm Diameter Nanoshells**

Nanoshells with ~120 nm silica cores and ~15 nm thick gold shells were synthesized by the Oldenburg method<sup>140</sup>. First, 3-4 nm diameter gold colloid formed by the Duff method<sup>141</sup> were combined and reacted with aminated silica spheres (Nanocomposix) and rocked for several days at room temperature to form “seed”. Unreacted gold colloid was removed from the seed by centrifugation (2800 rpm, 25 min) and resuspended in water. The purified seed solution was then combined with a solution of potassium carbonate containing H<sub>2</sub>AuCl<sub>4</sub> and formaldehyde to form complete gold shells. The synthesized silica core/gold shell NSs were purified by centrifugation (500g x 5 min, thrice) and resuspended in water, then 5 kDa mPEG-SH was added to the samples at a final concentration of 10 μM. After reacting overnight at 4°C, the PEG-coated NSs were purified by centrifugation to remove unbound mPEG-SH. Samples were diluted in PBS and stored at 4°C until use.

### **2.2.3 Nanoparticle Characterization**

Transmission electron microscopy (TEM) was used to visualize both AuNPs and NSs after synthesis. TEM samples were prepared by diluting AuNPs or NSs in water to an optical density (OD) of 0.3 or 1, respectively, at their peak plasmon resonance (520 nm for AuNPs; 800 nm for NSs) and placing a drop of sample on poly-l-lysine copper grids. Samples were imaged using a Zeiss Libra 120 Transmission Electron Microscope. The mean diameter of the AuNPs and NSs was determined by measuring the diameter of 20 particles manually in ImageJ.

The extinction spectra (and OD) of the NPs were recorded using a Cary60 UV-visible spectrophotometer, using water as a baseline. For dynamic light scattering and zeta potential measurements, the AuNPs were diluted in water to  $OD^{520nm}=0.3$  and the NSs were diluted in water to  $OD^{800nm}=1$ . Then, the samples were evaluated using an AntonPaar LiteSizer500 instrument. The reported hydrodynamic diameter and zeta potential are the mean and standard deviation of 20 sample measurements.

#### **2.2.4 In Vivo Pregnancy Murine Model**

All mice were maintained, bred, and used in accordance with Animal Use Protocols approved by the Institutional Animal Care and Use Committee at the University of Delaware (AUP #1320 and #1341). Timed-pregnant CD1 mice were bred and separated 12 hours later denoted as E0.5. At E9.5 or E14.5 mice were injected intravenously *via* the tail vein with 0.1  $\mu\text{g Au/g}$  mouse of either AuNPs, NSs, or the equivalent volume of saline. Three pregnant CD-1 mice were used for each treatment group for each gestation, totaling 18 mice for this study. Twenty-four hours post-injection, mice were humanely euthanized. This timepoint was selected for analysis because 24 hours of development results in the transition to a new Theiler Stage so it would be undesirable to examine distribution and effects on fetal growth at circulation times longer than this; additionally, most AuNPs or NSs should have reached their ultimate fate by twenty-four hours post injection. Maternal blood and nonreproductive organs (liver, kidney, spleen, heart, and lung) and embryos and

placentas were excised for each mouse and used for either histology or ICP-MS (discussed below). For reproductive organ analyses, two embryos (one proximal and distal to the maternal head) and their respective placentas were excised from each mouse, totaling 36 embryos and 36 placentas.

#### **2.2.5 Quantification of Gold Content in Tissues by ICP-MS**

Excised organs were weighed then lyophilized overnight to remove water content. Tissues were digested in 1 ml of 3% hydrochloric acid in nitric acid and heated to 60°C for 30 minutes or until completely dissolved. The digested tissue samples and standards of known gold concentration (prepared using TraceCERT® gold standard) were then diluted in a matrix containing 2% nitric acid and 2% hydrochloric acid. The gold content in each tissue sample and standard curve sample was analyzed on an Agilent 7500c ICP-MS instrument.

#### **2.2.6 Qualitative Evaluation of NP Presence in Tissues by Silver Staining**

Whole embryos and placentas and sections of maternal liver, spleen, kidneys, and lungs were excised from the pregnant mice at E10.5 or E15.5 and were fixed in 4% paraformaldehyde for 72 hours and washed in 70% ethanol twice prior to overnight processing. Processed paraffin samples were embedded and sectioned into 5-micron slices. Silver staining, which amplifies the size of NPs *via* deposition of silver on gold, was performed on embryos, placentas, livers and spleens to enable NP

visualization by optical microscopy. Briefly, the tissue sections were deparaffinized in xylene (10 min) and hydrated through a series of ethanol (100%, 90%, 70%) and water. Silver stain (Cytodiagnostics Silver Enhancer Kit) was incubated on the slides at room temperature for 10 minutes. The samples were then rinsed and counterstained with Hematoxylin and Eosin. Finally, samples were dehydrated and mounted with xylene based mounting media and imaged using a Zeiss Axioobserver microscope. Maternal kidneys and lung sections were only stained with Hematoxylin and Eosin to examine general morphology.

## 2.3 Results

### 2.3.1 Nanoparticle Characterization

AuNPs (15 nm diameter) and NSs (150 nm diameter) passivated with 5 kDa mPEG-SH as described in the Methods were characterized for their hydrodynamic diameter, zeta potential, and morphology using UV-visible spectrophotometry, dynamic light scattering (DLS), and transmission electron microscopy (TEM). Spectrophotometry revealed that the AuNPs had a peak plasmon resonance at ~520 nm (not shown), consistent with the extinction properties of 15 nm diameter AuNPs<sup>142</sup>. Similarly, the NSs had peak plasmon resonance at ~800 nm (not shown), consistent with the extinction features of NSs with 120 nm diameter silica cores and 15 nm thick gold shells<sup>143</sup>. DLS measurements indicated that uncoated AuNPs had a hydrodynamic diameter of  $23 \pm 8$  nm and a zeta potential of  $-23 \pm 5$  mV (**Figure**

**2.1A, B).** Following PEGylation, the AuNPs' hydrodynamic diameter increased to  $40 \pm 7$  nm and their zeta potential increased to  $-4.5 \pm 3$  mV. Since hydrodynamic diameters measured by DLS are typically larger than physical nanoparticle dimensions, the PEGylated AuNPs were further examined by TEM, which indicated the mean particle diameter was  $14 \pm 1$  nm (**Figure 2.1C**). NSs were characterized similarly and found to have a hydrodynamic diameter of  $150 \pm 2$  nm before PEG addition and  $176 \pm 4$  nm after PEG addition (**Figure 2.1D**). The NSs' zeta potential was  $-40 \pm 0.4$  mV and  $-3 \pm 2$  mV before and after PEGylation, respectively (**Figure 2.1E**), and TEM measurements showed the PEG-coated NSs had a mean diameter of  $151 \pm 13$  nm (**Figure 2.1F**)

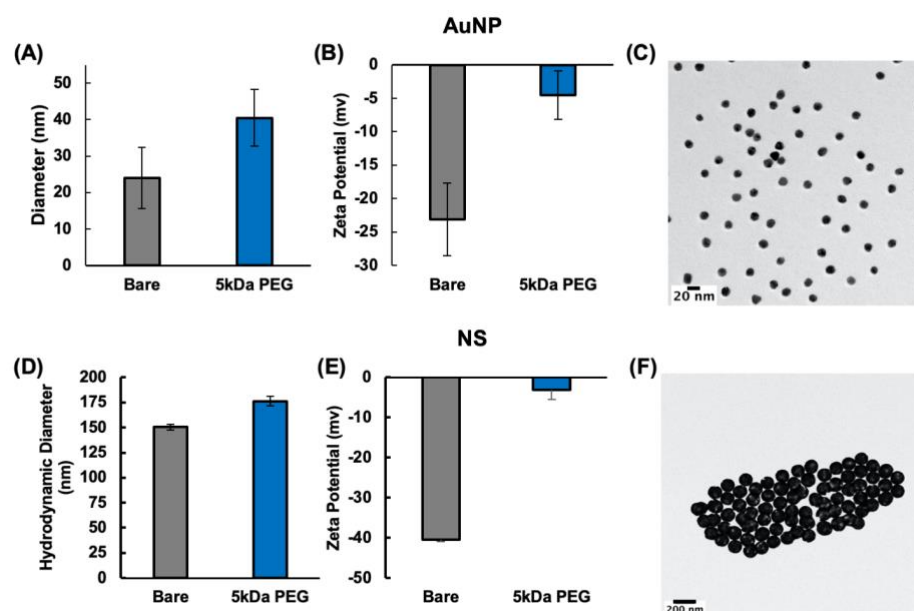


Figure 2.1: Nanoparticle characterization. (A) Hydrodynamic diameter and (B) zeta potential of AuNPs before and after PEGylation. (C) Electron micrograph of AuNPs. (D) Hydrodynamic diameter and (E) zeta potential of NSs before and after PEGylation. (F) Electron micrograph of NSs. Data in (A,B,D,E) are mean +/- standard deviation.

### **2.3.2 PEG-Coated 15 nm AuNPs 150 nm NSs Exhibit More Accumulation in Placentas and Embryos When Administered at E9.5 than at E14.5**

After characterizing the NPs, we sought to examine the gestational differences in their distribution to placentas and embryos following intravenous delivery. We injected 15 nm PEG-coated AuNPs, 150 nm PEG-coated NSs, or saline at doses of 0.1  $\mu\text{g Au/g}$  mouse into pregnant CD1 mice at E9.5 or E14.5 *via* the tail vein. Twenty-four hours later, the reproductive and major non-reproductive tissues of the mothers were excised and processed for either histological examination or quantification of gold content by ICP-MS. The ICP-MS data showed that both 15 nm AuNPs and 150 nm NSs coated in PEG accumulate to a greater extent in placentas than embryos at both E9.5 and E14.5 (**Figure 2.2A, B**). There is a notable decrease in the number of nanoparticles in the tissues at E14.5 relative to E9.5, indicating that particle distribution to reproductive organs is gestation-dependent (**Figure 2.2A, B**).

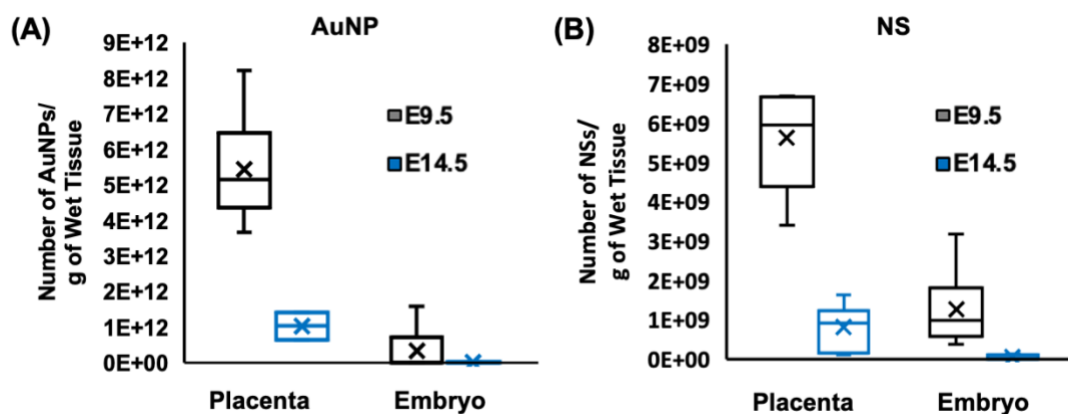


Figure 2.2: Nanoparticle distribution to placentas and embryos determined by ICP-MS. Analysis of gold content in placentas and embryos of dams that received intravenous injections of (A) 15 nm diameter AuNPs or (B) 150 nm diameter NSs on E9.5 or E14.5. Gold content in tissues was measured one day post-NP administration.

The gold content in the placentas and embryos was further evaluated by histological examination of silver-stained tissue sections to corroborate the ICP-MS results. Silver stain nucleates on the surface of gold-based NPs to enable their visualization by light microscopy. Both 15 nm AuNPs and 150 nm NSs were observed in E9.5 placentas, but fewer AuNPs and NSs were observed in placentas at E14.5 (**Figure 2.3A, Figure 2.4A, particle location indicated by white arrows**). These data confirm the quantitative ICP-MS results (**Figure 2.2**) that indicated NP accumulation in placentas is gestation dependent. Within embryos, neither AuNP nor NS presence was distinct in the silver-stained tissue sections at either gestation (**Figure 2.3B, Figure 2.4B**), in agreement with the ICP-MS results that showed both types of particles accumulate to a lesser degree in embryos than placentas. The

increased sensitivity of ICP-MS relative to silver staining likely explains why we could identify particles in the embryos by ICP-MS but not by silver staining.

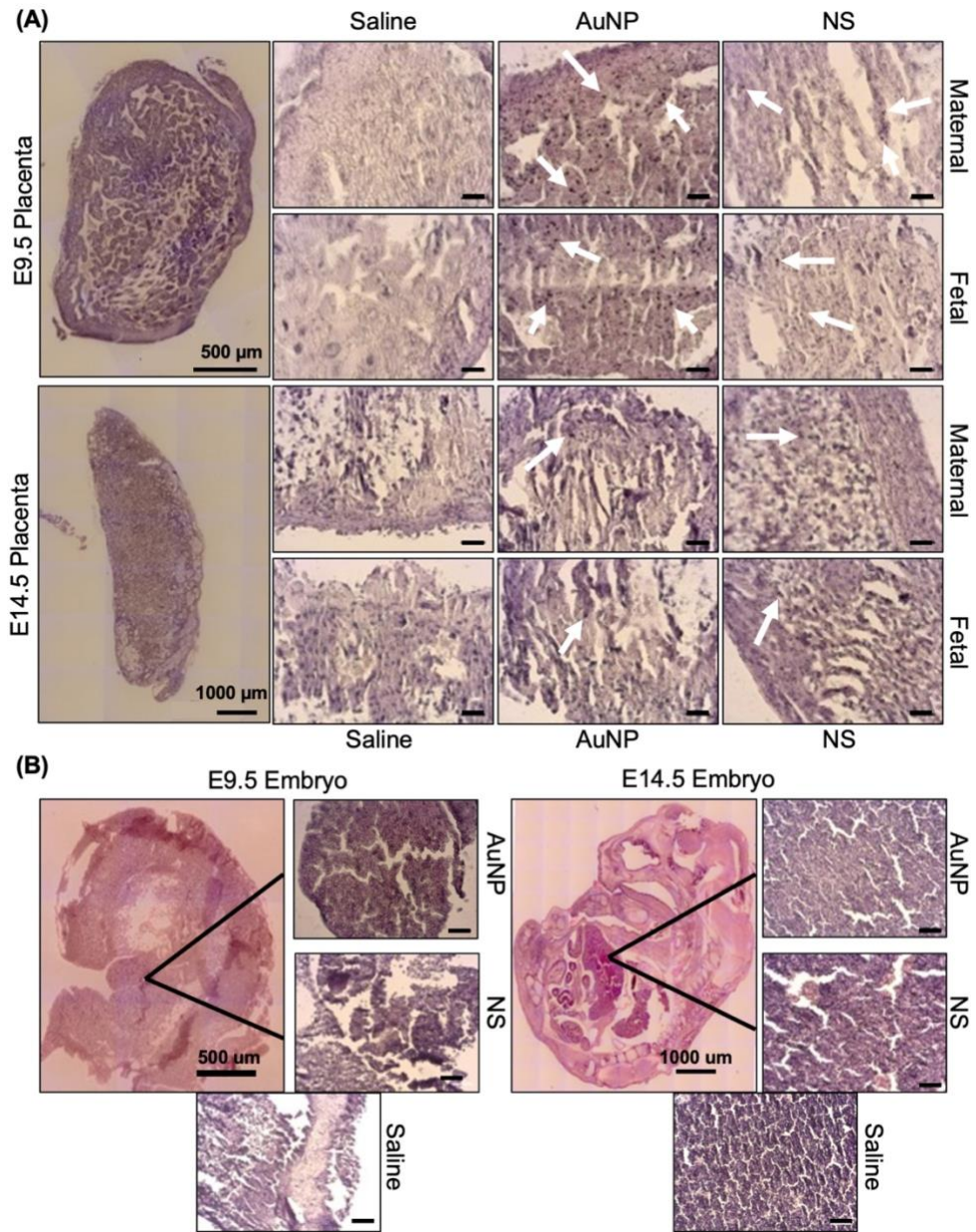


Figure 2.3: Histological examination of NP distribution to placentas and embryos one day post administration to dams at E9.5 or E14.5. Tissues were silver stained to enable visualization of AuNPs and NSs. (A) Images of placentas from dams treated with saline, AuNPs, or NSs. White arrows indicate representative NPs along the maternal or fetal sides of the placenta. Scale bars = 20 μm. (B) Images of embryos from dams treated with saline or NPs at E9.5 or E14.5. Insets depict lower abdomen area. Scale bars = 20 μm.

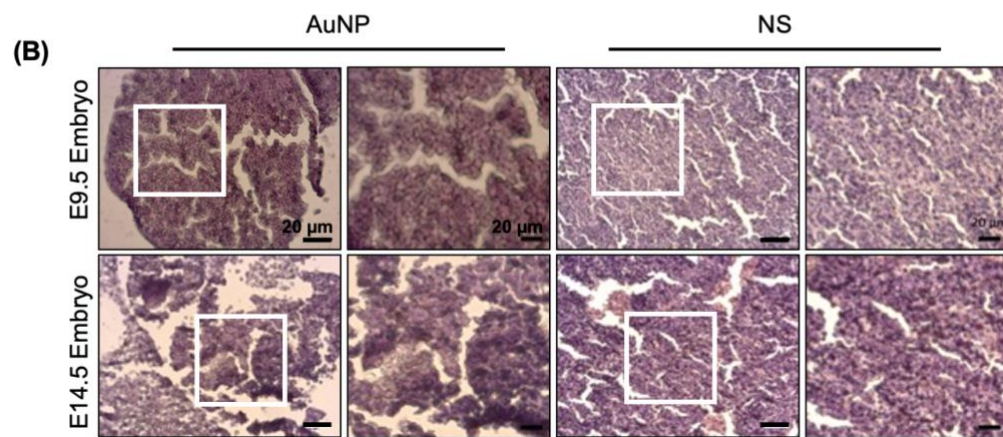
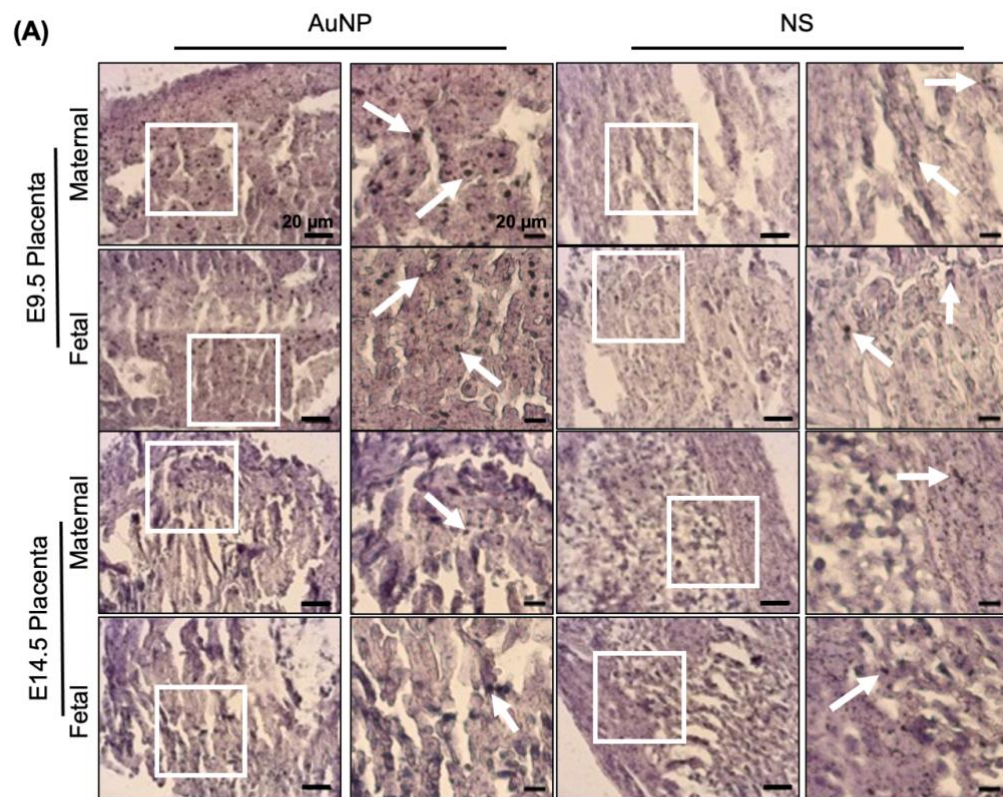


Figure 2.4: Nanoparticle biodistribution to maternal non-reproductive organs. (A,B) Number of NPs in non-reproductive organs of pregnant mice that were injected with AuNPs (A) or NSs (B) at E9.5 or E14.5, based on ICP-MS analysis of gold content measured one-day post intravenous administration of the NPs. Graphs in (A) and (B) are mean  $\pm$  standard error, with individual data points shown as circles. (C) Silver stained sections of liver and spleen from dams treated with saline, AuNPs, or NSs. White arrows point to representative NP locations. Scale bars = 20  $\mu$ m.

We also investigated if AuNP or NS accumulation in embryos is a function of embryo location in the uterus. Murine ovarian and uterine arteries supply blood and nutrients to placentas, and therefore, embryos at different positions in the uterus (**Figure 2.5A**). To investigate whether spatial differences exist in NP accumulation in embryos, we excised embryos and their respective placentas from the proximal (closest to ovary) or distal (closest to cervix) ends of the uterine horn and analyzed gold content in these tissues separately by ICP-MS. These two embryo positions were chosen as they represent both extremes of blood supply to the uterus; the ovarian artery supplies blood to the proximal embryos first, while the uterine artery supplies blood to the distal arteries first<sup>144</sup>. There was no significant difference in gold content between proximal and distal placentas or embryos at either gestational age for either NP type (**Figure 2.5B, C**). This result is different than originally expected as a previous study in which researchers clamped the uterine or ovarian arteries in mice to reduce perfusion to the gravid uterus showed that the uterine arteries appeared to be more important for survival of embryos than the ovarian arteries<sup>145</sup>. Therefore, we expected distal embryos and placentas would have more gold content than proximal

embryos and placentas. However, multiple studies have shown that the middle embryos are supplied with the least oxygen rich blood<sup>146–148</sup> compared to the distal and proximal embryos. Accordingly, while the distal and proximal embryos and placentas may have the same gold content due to their location at the blood supply entry points, as we have shown, the middle embryos may have less gold content. Future work should sample the proximal, distal, and middle embryos and placentas to test this hypothesis.

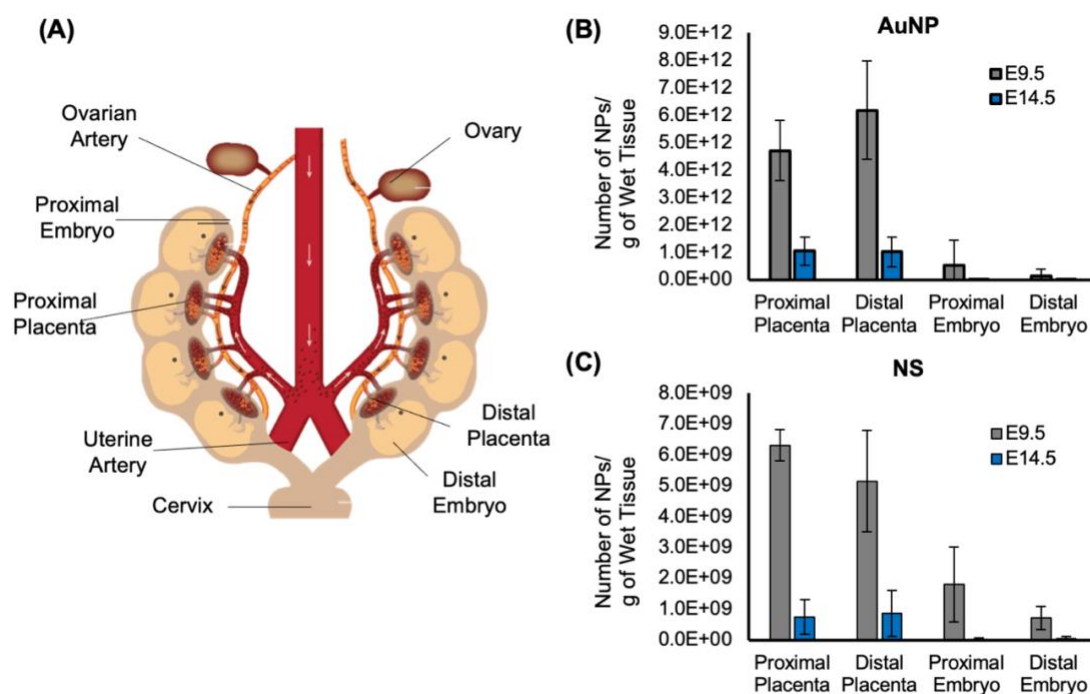


Figure 2.5: NP distribution to placentas and embryos by location in uterus. (A) Schematic of pregnant mouse uterus. Image reproduced with permission from Raz T, et al. *PLoS ONE*. 2012; 7(12): e52273 under a Creative Commons Attribution License. Number of (B) 15 nm AuNPs and (C) 150 nm NSs in proximal and distal embryos and placentas at E9.5 and E14.5 as determined by ICP-MS analysis of gold content in tissues.

### 2.3.3 15 nm AuNPs and 150 NSs Both Have Minimal Effect on Fetal Growth

To determine whether the intravenously administered AuNPs or NSs impacted fetal growth in pregnant mice, we compared the weight of embryos and placentas that were excised from pregnant mice 24 hours post-NP administration to those obtained from pregnant mice treated with saline. A 24-hour time point was chosen to ensure embryo development was not altered as 24 hours of development results in the transition into a new Theiler Stage. The embryo to placenta weight ratio (E:P), a measurement of placental efficiency, was calculated for each treatment group. An E:P ratio greater than 1, especially at late gestation, indicates efficient placental function leading to adequate fetal growth<sup>148,149</sup>. Embryos from dams treated with 15 nm PEG-coated AuNPs did not display any significant changes in E:P or mean weight when compared to saline at either gestational age (**Figure 2.6A, B**). Likewise, 150 nm PEG-coated NSs did not alter E:P or embryo weight at E9.5 compared to dams treated with saline, and there was no difference in E:P at E14.5 for dams treated with NSs or saline (**Figure 2.6C, D**). At E14.5, the embryo weights from dams treated with NSs were significantly higher than those treated with saline (**Figure 2.6D**). We attribute this difference to physiologic variability as the E:P ratio for NSs at E14.5 is greater than 1, indicating adequate fetal growth, and is not significantly different from that of the saline control. In aggregate, these results indicate that neither PEG-coated AuNPs nor NSs disrupt fetal growth within 24 hours of administration to pregnant mice.

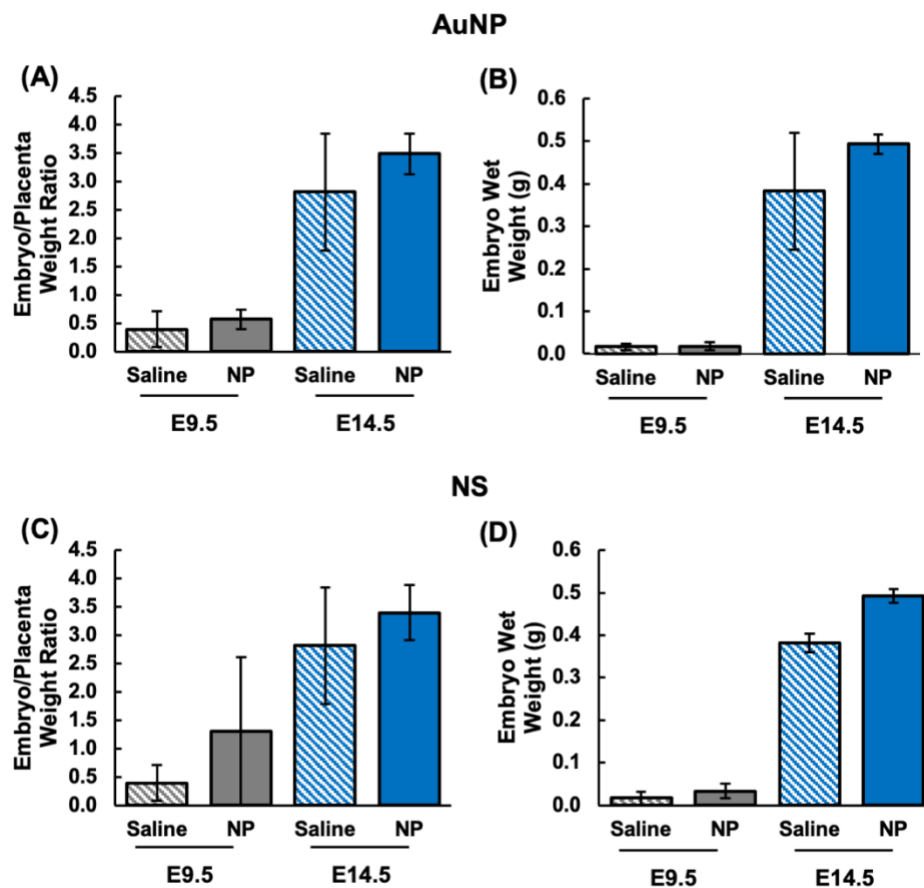


Figure 2.6: Analysis of embryo and placenta weight as a measure of NP safety. (A) Ratio of embryo weight to placenta weight in dams administered 15 nm AuNPs. (B) Embryo weights 24 hours post 15 nm AuNP injection in pregnant mice. (C) Ratio of embryo weight to placenta weight in dams one day after 150 nm NS administration. (D) Embryo weights in NS-treated mice 24 hours post injection. Data are mean  $\pm$  standard deviation. No significant differences were found between saline or NP-treated mice when analyzing E:P ratio or embryo weight by t-test.

## 2.4 Nanoparticle Distribution to Maternal Non-Reproductive Organs in Not Gestation Dependent

Given our finding that AuNP and NS accumulation in placentas and embryos is gestation dependent, we wanted to examine if their accumulation in maternal non-

reproductive organs is also gestation dependent. Therefore, we excised maternal organs (lungs, liver, kidney, spleen, heart, and blood) 24 hours post-intravenous delivery of the AuNPs or NSs for analysis of gold content by ICP-MS. Analysis revealed that 15 nm AuNPs exhibit the highest accumulation in liver and spleen of pregnant mice, with no significant difference in accumulation observed for any organ tested between E9.5 and E14.5 (**Figure 2.7A**). Tissues excised from the dams treated with 150 nm NSs displayed similar findings, with most NSs found in the liver and spleen, and no differences in accumulation identified as a function of gestation (**Figure 2.7B**). These data indicate that, independent of NP size or maternal gestation, most AuNPs and NSs are filtered by the liver and spleen. The liver functions to metabolize material in blood so it is not surprising that a large portion of the NPs accumulate there. Silver staining of histological sections of the liver and spleen corroborated the ICP-MS results. Both 15 nm AuNPs and 150 nm NSs were observed in the maternal liver and spleen at both gestations while tissue morphology appeared similar to that of the saline-treated mice (**Figure 2.7C, Figure 2.8, representative NPs indicated by white arrows**). It should be noted that maternal blood volume increases at later gestations, so although the density of AuNPs or NSs in blood is similar between E9.5 and E14.5 mice, the total amount of NPs in blood is likely greater at E14.5; future work should confirm this experimentally by measuring total blood volume and gold content at each gestation.

Our data show that PEG-coated AuNPs and NSs intravenously administered at E9.5 and E14.5 accumulate primarily in the liver and spleen at both gestational ages.

These results agree with other studies that have assessed NP distribution to major non-reproductive organs at different stages of pregnancy (E5.5-13.5). For example, one study found that there were no differences in the distribution of gold NPs ranging from 1.5 nm to 70 nm in diameter to major organs (liver, spleen, kidney, lung and heart) in pregnant (E9.5) and non-pregnant mice<sup>134</sup>. In this study, the lung was found to be a site of high accumulation, while specific biodistribution data for the spleen was not included<sup>134</sup>. This data, coupled with our results, indicates that NP accumulation in non-reproductive organs is not gestation dependent.

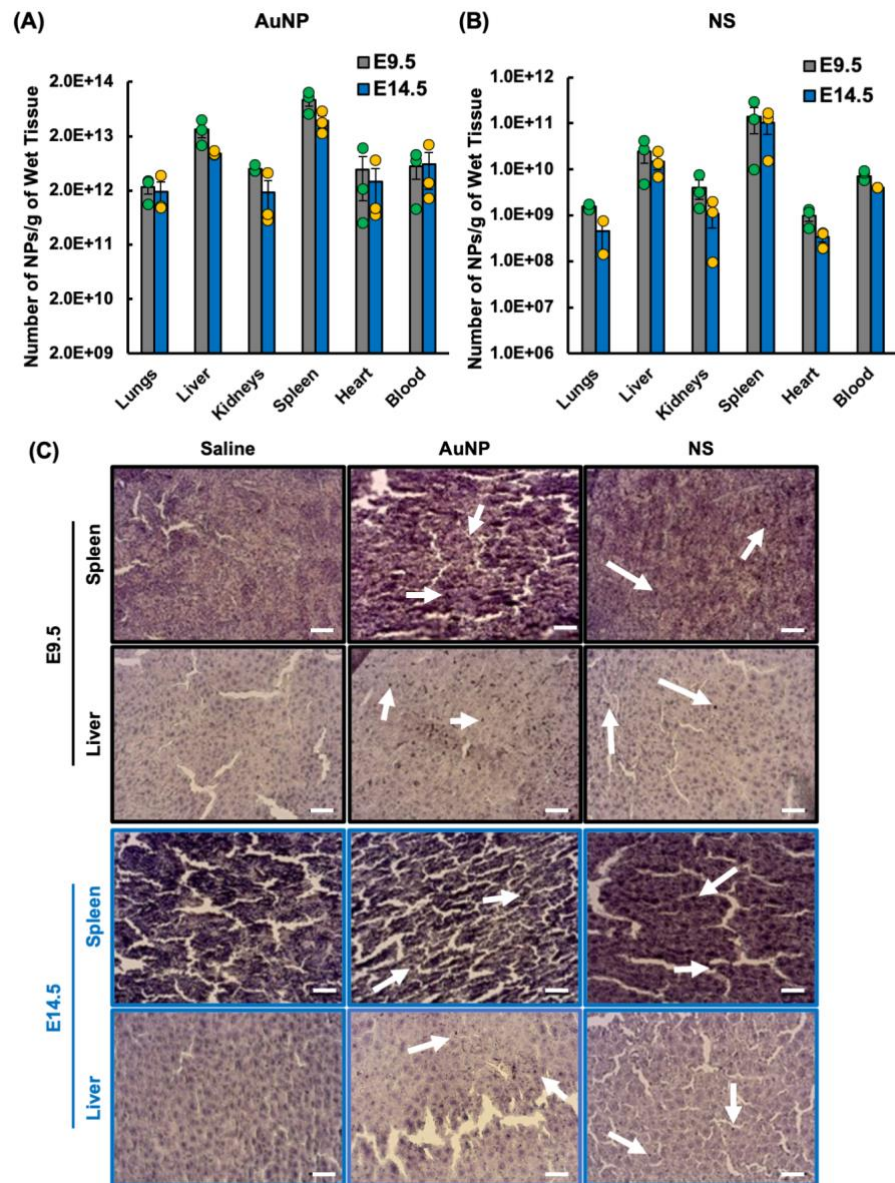


Figure 2.7: Nanoparticle biodistribution to maternal non-reproductive organs. (A,B) Number of NPs in non-reproductive organs of pregnant mice that were injected with AuNPs (A) or NSs (B) at E9.5 or E14.5, based on ICP-MS analysis of gold content measured one-day post intravenous administration of the NPs. Graphs in (A) and (B) are mean  $\pm$  standard error, with individual data points shown as circles. (C) Silver stained sections of liver and spleen from dams treated with saline, AuNPs, or NSs. White arrows point to representative NP locations. Scale bars = 20  $\mu$ m.

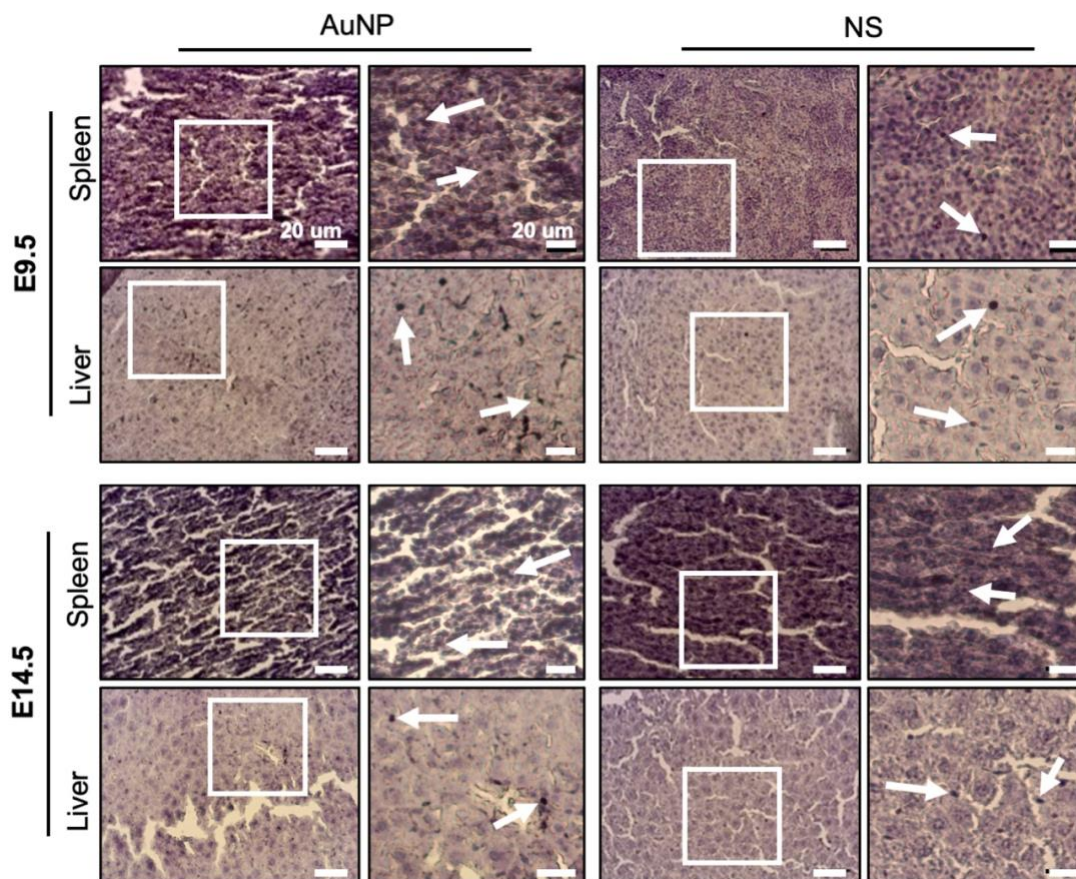


Figure 2.8: Silver-stained sections of livers and spleens from pregnant mice treated with AuNPs or NSs. White boxes indicate area of interest that is shown in magnified view to the right. White arrows point to representative AuNPs or NSs. These images provide additional fields of view and magnifications to supplement the data presented in Figure 5. Scale bar = 20  $\mu\text{m}$ .

## 2.5 Discussion

The results of this study show that intravenously administered AuNPs and NSs can minimally accumulate in the placenta and embryo during murine pregnancy, with greater amounts of NPs distributing to the maternal liver and spleen. At both E9.5 and

E14.5, more AuNPs and NSs were found in the placenta than in the embryo, and the levels of gold in these tissues decreased at E14.5 compared to E9.5, indicating that NP distribution to placentas and embryos is gestation dependent. The apparent decrease in the number of NPs/g of wet tissue at E14.5 compared to E9.5 may be attributed in part to increases in placenta and embryo weight at later gestations, as well as to altered transport mechanisms as discussed below. Importantly, the presence of the AuNPs or NSs in the body did not impact fetal development based on analysis of placental weight and embryo weight. This suggests that intravenously administered nanomedicines may be a viable treatment option for pregnancy complications in the future.

The finding that both 15 nm AuNPs and 150 nm NSs coated with PEG accumulate in the placenta and fetus to a greater extent at E9.5 than at E14.5 aligns with prior work that evaluated the distribution of 13 nm AuNPs coated with PEG five hours post-intravenous delivery to pregnant mice at different gestations (E5.5-E15.5)<sup>150</sup>. This study showed that PEG-coated AuNPs accumulated in fetal tissues, but fetal gold concentration decreased significantly after E11.5<sup>150</sup>. Our study corroborates this result and shows that a similar trend exists for larger PEG-coated NSs. We suspect dynamic changes in transplacental transport mechanisms are responsible for gestational differences in NP accumulation in placentas and fetuses. Transplacental transport can occur by active and passive mechanisms, with NPs trafficking through or between the cells that comprise the barrier. *In vitro* transport studies have shown that NPs may be taken up by placental syncytiotrophoblasts through phagocytosis, clatherin-

mediated endocytosis, caveolae-mediated endocytosis, or macropinocytosis<sup>151-155</sup>. After uptake, NPs typically exploit vesicular transport to transcytose across trophoblasts, although some cationic NPs may fuse directly with the basal membrane to escape the cell<sup>151,156</sup>. After crossing the trophoblast layer, NPs must diffuse through the villous stroma and pass-through endothelial cell walls (again, by passive or active mechanisms) to enter fetal circulation<sup>156</sup>. We hypothesize that these transport mechanisms may be differentially regulated throughout gestation. Indeed, several cell membrane nutrient transporters such as cholesterol transporter SR-B1<sup>157</sup> and glucose transporter GLUT4<sup>158</sup> have been noted previously to be differentially expressed over gestation. Therefore, it is reasonable to surmise that endocytosis mechanisms change with advancing gestation as well. In addition, placental architecture and development dramatically change over gestation and as such, the trophoblast tissue layer may have increased permeability between cells at earlier rather than at later stages. Overall, transplacental transport and the mechanisms involved with that process are complex, metabolite/item specific, and not well understood over different phases of placental development. Further study into the mechanism behind AuNP and NS gestational dependent transplacental transport properties are needed.

To bypass high amounts of hepatic clearance, local delivery routes (i.e., vaginal administration) should be investigated in the future to increase NP accumulation in reproductive organs. These studies should also be performed at various gestational ages since the properties of cervicovaginal mucus, a major barrier to vaginal drug delivery, are known to change throughout pregnancy<sup>103,106,107,159</sup>.

Safety studies should also be completed to ensure NP delivery does not induce toxicity; analyses could include histological evaluation, examination of fetal development, and assessment of pup cognitive function and behavior. Future work should also investigate NP material and surface coatings as factors that can affect delivery, as the results presented here only apply to gold-based NPs coated with PEG with diameters of 15 nm or 150 nm. Finally, mechanistic transplacental transport studies are needed to better understand how NPs cross the placenta. This information would allow researchers to better engineer NPs with reduced transplacental transport and increased fetal safety. Overall, the work presented here lays the foundation for additional studies of NP-based drug delivery for the advancement of maternal and fetal health during pregnancy.

## Chapter 3

### DELIVERY AND SHORT TERM MATERNAL AND FETAL SAFETY OF VAGINALLY ADMINISTERED PEG-PLGA NANOPARTICLES

The work presented in this chapter is adapted from a manuscript published in by Irvin-Choy NS\*, Nelson KM,\* Dang MN, Gleghorn JP#, Day ES#. Gold nanoparticle biodistribution in pregnant mice following intravenous administration varies with gestational age. *Nanomedicine: Nanotechnology, Biology, and Medicine*. 2021; 36: 102412. \*co-first authors; #co-corresponding authors.

#### 3.1 Introduction

Preexisting and newly emergent conditions affecting pregnant people are challenging to manage due to the limited availability of treatments with confirmed fetal and maternal safety. Without intervention, conditions including cervical cancer<sup>121,122</sup>, HIV<sup>126,160</sup>, endometriosis<sup>123,161</sup>, and bacterial vaginosis (BV)<sup>93,95</sup> may exacerbate pregnancy challenges. Consequently, pregnant people with these and other high-risk conditions face the difficult decision to terminate the pregnancy or risk their and the unborn baby's health by foregoing treatment for the duration of the pregnancy. These patients desperately need new treatment options that will not harm themselves or the developing fetus.

Nanoparticle (NP)-based carrier systems have emerged as effective tools for treating many diseases (e.g., cancers, COVID-19, wound healing) over the last decade. Prior advancements in nanomedicine have established that NP size, shape, and surface charge

dictate biodistribution following systemic delivery <sup>120,162–164</sup>. Although researchers have applied this knowledge to treating cervical cancer <sup>121,122</sup>, HIV <sup>126,160</sup>, endometriosis <sup>123,161</sup>, and BV <sup>95</sup> in non-pregnant conditions, it remains to be established how NP treatment systems can be used for maternal-fetal health applications during pregnancy. However, maternal-fetal nanomedicine is quickly growing <sup>120,127,165,166</sup>, with a few recent studies investigating the biodistribution and safety of NPs in pregnant murine models following systemic delivery <sup>134,150,167</sup>. One study found that gold nanoparticles (AuNPs) less than 10 nm in diameter could enter fetal circulation post intravenous (IV) administration <sup>134</sup>. Another study determined that both 15 nm diameter AuNPs and 150 nm diameter gold nanoshells could distribute to the placentas following IV delivery, with less accumulation observed when the NPs were administered at later gestational ages <sup>167</sup>. These studies have demonstrated a lack of short-term toxicity due to the presence of the NPs, supporting the potential use of nanomedicine to treat maternal-fetal health conditions.

To develop locally applied nanomedicine therapy for conditions affecting the vagina during pregnancy, it is essential to understand the distribution and safety of NPs following vaginal administration. The aforementioned studies indicated that IV administered NPs could reach placentas and embryos in pregnant mice despite a majority of systemic NPs being filtered out of circulation by the mononuclear phagocyte system (MPS) <sup>168,169</sup>. Systemic clearance by the MPS limits the number of NPs reaching the target tissue and increases the risk of off-target effects. Delivering NP treatments locally, directly to the tissue of interest, may help avoid these limitations to improve the management of vaginal disorders during pregnancy.

A significant challenge associated with vaginal delivery of therapeutics is the cervicovaginal mucus (CVM) barrier. CVM is a gel-like fluid comprised of glycoproteins that

lines the vaginal epithelium. This fibrous network traps foreign antigens, viruses, and bacteria, preventing them from ascending the reproductive tract into the uterus<sup>100,107</sup>. Previously, researchers have used neutralizing surface coatings, such as poly(ethylene glycol) (PEG), to minimize electrostatic interactions between NPs and CVM and thereby increase NP penetration through CVM<sup>110,170,171</sup>. Conversely, mucoadhesive coatings like chitosan have also been explored to increase NP retention in the vagina<sup>111,121,172</sup>. CVM viscosity and production increase over the course of pregnancy in response to hormonal changes, leading to decreased pore sizes in the fibrous networks<sup>100,107</sup>, which likely alters NP transport through the mucus.

Given the physiological changes of CVM during pregnancy, we evaluated the biodistribution of PEG-poly(lactic-co-glycolic acid) (PEG-PLGA) copolymer NPs following vaginal delivery in pregnant mice at two different gestational ages. PEG-PLGA NPs were used in this study because PLGA is a Food and Drug Administration-approved, hydrolytically degradable polymer that can encapsulate diverse types of cargo and can be easily modified with PEG to support CVM penetration. We vaginally delivered saline or PEG-PLGA NPs loaded with DiD fluorophores (DiD-PEG-PLGA NPs) to pregnant mice at gestational day (E)14.5 or E17.5 corresponding to early and late time points in the third trimester of human pregnancy, respectively. We also administered Cy5 labeled PEG-PLGA NPs (Cy5-PEG-PLGA-NPs) to separate mice at gestational age E17.5 to evaluate polymer distribution following vaginal administration. Immediately after NP or saline administration, the mice were fluorescently imaged with an *in vivo imaging system* (IVIS) to confirm successful injection. Twenty-four hours later, whole-body images were taken, and the major maternal and reproductive organs were excised and analyzed by IVIS and cryo-histology. These experiments revealed that DiD cargo was retained only in the vagina and did not distribute to

other organs within 24 hours of injection, whereas Cy5-labeled PLGA was observed in the vagina, placentas, and embryos. There were no significant differences in DiD signal in the vagina between gestational ages, indicating cargo biodistribution is not dependent on gestational age when vaginally delivered to pregnant mice. Importantly, vaginally administered NPs displayed no short-term effects on maternal and fetal growth and safety; however, future studies should more extensively investigate the long-term fetal effects of PEG-PLGA NPs and their efficacy as a treatment when loaded with therapeutic molecules. Overall, these findings indicate the potential for PEG-PLGA NPs in treating maternal conditions affecting vaginal health during pregnancy.

## **3.2 Materials and Methods**

### **3.2.1 Synthesis of DiD-Loaded PEG-PLGA NPs**

DiD-loaded PEG-PLGA NPs were synthesized by a single emulsification method. First, 50:50 PLGA (32 kDa) was dissolved in acetone at 1 mg/mL. Next, PEG (5 kDa)-PLGA (30 kDa) was dissolved in dichloromethane (DCM) at 1 mg/mL and then added at a 1:3 volumetric ratio to the PLGA/acetone solution. Fluorescent DiD was dissolved in dimethyl sulfoxide (DMSO) at 9 mM, and 0.5-3  $\mu$ L of this solution was added to the PLGA/PEG-PLGA solution. Lastly, the PLGA/PEG-PLGA/DiD solution was added dropwise to 0.2% polyvinyl alcohol (PVA) in MilliQ H<sub>2</sub>O at a 3:1 volumetric ratio. NPs were magnetically stirred for two hours at 800 rpm to allow solvent evaporation, then centrifuge filtered with 50 kDa molecular weight cutoff (MWCO) conical filter tubes for 25 minutes at 4200 rpm. The DiD-PEG-PLGA NPs were resuspended in 3 mL of MilliQ H<sub>2</sub>O and centrifuged a second time for 30 mins or until most of the water was removed. NPs were then diluted in phosphate-

buffered saline (PBS) to a fluorescent value of at least 10,000 (measured by reading 100  $\mu$ L of sample in a 96-well plate on a BioTek Synergy H1M plate reader with excitation/emission of 640 nm/670 nm) and transferred to Eppendorf tubes for a maximum of 2 hours before being delivered to mice.

After synthesis, an alternative filtration method was used to remove additional DiD from NP samples. Following the initial centrifugation in 50 kDa MWCO conical filters for 25 mins, NPs were resuspended in 500  $\mu$ L of 0.5% Triton X-100 to disrupt any DiD micelles that may have formed during synthesis. Subsequently, the NPs were centrifuge filtered in 50 kDa MWCO conical filters for 15 mins at 4200 rpm. NP washes were performed three times by resuspending NPs in 2 mL of MilliQ H<sub>2</sub>O between each centrifugal filtration step.

### **3.2.2 Synthesis of Cy5-PEG-PLGA NPs**

Cy5-PEG-PLGA NPs were synthesized also using a single emulsification method. First, Cy5-PLGA and PLGA (32 kDa) were dissolved in acetone in separate scintillation vials at 1 mg/mL concentrations. PEG (5 kDa)-PLGA (30 kDa) was dissolved in DCM at 1 mg/mL and 250  $\mu$ L of this solution was transferred to a clean Eppendorf tube. Next, 650  $\mu$ L of the PLGA/acetone solution and 100  $\mu$ L of the Cy5-PLGA/acetone solution were transferred to the Eppendorf tube already containing the PEG-PLGA/DCM solution for a total of 1 mL of solution. The Cy5-PLGA/PLGA/PEG-PLGA solution was then added dropwise to 3 mL of 0.2% PVA in MilliQ H<sub>2</sub>O while magnetically stirring at 800 rpm. NPs were covered with aluminum foil and stirred overnight. Following stirring, Cy5-PEG-PLGA NPs were centrifuge filtered in 100 kDa MWCO filters for 25 minutes at 4,200 rpm and 14°C. The Cy5-PEG-PLGA NPs were resuspended in 3 mL of MilliQ H<sub>2</sub>O then centrifuge filtered a second time

for 30 minutes at 4,200 rpm and 14°C. To prepare NPs for mouse injections, the fluorescence of 100 µL of Cy5-PEG-PLGA NPs was measured using a BioTek Syngery H1M plate reader at excitation/emission wavelengths of 640/670 nm and then diluted in PBS to a fluorescent value of 10,000. Cy5-PEG-PLGA NPs were stored in dark Eppendorf tubes at 4°C for a maximum of 2 hours before use.

### **3.2.3 Nanoparticle Characterization**

Following synthesis, DiD-PEG-PLGA NPs and Cy5-PEG-PLGA NPs were characterized by dynamic light scattering (DLS) and zeta potential measurements on a Litesizer500 instrument (Anton Paar). To prepare NP samples, 5-10 µL of NPs were diluted in 1 mL of MilliQ H<sub>2</sub>O in disposable or Omega cuvettes (Anton Parr) for DLS or zeta potential measurements, respectively. The reported intensity-based hydrodynamic diameter and the mean zeta potential are the averages of three DLS experiments. NP diameter and morphology were also evaluated by transmission electronic microscopy (TEM). TEM grids were stained with 2% uranyl acetate, dried, and examined with a Zeiss Libra 120 Transmission Electron Microscope.

### **3.2.4 Evaluation of DiD Encapsulation and Release from PEG-PLGA NPs**

DiD loading in PEG-PLGA NPs was determined by dissolving fully synthesized NPs in DMSO and measuring the resulting fluorescence. Purified DiD-PEG-PLGA NPs were dissolved in 500 µL of DMSO and placed on a rocker at room temperature for 30 minutes. Next, the solution of dissolved NPs and previously encapsulated DiD was centrifuged at 14,000 rpm for 30 minutes to separate the DiD from pelleted PEG-PLGA fragments. Following centrifugation, the fluorescence of the supernatant was measured in a Synergy H1

plate reader at an excitation/emission of 640/670 nm, respectively. All samples were compared to a standard curve of known DiD concentrations to calculate the amount of dye encapsulated. Encapsulation efficiency was found by dividing the measured amount of encapsulated dye by the known amount of dye added during synthesis.

To determine dye release from DiD-PEG-PLGA NPs in different conditions, the NPs were transferred to 1 mL of MilliQ H<sub>2</sub>O and stored at 4°C (storage conditions) or to 1 ml of 137 mM NaCl at pH 3.5 while shaking at 37°C (to represent the human vaginal environment)<sup>173</sup>. At 1, 2, 4, and 24 hours, the NPs were centrifuged for 20 minutes at 14,000 rpm to pellet the NPs. The supernatant with released DiD was removed and 100 µL was added to each well in a 96-well plate. As DiD is weakly fluorescent in water, 100 µL of DMSO was added to each well to allow measurement of the molecule's absorbance at 640 nm (which correlates with concentration) using a Synergy H1 plate reader. The NP pellet was resuspended in fresh solution, and the process was repeated at the remaining time points. After 24 hours, the remaining dye encapsulated was quantified by dissolving the NPs in DMSO, as described above. DMSO was added to all NP samples and compared to a standard curve of known DiD concentrations in DMSO/solvent to calculate the dye release over 24 hours.

### **3.2.5 In Vivo Pregnancy Murine Model and IVIS Imaging**

Female mice between 8-17 weeks of age were maintained, bred, and used in accordance with Animal Use Protocols approved by the Institutional Animal Care and Use Committee at the University of Delaware (AUP #1320 and #1341). Virgin CD1 mice were bred and separated 12 hours later, denoted as E0.5. Mice were regularly weighed throughout the study to monitor pregnancy progression. At E14.5 or E17.5,

mice were injected intravaginally with 20  $\mu$ L of either saline or freshly synthesized DiD-PEG-PLGA NPs at a fluorescence of at least 10,000 relative fluorescence units but less than 40,000 (measured in the plate reader as described above). Separate mice at E17.5 were injected intravaginally with 20  $\mu$ L of either saline or freshly synthesized Cy5-PEG-PLGA NPs at a fluorescence of 10,000 (measured in the plate reader as described above). To achieve a successful injection, mice were anesthetized with inhaled isoflurane. Anesthetized mice were placed dorsally, and the NP or saline solution was intravaginally injected using a glass microcapillary pipette. Mice were left in the dorsal position for at least 5 minutes after injection to ensure the solution remained in the vaginal canal. Mice were then moved to an *in vivo* imaging system (IVIS, Lumina III, Perkin-Elmer) to confirm successful injection via fluorescent detection of the DiD-loaded NPs or Cy5-labeled NPs (excitation/emission 640 nm/670 nm). Twenty-four hours post-injection, mice were humanely euthanized. Whole-body IVIS images were taken, then maternal organs (liver, kidney, spleen, heart, lung, vagina, and ovaries), embryos, and placentas were excised and IVIS imaged to detect the presence of a fluorescent signal. Subsequently, the embryos and placentas were counted and weighed, and all tissues from DiD-PEG-PLGA NP injected mice were flash-frozen to prepare cryosections (discussed below). IVIS images were analyzed in Living Image (Perkin-Elmer), and region of interest (ROI) areas were drawn around vaginas to measure their fluorescence.

### 3.2.6 Qualitative Evaluation of DiD Cargo Presence in Cryosections

The major maternal organs (liver, spleen, heart, kidney, and lungs) and reproductive organs (vagina, ovaries, embryos, and placentas) excised from the saline or DiD-PEG-PLGA NP injected pregnant mice at E15.5 or E18.5 were flash-frozen in isopentane to encourage uniform tissue freezing and limit cracking. First, isopentane was transferred to a metal container and chilled for 10 minutes in a Styrofoam box of approximately 15 mL of liquid nitrogen. Once the isopentane was chilled, tissues were transferred into it for 30-45 seconds or until frozen. Immediately after freezing, organs were cryo-embedded in optimal cutting temperature (OCT) compound and temporarily stored on ice. The embedded tissues were sliced into 5  $\mu\text{m}$  sections using a CryoStat Leica CM3050S at  $24^{\circ}\text{C}$ . Tissue sections were washed in PBS once for 5 minutes and air-dried while covered. Samples were immediately imaged using a Zeiss Axio Observer microscope and examined for fluorescent DiD signal in the DiD channel (670 nm) and general morphology in brightfield.

## 3.3 Results

### 3.3.1 Nanoparticle Characterization

DiD-PEG-PLGA NPs were synthesized (**Figure 3.1A**) and characterized for their hydrodynamic diameter, zeta potential, encapsulation efficiency, and dye release profiles using DLS, TEM, and a fluorescence plate reader. The NPs were spherical in morphology per TEM analysis (**Figure 3.1B**), with a hydrodynamic diameter of  $106 \pm 3$  nm and zeta potential of  $-19 \pm 0.3$  mV (**Figure 3.1C**). When 1  $\mu\text{l}$  of 9 mM DiD was added during the synthesis procedure, the encapsulation efficiency was  $39 \pm 6$  %, equating to  $3.7 \pm 0.5$   $\mu\text{g}$  of dye encapsulated per mg of PEG-PLGA (**Figure 3.1C**). DiD saturation was also evaluated by loading different volumes (0.25, 0.5, 1, 2, 3  $\mu\text{l}$ ) of 9 mM DiD during NP synthesis. This

analysis determined that dye volume did not affect the hydrodynamic diameter or zeta potential of the NPs (**Figure 3.2**). It also indicated that adding more than 1  $\mu$ l of dye did not increase NP fluorescence despite higher loading, suggesting that quenching may occur above this threshold (**Figure 3.2**). DiD release kinetics were evaluated in storage conditions (water, 4°C, pH 7) and conditions approximating the acidic human vaginal microenvironment (NaCl, 37°C, pH 3.5) over 24 hours using absorbance values of dye no longer encapsulated in the NPs. The absorbance measurements revealed that  $90 \pm 6$  % of the encapsulated DiD was released at 24 hours under physiologic conditions, whereas  $78 \pm 4$  % of the dye was released under storage conditions (**Figure 3.1D**). Together, these data indicate that DiD was successfully encapsulated in the PEG-PLGA NPs, and more dye was released over 24 hours in physiologic conditions. This agrees with previous research that shows cargo release is accelerated from PEG-PLGA NPs placed in acidic and/or elevated temperature conditions<sup>174-176</sup>. Cy5-PEG-PLGA NPs were synthesized as described (**Figure 3.1E**) and characterized for their hydrodynamic diameter and zeta potential (**Figure 3.1F**). Compared to DiD-PEG-PLGA NPs, the Cy5-PEG-PLGA NPs had a slightly larger hydrodynamic diameter of  $139 \pm 25$  nm and a similar zeta potential of  $-15 \pm 2$  mV across four batches (**Figure 3.1F**). The hydrodynamic diameter and zeta potential of the specific batch of NPs injected into the mice was  $165 \pm 20$  nm and  $-20 \pm 2$  mV.

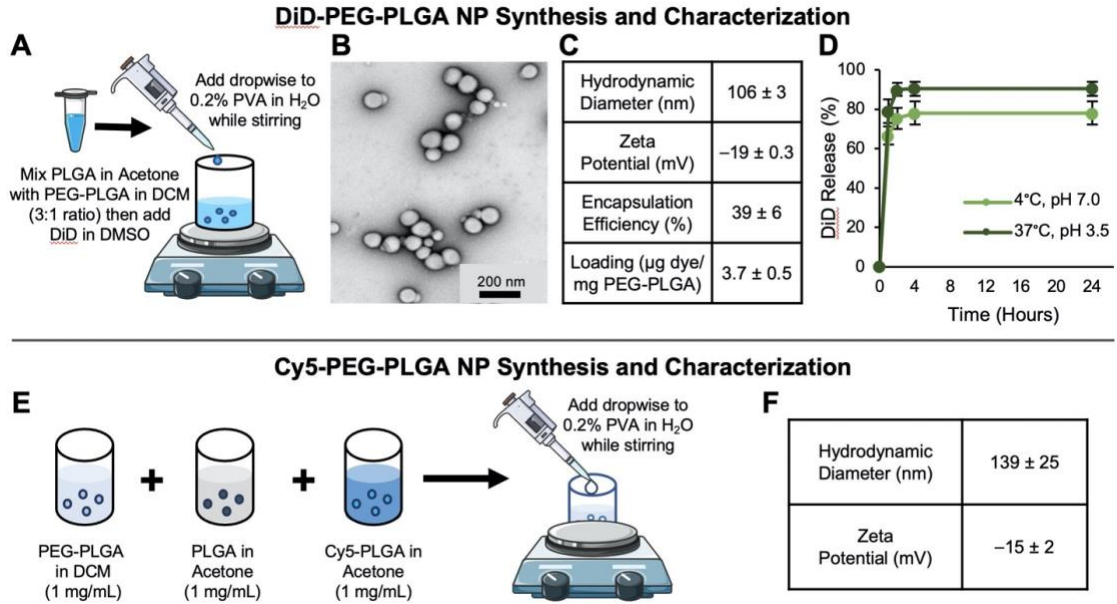


Figure 3.1: Synthesis and characterization of DiD-PEG-PLGA NPs and Cy5-PEG-PLGA NPs. **A.** Schematic of DiD-PEG-PLGA NP synthesis. **B.** Transmission electron micrograph of NPs. **C.** Hydrodynamic diameter, zeta potential, encapsulation efficiency, and DiD loading of NPs after synthesis and removal of excess dye by suspension in Triton X-100 and centrifugal filtration. Data indicate mean  $\pm$  standard deviation.  $n=4$  **D.** DiD release profile over 24 hours under storage (pH 7.0, 4°C) and physiologic (pH 3.5, 37°C) conditions. Data are mean  $\pm$  standard deviation of  $n=3$  experiments. **E.** Schematic of Cy5-PEG-PLGA NP synthesis. **F.** Hydrodynamic diameter and zeta potential of Cy5-PEG-PLGA NPs following synthesis and purification. Data show mean  $\pm$  standard deviation of  $n=4$  experiments.

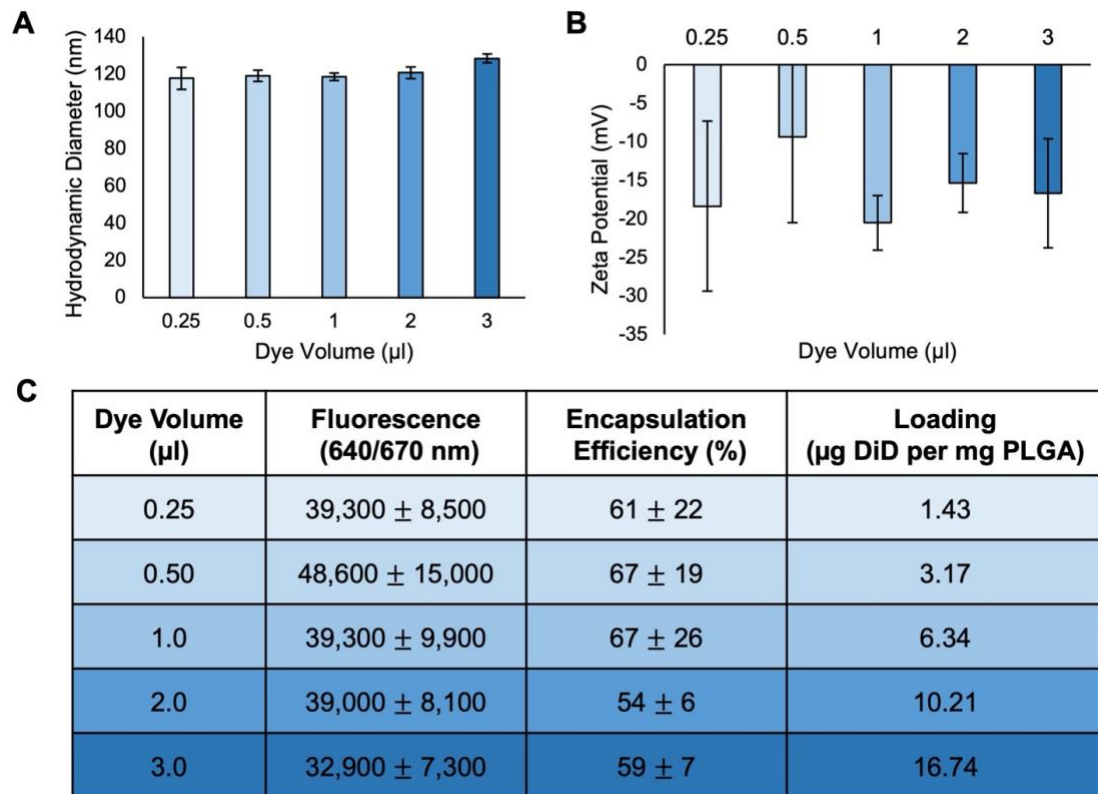


Figure 3.2: NP characteristics as a function of DiD volume added during synthesis. **A.** Hydrodynamic diameter, **B.** Zeta potential, **C.** Fluorescence intensity measured in a plate reader at excitation/emission of 640 nm/670nm, and **D.** the encapsulation and DiD loading efficiency of synthesized PEG-PLGA NPs. NP characterization was performed without the Triton X-100 purification method. Data show mean  $\pm$  standard deviation. n = 3

### 3.3.2 DiD-PEG-PLGA NPs Administered Vaginally at E14.5 and E17.5 Show

#### Localized Fluorescence in Vagina Twenty-Four Hours Post-Injection

After the DiD-PEG-PLGA NPs were characterized, we examined DiD distribution in pregnant mice following vaginal delivery at gestational ages E14.5 and E17.5. Using a glass microcapillary pipette, we injected 20 µL of saline or DiD-PEG-PLGA NPs suspended in 1x PBS into pregnant CD1 mice (**Figure 3.3A**). Whole-body images of mice were taken by IVIS

immediately following the injection and 24 hrs later, at gestational ages E15.5 and E18.5. IVIS imaging of the injected mice showed that fluorescence was present in the vagina immediately after delivery, confirming the DiD-PEG-PLGA NPs were injected successfully (**Figure 3.3B**). After whole-body IVIS images were taken 24 hrs after injection, the mice were sacrificed, and major organs (liver, spleen, heart, kidney, lungs, vagina, ovaries) and placentas and embryos were excised, imaged, and processed for histological examination. IVIS imaging determined that DiD was present in the vagina twenty-four hours post-injection at both gestational ages but was not seen in any other organs (**Figure 3.4A**). Quantification of the average radiant efficiency in the vaginal tissue confirmed NP injected mice displayed a significantly higher fluorescence than the saline mice at both gestational ages (**Figure 3.4B**). No significant difference in fluorescence between gestational ages for NP-treated mice was observed. To corroborate that the observed signal was not due solely to unencapsulated free dye remaining in the NP solution after synthesis, the experiment was repeated with NPs that were further purified by suspension in 0.5% Triton X-100 and washing several times by centrifugal filtration before vaginal injection into E14.5 mice. The signal from vaginas treated with purified NPs was similar to previous findings (**Figure 3.5**). However, considering the quick release of DiD from the PEG-PLGA NPs in physiological conditions (**Figure 3.1D**), we decided to conduct further analyses with Cy5-PEG-PLGA NPs to understand where the polymer distributes to after vaginal NP administration, as well as further histological analysis to understand DiD cargo distribution within tissues, particularly the vagina.

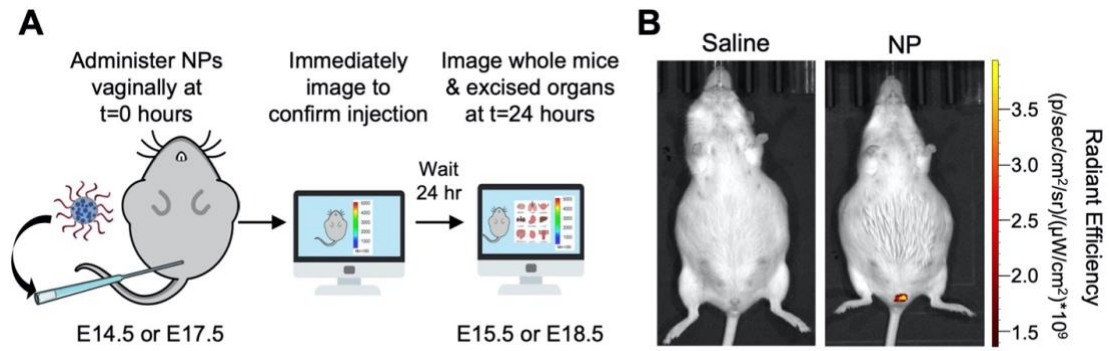


Figure 3.3: Vaginal delivery method. **A.** Experimental timeline, from vaginal injection at  $t=0$  hours through tissue collection and imaging at  $t=24$  hours. **B.** Whole body IVIS imaging of E14.5 mice at  $t=0$  hours after DiD-PEG-PLGA NP or saline injection.

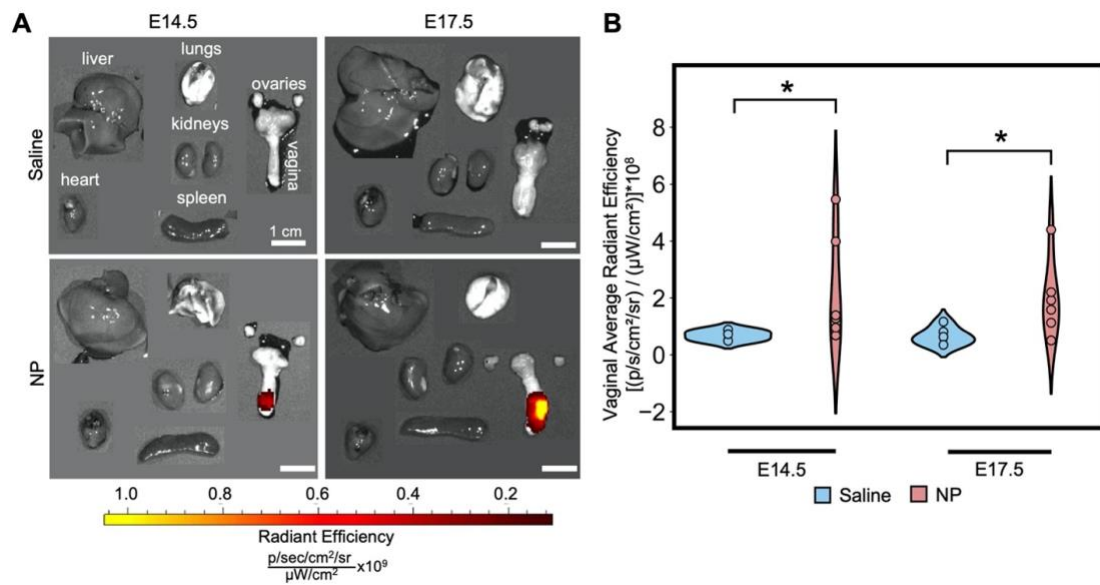


Figure 3.4: Assessment of DiD cargo accumulation in maternal organs. **A.** IVIS imaging of maternal non-reproductive and reproductive organs taken 24 hours post-DiD-PEG-PLGA NP or saline administration at E14.5 or E17.5. **B.** Average radiant efficiency of vaginas excised from mice 24 hours after DiD-PEG-PLGA NP or saline administration at E14.5 or E17.5. \*indicates  $p < 0.05$  by t-test. There were no significant differences in vaginal radiant efficiency between gestational ages (i.e., between E14.5 and E17.5 mice exposed to NPs) as confirmed by a t-test.  $n=6$  mice per group

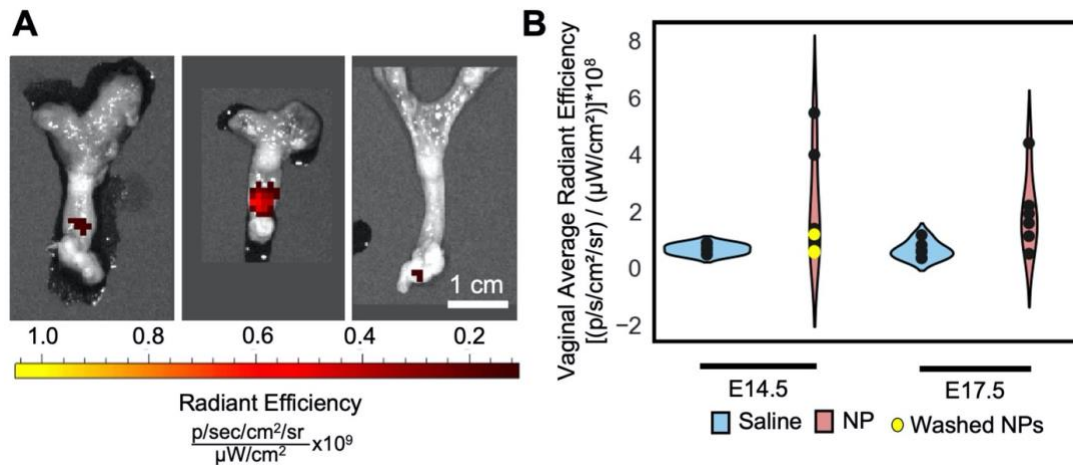


Figure 3.5: NP delivery to E14.5 mice following additional purification by Triton-X washing to remove any unencapsulated DiD. **A.** IVIS of three mouse vaginas injected with purified NP samples. **B.** Overlay of average radiant efficiency of Triton X-washed NPs (yellow circles) compared to signal from NPs washed by standard methods and injected into vaginas of mice at E14.5. There is no statistical difference between NPs washed by standard methods or Triton X purification ( $\alpha = 0.24$ ). n = 3

DiD presence in the maternal organs was evaluated by histological examination of cryo-sectioned tissues to validate and expand upon the IVIS results. Tissues were flash-frozen in isopentane, cryo-embedded in OCT, cryo-sectioned, and imaged the same day to observe DiD signal. Fluorescence microscopy confirmed DiD signal was present only in the vagina and no other reproductive or major maternal organs. Specifically, DiD signal was present along the vaginal canal, nearest the vaginal opening (the site of injection) (**Figure 3.6**). DiD fluorescence was not observed at or beyond the cervix, indicating DiD remained in the vagina over the 24-hr period after vaginal administration. The livers and spleens were also evaluated for fluorescence by histology, as NPs are known to distribute to these organs following IV injections. Microscopic examination of the livers and spleens indicated DiD signal was absent in these organs at either gestational age (**Figure 3.7**). The ovaries were also assessed by cryo-

histology since previous research has shown that IV-administered NPs distribute to the reproductive tissues in non-pregnant mice during the estrus phase of the estrus cycle<sup>99</sup>. In our study, we assessed all reproductive tissues at two different stages of pregnancy. We determined via histological examination that DiD did not reach the ovaries of pregnant mice within 24-hr following vaginal administration at either gestational age E14.5 or E17.5 (**Figure 3.8**). These data confirm the quantitative IVIS data that showed DiD is present only in the vagina after vaginal NP administration.



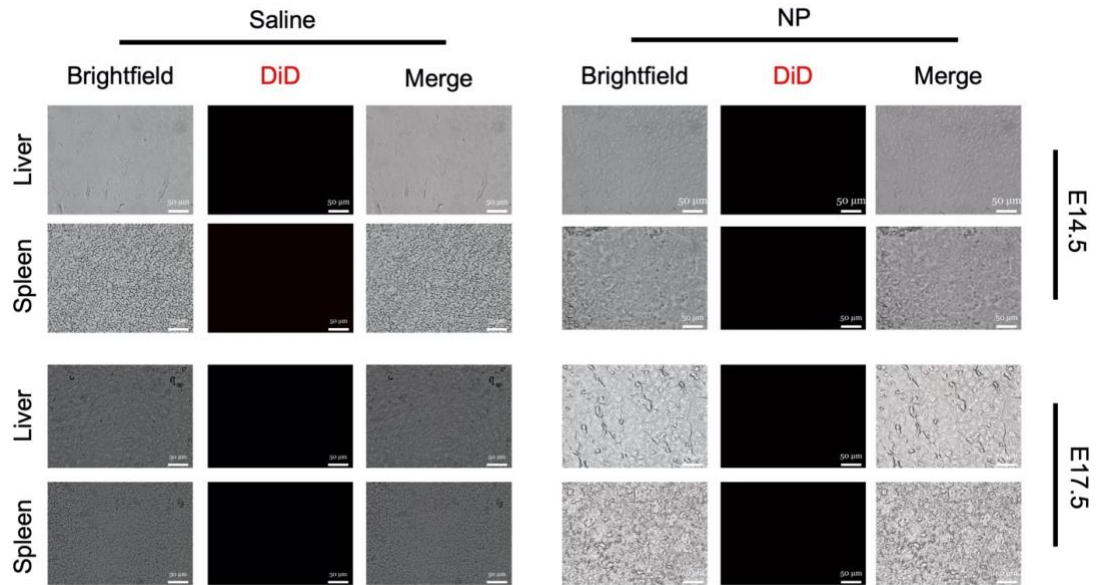


Figure 3.7: Evaluation of spleen and liver cryosections. The spleens and livers of pregnant mice that received vaginal NP or saline injection at gestational age E14.5 or E17.5 were excised 24 hours post injection, cryo-sectioned, and examined by fluorescence microscopy for DiD fluorescence. Minimal/no signal was observed in these tissues. Scale bars = 50  $\mu$ m.

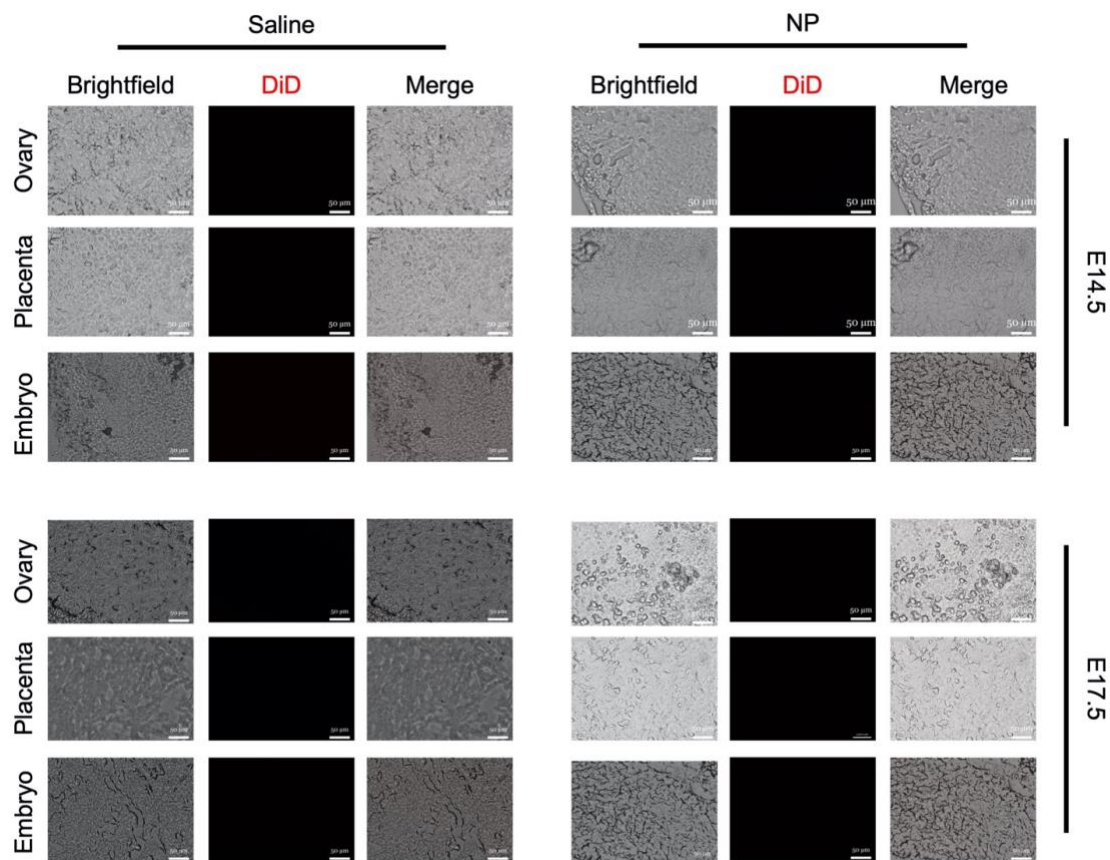


Figure 3.8: Examination of maternal reproductive organs. The ovaries, placentas, and embryos from pregnant mice treated with NPs or saline at both gestational ages were cryo-sectioned and observed by fluorescence microscopy for DiD presence. Minimal/no signal was observed in these tissues. Scale bars = 50  $\mu\text{m}$ .

To ensure DiD did not distribute to the embryos, we examined the placentas and embryos excised at E15.5 and E18.5 by IVIS imaging and histology. IVIS images of the placentas and embryos revealed that DiD signal was absent in fetal tissues (**Figure 3.9A**). Histological examination of the placentas and embryos confirmed these findings in that the DiD signal was not observed at either gestational age (**Figure 3.8**). Taken together, these data suggest DiD cargo distributes only to the vagina following vaginal NP delivery at E14.5 and E17.5.

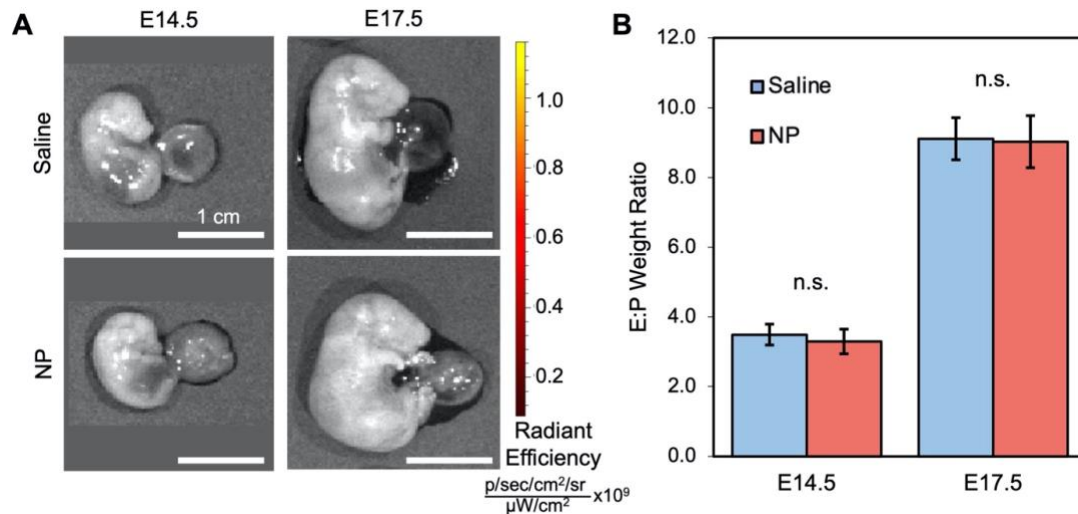


Figure 3.9: Evaluation of NP distribution to placentas and embryos and NP effects on short-term embryo and placenta growth. **A**. IVIS imaging of representative embryos and placentas excised from pregnant mice 24 hours after saline or NPs were injected on E14.5 and E17.5. **B**. Embryo-to-placenta weight ratio (E:P ratio) from mice treated with NPs or saline at each gestational age. Data show mean  $\pm$  standard deviation. n = 6 litters of 307 embryos and 307 placentas total. A student's t-test determined no significant differences between the NP and saline-treated mice.

### 3.3.3 Cy5-PEG-PLGA NPs Administered Vaginally at E17.5 Exhibit

#### Fluorescence in Vaginas, Placentas, and Embryos Twenty-Four Hours

##### Post-Injection

To determine the distribution of the polymer within the NPs following vaginal administration, we synthesized Cy5-PEG-PLGA NPs using Cy5-labeled PLGA. Unlike the DiD cargo, which is rapidly released from DiD-PEG-PLGA NPs within the 24-hour observation period, the Cy5 fluorophore remains tethered to the PLGA, allowing for tracking of the Cy5-PEG-PLGA NPs over the 24-hours following administration. Cy5-PEG-PLGAs were administered vaginally to pregnant CD1 mice at E17.5 and IVIS images from the NP-injected mice revealed Cy5 signal was present in the vagina (**Figure 3.10A**). Cy5 signal was

also observed in placentas and embryos (**Figure 3.10B**). Quantitative analysis determined that the average radiant efficiencies of the vagina, placentas, and embryos were significantly higher for the NP-injected mice compared to the saline-injected mice (**Figure 3.10C**). Collectively, these data suggest that PEG-PLGA NPs can distribute to the vagina, placenta, and embryo following vaginal administration, but that cargo that is rapidly released from these NPs in the acidic vaginal environment is strictly retained in the vagina.

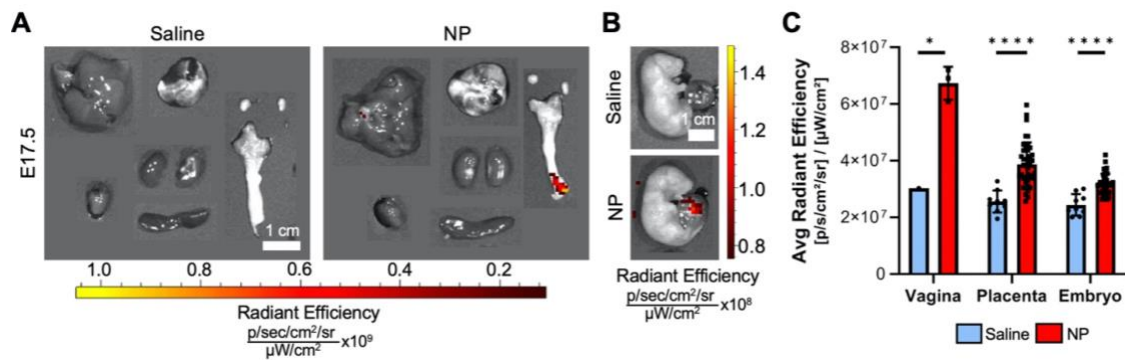


Figure 3.10: Assessment of Cy5-PEG-PLGA NP accumulation in maternal organs and embryonic tissues. **A**. IVIS imaging of maternal non-reproductive and reproductive organs taken 24 hours post-NP or saline administration at E17.5. **B**. Average radiant efficiency of vaginas, placentas, and embryos excised from mice 24 hours after administration of NPs or saline at E17.5. \*indicates  $p < 0.05$ , \*\*\*\* indicates  $p < 0.0001$  by t-test.  $n=1$  saline mouse with 9 placentas and embryos,  $n=3$  NP injected mice with a combined total of 41 placentas and embryos.

### 3.3.4 DiD-PEG-PLGA NPs Do Not Directly Affect in utero Fetal and Maternal Growth over Twenty-Four Hours of Exposure

Gross morphological examination of the embryos and placentas ensured no major defects were seen due to NP administration. No gross differences were observed between embryos and placentas from NP-treated dams compared to saline-treated dams at either time

point (**Figure 3.9A**). To determine if the vaginal administration of DiD-PEG-PLGA NPs to pregnant mice affected fetal or maternal growth, we calculated the embryo-to-placenta (E:P) weight ratio of saline and NP-injected mice. The E:P weight ratio is a measure used to determine the overall placental efficiency *in utero*. An E:P ratio greater than one indicates an efficient placenta and adequate fetal growth<sup>148,149</sup>. Our study showed no significant differences between the E:P ratios of the mice treated with saline and those treated with DiD-PEG-PLGA NPs for either gestational age (**Figure 3.9B**). The maternal weight gain was also evaluated over the pregnancy and injection period to observe potential maternal stress. The DiD-PEG-PLGA NP treatment group did not display any significant differences in overall maternal weight gain throughout gestation compared to the saline treatment group in either gestational age (**Figure 3.11A**). Additionally, there were no significant differences between the saline and NP groups in maternal weight gain within the 24-hour treatment period at either gestational age (**Figure 3.11B**). The number of resorptions per litter was also quantified during dissection to ensure DiD-PEG-PLGA NPs did not cause acute fetal distress. Here, it was determined that the number of resorptions in the NP treatment group was not significantly different from that of the saline treatment group (**Figure 3.11C**). Similarly, there were no significant differences in the number of embryos in each litter between the treatment groups (**Figure 3.11D**). These results en masse indicate that DiD-PEG-PLGA NPs do not cause any short-term, direct effects on maternal or fetal growth.

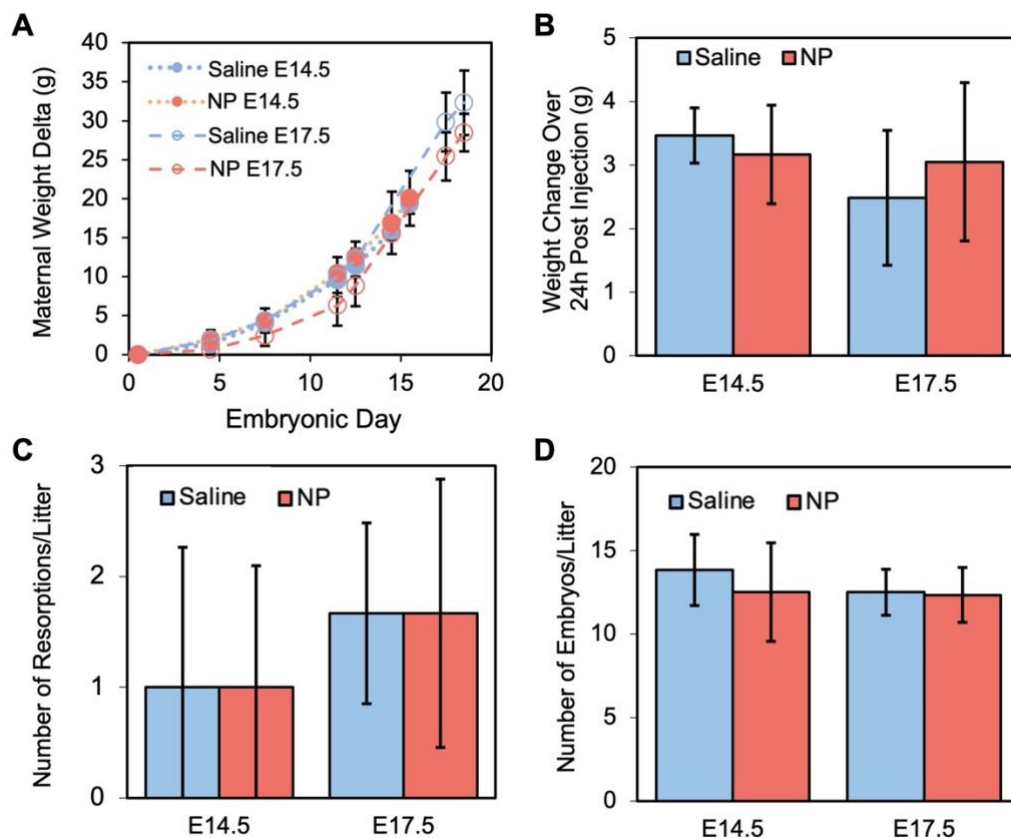


Figure 3.11: Short-term effects of NPs on maternal and fetal growth. **A.** Maternal weight gain from embryonic day 0 to the end of the study. **B.** Maternal weight change over the 24 hours after NP or saline injection. **C.** The number of embryonic resorptions per litter in each treatment group. **D.** Number of embryos in utero per litter. There were no significant differences between the treatment groups across any of these metrics, as confirmed by a t-test comparing saline to NP-exposed mice. Data show mean  $\pm$  standard deviation.  $n = 6$  pregnant mice per group, with a total of 307 embryos.

### 3.4 Discussion

This study shows that DiD released from vaginally administered PEG-PLGA NPs is retained in the vagina and does not accumulate in other organs when administered at E14.5 and E17.5 gestational ages of murine pregnancy (**Figure 3.4, Figure 3.5**). Quantitative IVIS analysis indicated no significant difference in DiD signal in the vaginas between E14.5 and

E17.5 NP-treated mice (**Figure 3.4**), indicating DiD cargo retention in the vagina is not gestation dependent at these time points. Interestingly, the quantitative analyses of Cy5-PEG-PLGA NP distribution 24 hrs after vaginal administration at E17.5 revealed that the NPs could accumulate in the vagina, placenta, and embryo (**Figure 3.10**). There was no effect of the DiD-PEG-PLGA NPs on maternal weight gain indicating they did not influence maternal wellbeing over the duration of the study compared to the saline-injected dams (**Figure 3.11**). Further, the NPs did not impact fetal development based on the placenta and embryo weights and morphology (**Figure 3.9**). Lastly, dams injected with NPs did not display differences in litter size or resorption number compared to saline-injected dams (**Figure 3.11**). These data suggest the potential to use PEG-PLGA NPs as vaginal delivery vehicles to treat conditions affecting the vagina during pregnancy.

We observed that DiD encapsulated in PEG-PLGA NPs is retained in the vagina for twenty-four hours after vaginal administration, consistent with other studies that have evaluated polymer-based NP retention following vaginal administration in non-pregnant mice<sup>177</sup>. Cu *et al.* delivered coumarin-loaded PEG-PLGA NPs vaginally to mice during the diestrus phase to correspond to the follicular phase or the onset of menstruation in humans for the vaginal delivery of therapeutics. Our study shows similar results to the Cu study but was performed in pregnant mice at E14.5 and E17.5 gestational ages and adds new information about polymer distribution (based on Cy5-PLGA) compared to cargo distribution (based on DiD). Notably, cargo retention in the vagina is likely due to entrapment within the cervicovaginal mucus. Numerous studies<sup>109,110</sup> have shown that NP physicochemical properties, such as size, surface charge, PEG coating density, and molecular weight, influence transport within CVM. Therefore, future studies that build on our work could seek to understand how different PEG coating densities, alternative surface coatings, and larger and

smaller diameters affect NP retention time in the vagina and distribution to placentas and embryos during pregnancy. Also, to ensure local delivery is feasible clinically, the length of time that the particles and their cargo are retained in the vaginal canal should be evaluated *in vivo* and in clinical settings; our study only investigated 24 hours post-delivery because the transition to a new Theiler Stage occurs after 24 hours of development. Characterization of the stability of the particles *in vivo* over extended periods of time would be informative for drug formulation.

Previous research has shown that NP distribution in the pregnant murine model is gestation-dependent following IV delivery<sup>134,150,167</sup>. Given these findings and the physiological changes in CVM throughout pregnancy, we expected DiD cargo retention following vaginal NP delivery would also be gestation dependent. While E14.5 and E17.5 both represent the third trimester of human pregnancy, murine CVM continues to thicken as pregnancy progresses<sup>178</sup>. We hypothesized that DiD retention would differ as gestational age increased. However, quantifying IVIS images determined no difference in DiD signal in the vaginas between the E14.5 and E17.5 NP mice. Additionally, the histological examination showed no notable differences in vaginal DiD signal between the two gestational ages. These data indicate that gestational age does not play a role in DiD retention in the vagina after NP delivery in the pregnant murine model. This may be due to the rapid release of the DiD from the NPs or to minimal changes in CVM properties between E14.5 and E17.5. Future work could characterize murine CVM pore size, viscosity, and other characteristics as a functional of gestational age to shed light on the results observed here.

Our study was focused on examining significant metrics of short-term toxicity. In the future, the long-term effects of local NP administration should be evaluated to ensure fetal and maternal safety. The analyses should include an evaluation of liver enzymes to indicate liver

toxicity, an assessment of serum cytokines in pregnant subjects to reveal any immunogenicity, and an analysis of fetal development, fetal immune response, and neonatal cognitive function and behavior. To explore the potential of vaginally administered NP treatments, PEG-PLGA NPs should be loaded with a therapeutic agent, and NP efficacy and stability should be evaluated *in vitro* and *in vivo*. The knowledge acquired would allow researchers to develop nanocarriers that can effectively treat maternal conditions during pregnancy while maintaining the safety of the developing fetus and pregnant people. In conclusion, the work shown here is foundational for the future development and use of nanomedicine in maternal-fetal applications.

## Chapter 4

### CLINDAMYCIN-LOADED PEG-PLGA NPs INHIBIT GARDNERELLA VAGINAL GROWTH IN VITRO

#### 4.1 Introduction

Bacterial vaginosis (BV) is a common vaginal infection characterized by an imbalance in the bacterial ecosystem of the vagina. It occurs when healthy *Lactobacilli* bacteria, which help to maintain a healthy vaginal environment, are outnumbered by other types of pathogenic bacteria, the most predominant being *G. vaginalis*<sup>93,95,179</sup>. Patients with the condition experience symptoms such as a fishy odor, thin grayish-white vaginal discharge, itching, and irritation, although some individuals with BV may experience no symptoms at all<sup>93</sup>. While the exact causes of BV are not fully understood, factors such as douching, multiple sexual partners, and the use of certain soaps or hygiene products can contribute to the disruption of the vaginal microbiota.

Antibiotic treatments, such as clindamycin oral tablets or vaginal creams, are typically recommended, that can help alleviate symptoms and restore the vaginal balance. Clindamycin is a commonly prescribed antibiotic that has demonstrated efficacy in the treatment of bacterial vaginosis (BV)<sup>180,181</sup>. Clindamycin is effective in reducing the symptoms of BV, such as abnormal discharge and odor, and restoring the

natural balance of bacteria in the vagina. However, it's important to note that like any antibiotic, clindamycin may also affect the beneficial bacteria, such as the *Lactobacillus* species, leading to potential disruptions in the vaginal microbiota. In some cases, this can result in the recurrence of BV, which occurs in 15-20% of BV patients within 3 months of treatment<sup>182</sup>.

BV can have unique implications for pregnant patients. During pregnancy, hormonal changes can alter the vaginal environment, making pregnant individuals more susceptible to BV. If left untreated, BV in pregnancy can increase the risk of complications such as preterm birth, low birth weight, and postpartum infections<sup>183</sup>. Treatment options for pregnant patients with BV may vary, as some antibiotics commonly used to treat BV may not be safe during pregnancy. It is essential for patients to follow the healthcare provider's recommendations for managing BV during pregnancy to minimize potential risks and ensure the health and well-being of both the pregnant individual and the developing fetus<sup>180,181,184</sup>. Given the safety concerns and delicacy required to protect the fetus, there needs to be a new treatment strategy for pregnant patients with BV.

Nanoparticles (NPs) are drug delivery vehicles with great potential to be used to treat BV in pregnant and non-pregnant patients. Due to their small size and large surface area, NPs with correctly tuned surface chemistry can efficiently penetrate the vaginal epithelium and reach the site of infection<sup>10</sup>. Additionally, their unique physicochemical properties allow for controlled drug release, ensuring sustained therapeutic levels over an extended period. Encapsulating antimicrobial agents within

NPs protect the drug from degradation, enhance its stability, and improve its bioavailability. With respect to PLGA nanocarriers which are hydrolytically degradable, the lactic to glycolic acid (L:G) ratio is critical in determining the release profile of the drug from the NP<sup>185-187</sup>. Previous work has shown that PLGA NPs with higher lactic acid content exhibit slower release profiles, while those with an L:G ratio of 50:50 exhibit the fastest release<sup>185</sup>. In addition to tailoring the release kinetics, NPs can be surface modified to enhance their targeting capabilities<sup>10</sup>, enabling them to selectively bind to bacteria or biofilms associated with BV. Collectively, these benefits of drug nanocarriers allow them to minimize systemic side effects and enhance the efficacy of treatment compared to freely delivered (unencapsulated) drugs.

In this study, we investigated the potential to load clindamycin (CLN) in PEG-PLGA NPs (CLN-PEG-PLGA NPs) of varying L:G ratios (50:50, 75:25, and 85:15), characterized their drug release kinetics, and examined their ability to inhibit *G. vaginalis* growth *in vitro*. For these experiments, *G. vaginalis* was cultured in suspension in broth or adhered onto chocolate agar plates, then treated with free CLN or CLN-PEG-PLGA NPs of each L:G ratio. *G. vaginalis* growth in suspension culture was measured every two hours using ultraviolet-visible spectrophotometry (measuring absorbance at 600 nm) and growth in adherent culture was monitored by imaging plates after twelve hours using a Nikon digital camera. We also evaluated the velocity of PEG-PLGA NPs in the presence of mucus to understand how they might move through cervicovaginal mucus in the vaginal environment. Fluorescent DiD-PEG-PLGA NPs were synthesized and suspended in reconstituted porcine gut mucus or

water. Time lapse images of DiD-PEG-PLGA NPs were taken at 33 frames per second for a total of 1 second on a fluorescent microscope and NPs were tracked manually in ImageJ. This revealed NP movement is slowed in mucus compared to water, but that L:G ratio does not influence velocity in mucus. Lastly, CLN-PEG-PLGA NPs of varying L:G ratios were administered to adherent *G. vaginalis* cultures with a mucosal layer to represent the CVM layer in BV patients. These experiments revealed CLN-PEG-PLGA NPs can successfully inhibit *in vitro* *G. vaginalis* growth in suspension and when adhered in the absence or presence of mucus within a 12-hour treatment period (though the extent of inhibition was less than that observed for free CLN, likely due to the differences in the bolus dose applied for free CLN versus the sustained drug release for encapsulated CLN). There were also no significant differences in bacterial growth inhibition between the three L:G ratios, indicating the L:G ratio (and corresponding changes to drug release kinetics) does not have an impact on short-term antibacterial treatment *in vitro*. Overall, these findings indicate that CLN maintains its antibacterial activity upon loading into PEG-PLGA NPs, suggesting there is potential for the use of CLN-PEG-PLGA NPs for treating pregnant and non-pregnant patients with BV.

## **4.2 Methods**

### **4.2.1 Synthesis of CLN-PEG-PLGA NPs**

Clindamycin-hydrochloride (CLN) loaded polyethylene glycol (PEG) – poly(lactic-co-glycolic) acid (PLGA) NPs were synthesized using a single emulsion method. Custom mPEG (MW 5kDa)- PLGA (MW 30 kDa) polymers with varying lactic to glycolic (L:G) acid ratios of 50:50, 75:25, and 85:15 (Nanosoft polymers) were dissolved in dichloromethane (DCM) at concentrations of 1 mg/mL. CLN (research grade, Sigma Aldrich) was dissolved in dichloromethane (DCM) at a concentration of 1mg/mL and added to the PEG-PLGA solution at a ratio of 1:1. Then, 1 ml of the CLN/PEG-PLGA solution was added dropwise to a 3 mL solution of 0.2% poly(vinyl alcohol) in MilliQ H<sub>2</sub>O while stirring at 800 rpm. CLN-PEG-PLGA NPs were pulse sonicated in 5 second cycles (5 seconds on, 5 seconds off) for a total of 2 minutes using Fisherbrand Model 120 Sonic Dismembrator (Fisher Scientific) at 80% amplitude. The CLN-PEG-PLGA NP solutions were then magnetically stirred overnight to allow for solvent evaporation. NPs were centrifuge filtered in 100 kDa molecular weight cut off (MWCO) conical filter tubes (Amincon Ultra-4, MilliporeSigma) for 25 minutes at 4200 rcf at at 14°C. Following centrifugation, NPs were resuspended in 3 mL of MilliQ H<sub>2</sub>O and centrifuged a second time for 30 mins or until H<sub>2</sub>O was removed. CLN-PEG-PLGA NPs were used immediately after purification for each experimental study.

#### **4.2.2 Synthesis of DiD-PEG-PLGA NPs**

DiD PEG-PLGA NPs were also synthesized using a single emulsion method in which DiD (ThermoFisher) was dissolved in dimethyl sulfoxide (DMSO) at a concentration of 9 mM. Next, 1  $\mu$ L of fluorescent DiD was added to 1 mL of PEG-PLGA dissolved in DCM at a concentration of 1mg/mL. The DiD/PEG-PLGA solution was added dropwise to 3 mL of 0.2% PVA, then pulse sonicated in 5 second cycles (5 seconds on, 5 seconds off) for a total of 2 minutes. NPs were magnetically stirred overnight for solvent evaporation, then centrifuged filtered in 100 kDa MWCO conical filters for 25 minutes at 4200 rpm. To ensure unencapsulated DiD was removed from the solution, 500  $\mu$ L 0.5% Triton X-100 was added to each sample and NPs were centrifuged filtered for 15 minutes at 4200 rpm. NP washing was performed twice by resuspending NPs in 2 mL of MilliQ H<sub>2</sub>O and centrifuge filtering for 15 minutes at 4200 rpm at 14°C. DiD-PEG-PLGA NPs were used immediately after synthesis and purification for experimental studies.

### **4.2.3 Nanoparticle Characterization**

CLN-PEG-PLGA NPs were characterized for their hydrodynamic diameter and zeta potential using Dynamic Light Scattering (DLS) on an AntonPaar LiteSizer 500 instrument. DLS samples were prepared in disposable or Omega cuvettes (Anton Parr) by dissolving 5-10  $\mu$ L of the purified NPs in 1 mL of MilliQ H<sub>2</sub>O. The reported hydrodynamic diameter and zeta potential are the averages of three DLS experiments. Similar procedures were used for DiD PEG-PLGA NPs.

#### **4.2.4 CLN-PEG-PLGA NPs Loading Efficiency and Drug Release Profile**

To determine CLN loading in CLN-PEG-PLGA NPs, the filtrate of unencapsulated CLN was collected in 15 ml conical tubes following each wash step during NP synthesis. The absorbance of the unencapsulated drug was measured on a NanoDrop One microvolume spectrophotometer at 210 nm using MilliQ H<sub>2</sub>O as a baseline. The absorbance of the unencapsulated CLN sample was compared to a standard curve of known concentrations of CLN in MilliQ H<sub>2</sub>O to determine the concentration of unencapsulated drug. The amount of drug loaded in the NPs was then determined by subtracting this amount of drug from the original amount added to the synthesis solution.

To determine the drug release profile, CLN-PEG-PLGA NPs were added to disposable cuvettes containing 1 mL of MilliQ H<sub>2</sub>O and stored at 4°C (storage conditions) or 1 ml of 137 mM NaCl at pH 5.0 while shaking at 37°C (to represent the murine vaginal environment with BV infection). At 1, 2, 4, and 24 hours, NP solutions were transferred to 15 mL 100 kDa MWCO Amicon filters then centrifuged for 30 minutes at 14,000 rcf at 14°C. The filtrates were collected and transferred to 1.5 mL Eppendorf tubes. The NPs collected in the filters were resuspended in 1 mL of fresh solvent and placed back in their respective locations. The absorbance of the filtrates was measured on the Nanodrop at 210 nm and the measurements were compared to a standard curve of known concentrations of CLN in MilliQ H<sub>2</sub>O to quantify the amount of release drug.

#### **4.2.5 DiD-PEG-PLGA NP Microscopy Tracking**

Following DiD-PEG-PLGA NP synthesis, NPs were added to either MilliQ H<sub>2</sub>O or reconstituted porcine gut mucus and their motion manually tracked using fluorescence microscopy to calculate the average root mean square displacement. The mucus solution was prepared by reconstituting porcine gut mucus (Sigma Aldrich) in NaOH at a concentration of 20 mg/mL. To construct a device for NP tracking, two thin strips of double-sided tape were placed on the edge of a coverslip to create a 0.5 cm wide channel<sup>188</sup>. A second coverslip was placed on the first coverslip to create a thin slide. Then, 2  $\mu$ L of freshly synthesized DiD-PEG-PLGA NPs were added to 1 mL of either mucus or MilliQ H<sub>2</sub>O. Next, 10  $\mu$ L of NPs in solution were carefully inserted into the channel. Channels containing NP solutions were imaged on a Axio Observer Z1 Inverted Fluorescence Microscope (Zeiss) using a 63x oil lens. NPs were viewed using the 640 nm - 670 nm DiD channel. Time lapse images were acquired for a total of 1 sec at 33 frames per second with an exposure time of 10 milliseconds.

Following imaging, NPs were manually tracked using the Manual Tracking Plugin on ImageJ. Briefly, NPs that remained in focus for the duration of the time lapse video were selected for analysis. The position of a NP was tracked in each frame and the root mean squared displacement of each NP type was calculated in each solvent. For analysis, 20 NPs were tracked in a single time lapse video and 20-time lapse videos were taken, totaling 400 NPs analyzed per treatment group.

#### **4.2.6 *Gardnerella Vaginalis* Culture**

*Gardnerella Vaginalis* (*G. vaginalis*) (ATCC 49145) was cultured in suspension and on chocolate agar plates. For suspension cultures, *G. vaginalis* was incubated at 37°C in an atmosphere of 5% CO<sub>2</sub> in bioreaction tubes in ATCC 1685: NYC III Medium. After 24-48 hours, cells were resuspended at a ratio of 1:1000 in fresh broth. Bacteria concentration was determined by measuring absorbance at 600 nm on a Cary60 UV-vis spectrophotometer, then calculating the number of cells based on OD<sub>600</sub> 0.1 = 5.7x10<sup>8</sup> cells/mL. Agar plates for adhered cultures were made using ATCC Medium 814 GC Agar on 10 cm petri dish plates that were stored in 4°C until use. Prior to inoculation, plates were air-dried in a sterile biosafety cabinet for 15 minutes. *G. vaginalis* was inoculated using 10 µL inoculation loops and incubated at 37°C in an atmosphere of 5% CO<sub>2</sub>.

#### **4.2.7 *G. Vaginalis* Growth Following Free Clindamycin and CLN-PEG-PLGA NP Treatment**

To evaluate the effect of free CLN and CLN-PEG-PLGA NPs on *G. vaginalis* growth, bacteria cultured in suspension were diluted to an initial OD<sub>600</sub> = 0.1 (**Figure 3.1**). Free CLN dissolved in MilliQ H<sub>2</sub>O or CLN-PEG-PLGA NPs diluted in broth were added at various concentrations ranging from X to Y to separate bioreaction tubes of *G. vaginalis*. To verify the initial OD<sub>600</sub>, 500 µL of each sample was aseptically transferred to a disposable cuvette and the OD<sub>600</sub> measured on a Cary 60

spectrophotometer (Agilent), after which the sample was aseptically transferred back into its original tube. To measure bacterial growth over time, absorbance measurements were taken every two hours for a total of 12 hours.

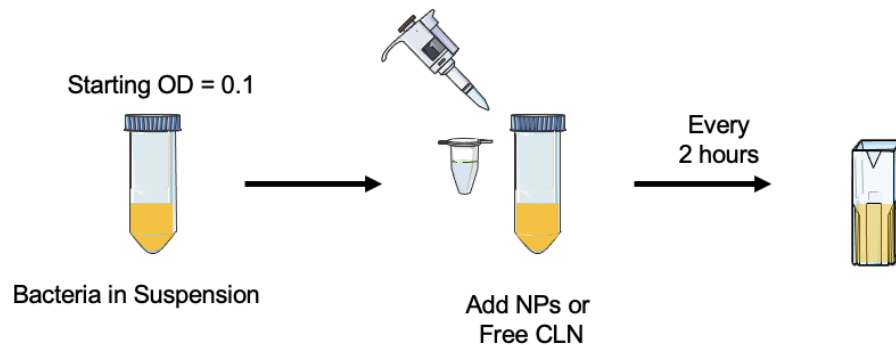


Figure 4.1: Schematic of NP Treatment on *G. Vaginalis* Culture in Suspension

#### 4.2.8 CLN-PEG-PLGA NP Treatment of Adhered *G. vaginalis*

The effect of CLN-PEG-PLGA NP treatment on adhered *G. vaginalis* cultures was determined by first culturing *G. vaginalis* on chocolate agar plates (**Figure 4.2**). To prepare the bacteria, *G. vaginalis* was diluted to a starting  $OD_{600} = 0.1$  then diluted a second time  $10^6$  from the  $OD_{600} = 0.1$  stock. Plates were inoculated by adding 100  $\mu$ L of the diluted stock to the center of the agar plate then cells were spread one time in a clockwise direction using a plastic cell spreader. The inoculated plates were incubated for 6 hours at 37°C in an atmosphere of 5%  $CO_2$ . Following incubation, treatments (no drug, free CLN, or CLN-PEG-PLGA NPs) were added to each plate

and incubated for another 6 hours. At 12 hours total, plates were imaged using a Nikon EOS Rebel T7 EF-S 18-55mm camera. The number of bacteria in each plate was quantified using ImageJ bacteria cell counter, where bacteria in an outer region close to the edge of the plate were excluded from the analysis to account for edge effects (i.e., only bacteria in a central region of interest were counted).

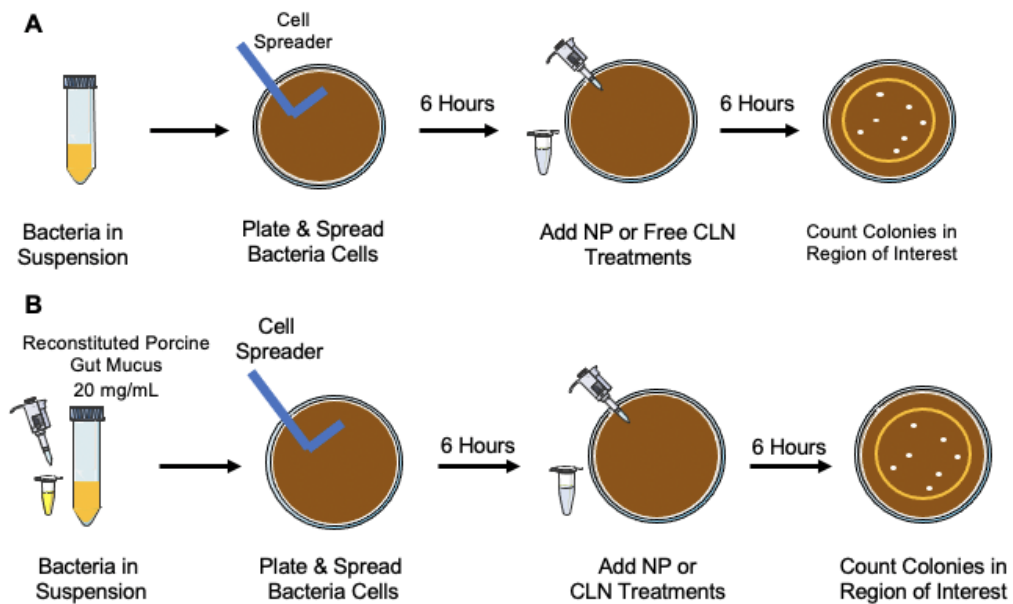


Figure 4.2: Schematic of NP Treatment on Adhered *G. Vaginalis*. **A.** Method for *G. Vaginalis* cultures adhered on chocolate agar plates without, and **B.** with porcine gut mucus reconstituted in NaOH.

The study was repeated in the presence of reconstituted gut mucus to determine NP impact on *G. vaginalis* with a mucosal barrier. Reconstituted gut mucus was dissolved in NaOH at 1mg/mL then 100  $\mu$ L was added to 1 mL of the diluted

bacteria stock. Plates were inoculated with 100  $\mu$ L of the mucus/bacteria mixture and cells were spread in a clockwise direction on the agar plate using a plastic cell spreader. The bacteria/mucus plates were incubated for 6 hours then 100  $\mu$ L of free CLN or CLN-PEG-PLGA NPs were drizzled on the plates so that treatments were dispersed as evenly as possible. Agar plates were incubated for another 6 hours, then imaged and quantified to measure bacterial growth.

### 4.3 Results

#### 4.3.1 Nanoparticle Characterization

CLN-PEG-PLGA NPs with three different L:G ratios (50:50, 75:25, and 85:15) were synthesized (**Figure 4.3A**) and characterized for their hydrodynamic diameter, zeta potential, CLN loading, and drug release in storage and physiologic conditions. Based on DLS measurements, the hydrodynamic diameters of the CLN-PEG-PLGA NPs ( $226 \pm 6$  nm for 50:50 NPs,  $226 \pm 26$  nm for 75:25 NPs, and  $236 \pm 48$  nm for 85:15 NPs) were slightly larger than those of unloaded PEG-PLGA NPs (**Figure 4.3B**). The zeta potentials of each respective CLN-PEG-PLGA NP were  $-28 \pm 2$  mV,  $-21 \pm 8$  mV, and  $-26 \pm 2$  mV, and there were no significant differences in surface charge compared to unloaded PEG-PLGA NPs (**Figure 4.3C**).

The loading content of each CLN-PEG-PLGA NP was also evaluated to ensure the NPs with different L:G ratios had similar drug loading. There were no significant differences in CLN loading between each CLN-PEG-PLGA NP (**Figure 4.3D**),

meaning any differences in observed effect on bacterial growth could be attributed to the release kinetics of the drug from each formulation. Lastly, CLN release kinetics were evaluated for each NP in storage conditions (water, pH 7,4 °C) and physiologic conditions (NaCl, pH 5, 37 °C) mimicking the vaginal microenvironment of mice with BV. There were no significant differences in CLN release between L:G ratios when NPs were placed under storage conditions (**Figure 4.3**). However, in physiologic conditions, the CLN-PEG-PLGA NPs (50:50) displayed the fastest release of 67% at 24 hours compared to 50% for CLN-PEG-PLGA NPs (75:25) and 47% for CLN-PEG-PLGA NPs (85:15) (**Figure 4.3F**). Together, these data indicate that CLN can be successfully encapsulated in PEG-PLGA NPs with 3 different L:G ratios, and that while these NPs have similar hydrodynamic diameter, zeta potential, and CLN loading, the release kinetics are accelerated in physiologic conditions as the lactic acid content decreases.

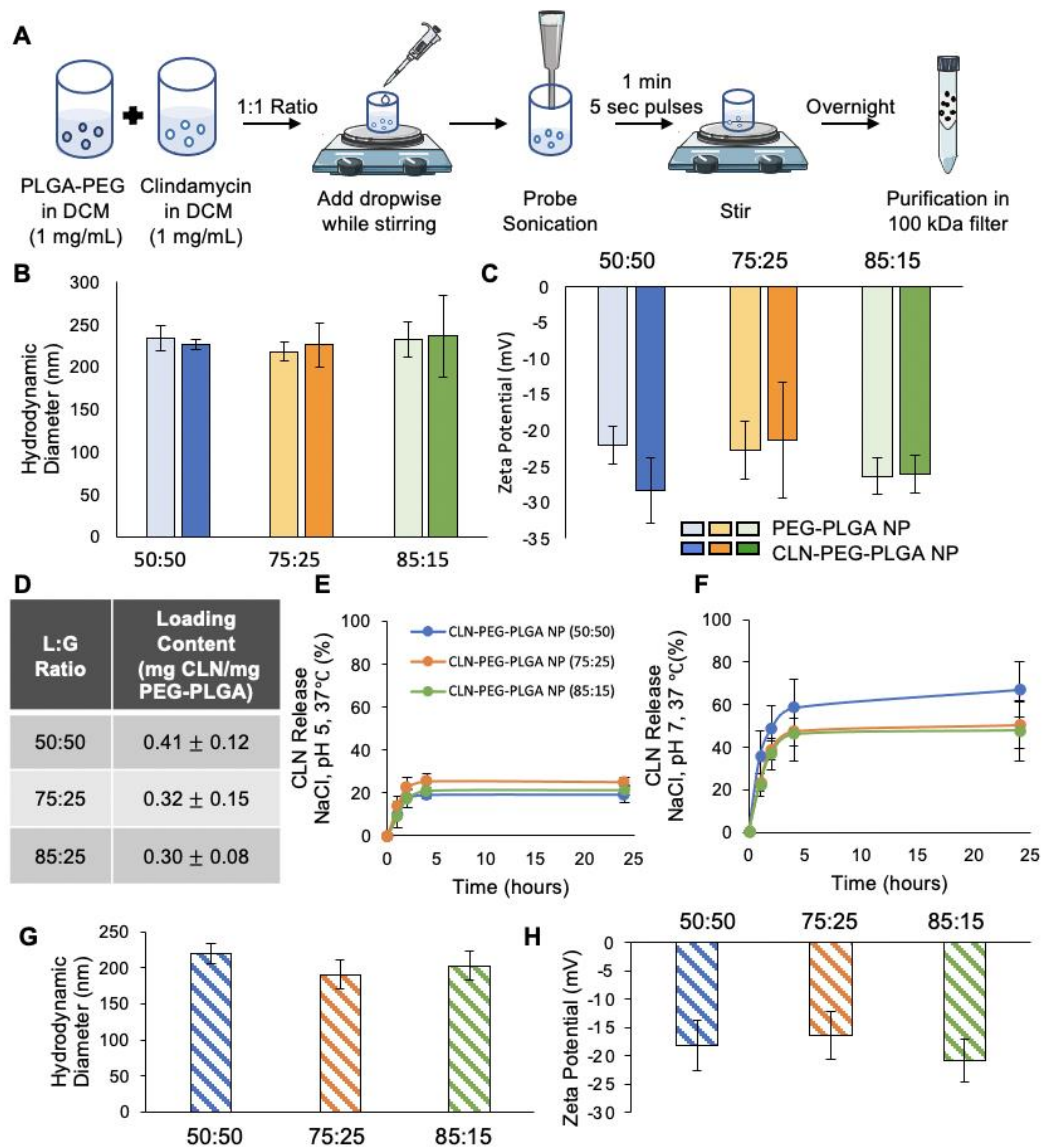


Figure 4.3: Nanoparticle Characterization. **A**. Schematic of NP synthesis procedure. **B-D**. CLN-PEG-PLGA NPs **B**. hydrodynamic diameter, **C**. Zeta potential, and **D**. drug loading content. **E-F**. CLN release profile from the NPs over 24 hours under **E**. storage (Water, pH 7.0, 4°C) and **F**. physiologic (NaCl, pH 5.0, 37°C) conditions. **G-H**. The **G**. hydrodynamic diameter and **H**. zeta potential of DiD-PEG-PLGA NPs. Data are mean ± standard deviation of n=3 experiments.

### **4.3.2 DiD-PEG-PLGA NP Velocity is Decreased in the Presence of Reconstituted Mucus**

Following synthesis, DiD-PEG-PLGA NPs were suspended in either reconstituted mucus or water then inserted into an imaging device made from two coverslips bound together by double-sided tape (**Figure 4.4**). Time lapse videos of the DiD-PEG-PLGA NPs in suspension were taken for each L:G ratio group for a total of 1 second and NPs were manually tracked using ImageJ. Data from this experiment revealed DiD-PEG-PLGA NPs in mucus had a dramatically lower mean square displacement (MSD) when suspended in mucus compared to being suspended in water (**Figure 4.4**). Further, the L:G ratio did not significantly impact the DiD-PEG-PLGA NP MSD within either medium.

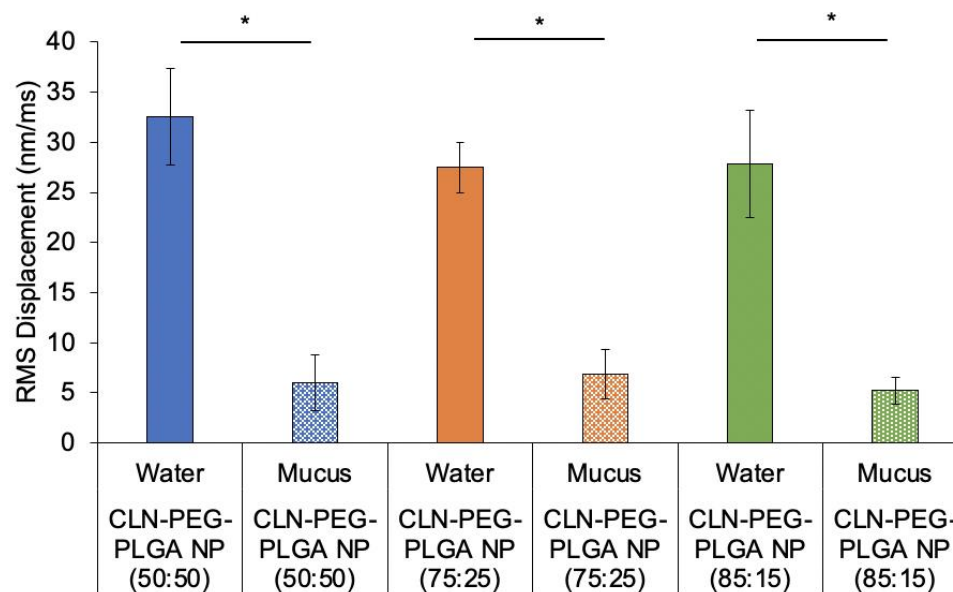


Figure 4.4: Analysis of DiD-PEG-PLGA NPs movement when placed in different media. Root mean square (RMS) displacement of DiD-PEG-PLGA NPs in water and reconstituted mucus. \*indicated  $p < 0.05$  by t-test. Data are mean  $\pm$  standard deviation of  $n=200$  nanoparticles.

### 4.3.3 CLN-PEG-PLGA NPs Inhibit *G. Vaginalis* Growth in Suspension

To evaluate the inhibition of *G. vaginalis* growth in suspension, free CLN was incubated in *G. vaginalis* cultures for 12 hours. CLN dissolved in MilliQ H<sub>2</sub>O was added at varying concentrations, including 0.1, 0.25, 0.5, 1, 2, 4, and 8  $\mu\text{g/mL}$ , to *G. vaginalis* and growth was measured and tracked every 2 hours for a total of 12 hours (**Figure 4.5A**). The final growth measurements of the free CLN treatments at 12 hours was compared to the NT group (**Figure 4.5A**) and it was determined all concentrations administered inhibited *G. vaginalis* growth by at least 50%. Further, *G. vaginalis*

growth inhibition increased as the concentrations increased, excluding the 4 and 8  $\mu\text{g/ml}$  concentrations.

To evaluate the ability of CLN-PEG-PLGA NPs to inhibit *G. vaginalis* growth, *G. vaginalis* was also treated with CLN-PEG-PLGA NPs in suspension. The OD<sub>600</sub> was measured every two hours to measure *G. vaginalis* growth over a total of 12 hours. All CLN-PEG-PLGA NPs dosed at a CLN concentration of 4  $\mu\text{g/mL}$  successfully inhibited *G. vaginalis* growth when compared to the NT group (**Figure 4.5B**). However, there were no significant differences in *G. vaginalis* growth inhibition between each CLN-PEG-PLGA NP group, indicating the L:G ratio (and corresponding altered drug release kinetics) does not impact efficacy over the 12-hour period in this *in vitro* setting (**Figure 4.5**). The MIC<sub>50</sub> or minimum inhibitory concentration, is the concentration of CLN that inhibits *G. vaginalis* growth by 50% and was calculated by multiplying the OD<sub>600</sub> value (number of isolates) at t=12 hours by 0.5 and comparing the no treatment group to the CLN treatment groups. Overall, *G. vaginalis* growth was inhibited more in a 12-hour period when using smaller concentrations of free CLN than CLN-PEG-PLGA NPs (**Figure 4.5C**). This is likely because the cells receive a bolus dose of free CLN, compared to slow release of CLN from the nanoformulations.

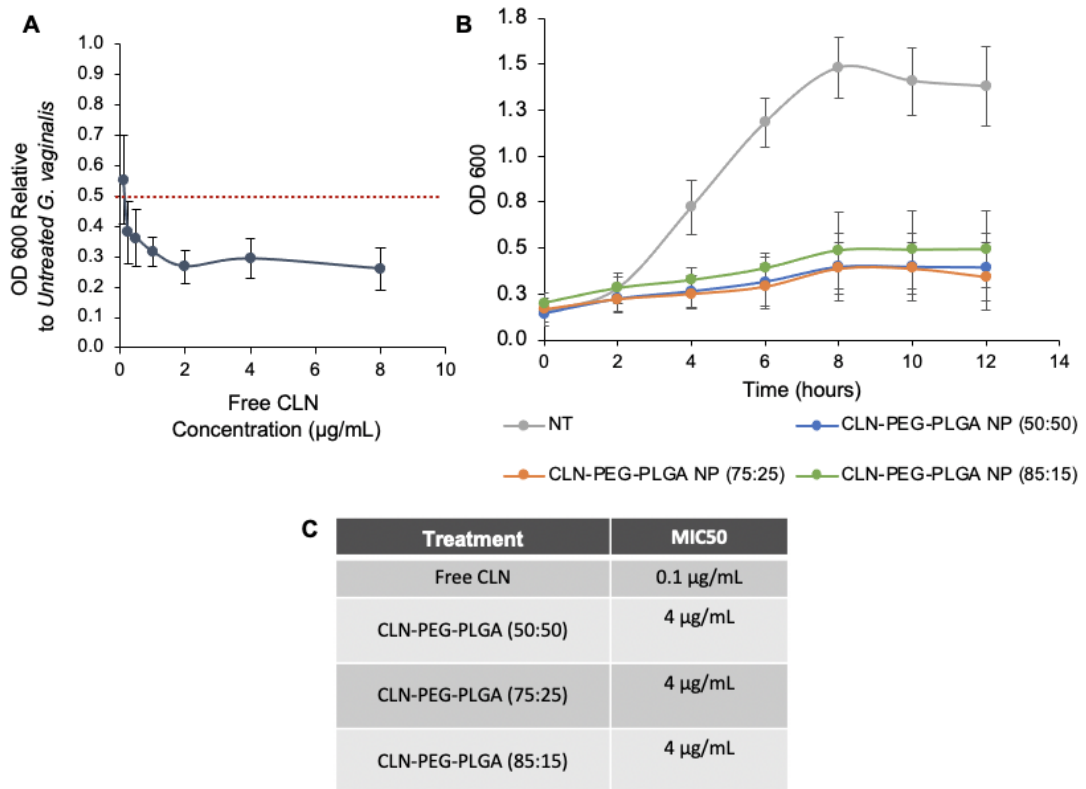


Figure 4.5: *G. vaginalis* Growth Following Free CLN and CLN-PEG-PLGA NPs Treatment in Suspension **A.** *G. vaginalis* growth after 12 hours of free CLN treatments only. **B.** *G. vaginalis* growth following CLN-PEG-PLGA NPs dosed with 4  $\mu\text{g/ml}$  of loaded CLN over 12 hours **C.** MIC<sub>50</sub> values of Free CLN and CLN-PEG-PLGA NP treatments. Data are mean  $\pm$  standard deviation of n=3 experiments.

#### 4.3.4 CLN-PEG-PLGA NPs Inhibit Adhered *G. Vaginalis* Growth in the Presence of a Mucus Barrier

After determining CLN-PEG-PLGA NPs could inhibit *G. vaginalis* growth in suspension, it was critical to evaluate their effect in a more physiologically relevant model. To create such model, *G. vaginalis* was cultured for 6 hours on chocolate agar plates, then CLN-PEG-PLGA NP treatments of 4  $\mu\text{g/mL}$  for each L:G ratio were

added to the plates and incubated for another 6 hours. After a total of 12 hours, bacteria plates were imaged, and colonies were counted within the ROI, indicated by the yellow circle (**Figure 4.6A**). The ROIs were 6 cm in diameter, with 2 cm of space on each side of the circle, to eliminate effects of bacterial cell culture. The treatment that yielded the most *G. vaginalis* growth inhibition compared to the NT group was the free CLN. However, all CLN-PEG-PLGA NPs also decreased *G. vaginalis* growth when compared to the NT group (**Figure 4.6B**). To determine the effect of each treatment in the presence of a mucosal barrier, 100  $\mu$ L of mucus reconstituted in NaOH was added to 1 mL of *G. vaginalis* cultures prior to inoculating the chocolate agar plates. The bacteria plates with mucus were incubated for 6 hours before the treatment groups were administered, and samples then incubated for another 6 hours. In the presence of mucus, both the free CLN and the CLN-PEG-PLGA NPs maintained their ability to inhibit bacterial growth (**Figure 4.6C**). The largest effect was due to the free CLN, again likely due to the bolus dose delivered to the bacteria (whereas the NPs release only about 50% of their encapsulated drug within 6 hours). Together, this data indicates CLN remains functional after being loaded into PEG-PLGA NPs.

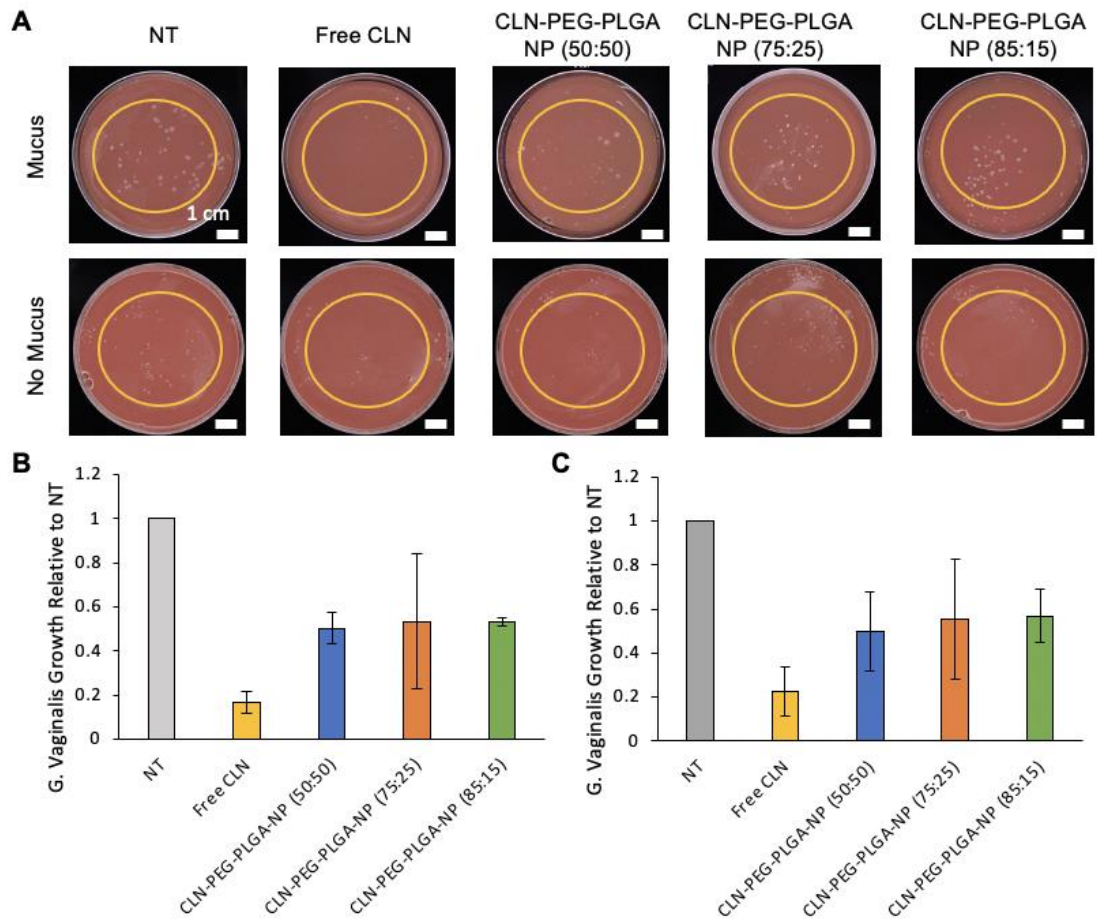


Figure 4.6: Growth of adherent *G. vaginalis* cultures following CLN-PEG-PLGA NP treatment in the absence of presence of mucus. **A.** Representative images of *G. vaginalis* grown on chocolate agar plates following CLN-PEG-PLGA NP or free CLN treatments with and without mucus. **B.** Quantification of bacterial colonies within the ROI of sample without and **C.** with mucus present. Data are mean  $\pm$  standard deviation of n=3 experiments.

#### 4.4 Discussion

This study shows that CLN-PEG-PLGA NPs can inhibit *in vitro* *G. vaginalis* growth over a 12-hour period, although to a lesser extent than free CLN (likely due to

the slower drug release and exposure to the cells versus the bolus dose applied for free drug). CLN-PEG-PLGA NPs administered in suspension decreased *G. vaginalis* growth by more than 50% (**Figure 4.5A**), and there were no significant differences in growth inhibition between NP groups of differing L:G ratios (**Figure 4.5B**). This suggests that the changes in drug release kinetics between the three formulations were not significant enough to substantially alter bacterial response over this timeframe. Similarly, when the CLN-PEG-PLGA NPs were used to treat *G. vaginalis* in adherent culture models with and without mucus present, all three inhibited *G. vaginalis* growth with no difference in growth inhibition observed based on L:G ratio (**Figure 4.6**). Free CLN yielded the greatest bacterial growth inhibition, likely due to the burst exposure to the cells. Overall, these data indicate CLN remains functional after encapsulation in PEG-PLGA NPs, but that the slower release kinetics and drug exposure to the cells results in less growth inhibition. In the future it will be important to determine how these *in vitro* observations translate into the *in vivo* setting.

One limitation of our study is that we could not extend the timeframe of analysis because *G. vaginalis* colonies become overgrown and unable to be accurately quantified after 24 hours of incubation. Due to this limitation, the experiments were limited to a 6- to 12-hour treatment period. Across this timeframe the NPs release approximately 50% of their encapsulated cargo, so they might be more effective at later timepoints after all drug has been released. Another limitation to this study is the *in vitro* model used. Unlike the physiologic conditions of BV, there is a limited mucosal barrier in the model presented. Moreover, there isn't a clearance mechanism

in the model to represent the discharge/removal of CVM and foreign pathogens that occurs in the human body. With the presence of a thicker barrier or a clearance mechanism, we would expect the efficacy of free CLN to decrease drastically because there isn't a nanocarrier present to promote its penetration through CVM and limit its early removal from the system. Conversely, we would expect the CLN-PEG-PLGA NPs to maintain their efficacy because the nanoformulation would improve penetration through the mucus barrier, reduce its removal from the body, and enhance its ability to reach pathogenic bacteria. Beyond more advanced *in vitro* models<sup>173</sup>, future work could also employ *in vivo* models to compare the efficacy of free versus encapsulated CLN in a more physiologically relevant system.

In our study, we synthesized DiD-loaded PEG-PLGA NPs that were of a similar size and charge to the CLN-PEG-PLGA NPs then tracked their movement in a suspension of reconstituted porcine gut mucus to evaluate the potential of PEG-PLGA NPs as a drug vehicle in the presence a mucosal barrier. Considering porcine gut mucus has the same mucins present as human CVM, we used this as a model for NP displacement in CVM. We also synthesized our NPs to include PEG because literature has also shown PEG-coatings on NPs increase the MSD when NPs are suspended in mucus<sup>110,189,190</sup>. The results from our study were consistent with previous work that has shown the MSD of polystyrene NPs that are suspended in *ex vivo* human CVM is significantly slowed when compared to polystyrene NPs suspended in water<sup>109</sup>. However, the DiD-PEG-PLGA NPs are still able to move somewhat through the mucus, illustrating the NPs are not completely trapped in the mucosal barrier. While

our model did not account for the physiologic changes that occur throughout pregnancy or throughout the menstrual cycle for non-pregnant patients, future work should investigate how PEG-PLGA NP design can be improved to escape the decreasing pore size of the mucus networks. NP characteristics that can be tailored to improve NP displacement would be the PEG-coating density, the MW of the PEG-PLGA, the NP size, and potentially the use of other coatings to enhance mucus penetration.

Our study focused on evaluating CLN-PEG-PLGA NPs effect on *G. vaginalis* growth *in vitro* in a 12-hour treatment period after a single dose. Given that BV is a recurring condition that often resists initial drug treatment<sup>87,93</sup>, future studies should investigate how multiple doses of CLN-PEG-PLGA NPs impacts *G. vaginalis* growth over a long-term period. Researchers should also assess the frequency and concentration of doses required for longer-term treatments, because the recurrence rate of BV is 15-20% within 3 months of initial diagnosis<sup>182</sup>. To further explore the potential of using CLN-PEG-PLGA NPs for pregnant and non-pregnant BV patients, a more complex *in vitro* model should be developed to include a thick CVM layer that would be present during pregnancy or different phases of the menstrual cycle, or an *in vivo* model should be employed. The knowledge from these studies would allow researchers to understand how NP-based systems can treat BV while maintaining the safety of the patient. In conclusion, the work shown in this chapter is essential to improving treatment strategies for pregnant and non-pregnant patients with BV.

## Chapter 5

### CONCLUSIONS AND FUTURE WORK

#### 5.1 Introduction

This thesis provided insight into the potential of nanomedicine for maternal/fetal health applications by defining NP biodistribution following systemic or vaginal delivery in pregnant murine models as a function of gestational age. It also demonstrated that clindamycin, an antibiotic used to fight bacterial vaginosis (BV), a common vaginal infection in pregnant and non-pregnant women, could be loaded in NPs with tunable release kinetics and that the encapsulated drug maintained its ability to hinder bacteria growth *in vitro*. This chapter will provide a concise overview of each contribution in the thesis, highlighting the importance, significations, and implications of the research conducted. Furthermore, it will outline various potential avenues for future development of nanomedicine for maternal/fetal health, including promising routes of research exploration and clinical applications that should be considered as the field advances.

#### 5.2 Overview of the Work Presented

Chapter 2 investigated the biodistribution of gold-based nanoparticles (NPs) of two different sizes in pregnant mice after systemic delivery. Pregnant mice were

intravenously administered either 15 nm gold nanoparticles or 150 nm diameter silica core/gold nanoshells, both coated with PEG, at gestational days (E)9.5 or 14.5. After twenty-four hours, the NPs' tissue distribution was analyzed using inductively coupled plasma-mass spectrometry and silver staining of histological samples. The results revealed that more NPs accumulated in the placentas compared to the embryos, with greater delivery to these tissues observed at E9.5 than E14.5. Neither type of NP affected the weight of the fetus or the placenta, indicating minimal short-term toxicity during early to mid-stage pregnancy. These findings suggest the importance of further developing NPs as safe tools for delivering therapeutics to reproductive tissues.

Chapter 3 examined how PEG-PLGA NPs distribute in pregnant mice after vaginal delivery, as well as their short-term toxicity. Two types of NPs were used: DiD-PEG-PLGA NPs loaded with fluorophores for cargo tracking, and Cy5-PEG-PLGA NPs incorporating tagged polymer for distribution analysis. DiD-PEG-PLGA NPs were administered on either gestational day (E)14.5 or 17.5, and 24 hours later, the distribution of cargo was examined in excised tissues and histological sections using fluorescence imaging. No differences were found in DiD distribution between the gestational periods, so Cy5-PEG-PLGA NPs were administered only on E17.5 to assess polymer distribution in reproductive organs. The Cy5-PEG-PLGA NPs were found in the vagina, placentas, and embryos, while DiD cargo was limited to the vagina. Maternal, fetal, and placental weight were not affected by the NPs, indicating no immediate adverse effects on maternal or fetal growth. These findings warrant

future exploration of vaginally delivered NP therapies to manage vaginal conditions during pregnancy.

Chapter 4 examined the effectiveness of clindamycin-loaded PEG-PLGA NPs (CLN-PEG-PLGA NPs) with different L:G ratios (50:50, 75:25, and 85:15) in inhibiting the growth of *G. vaginalis*, a pathogenic bacteria that is overabundant in bacterial vaginosis (BV) infections. *G. vaginalis* was cultured in both suspension and on agar plates and treated with CLN-PEG-PLGA NPs of each L:G ratio. The growth of *G. vaginalis* was monitored at regular intervals using spectrophotometry or imaging and these experiments demonstrated that CLN-PEG-PLGA NPs effectively inhibited the growth of *G. vaginalis* in suspension and on surfaces both in the absence and presence of mucus within a 12-hour treatment period. However, there were no significant differences in bacterial growth inhibition among the three L:G ratios, indicating that the ratio does not impact short-term antibacterial treatment (likely due to minimal differences in the total amount of drug released between each formulation within the 12-hour treatment period). While freely delivered clindamycin was more potent against *G. vaginalis* in these studies, this was not surprising given that the bacteria receive a bolus dose of free drug compared to slow and sustained exposure to released drug from the NPs. Importantly, these results indicate clindamycin maintains its efficacy after encapsulation in and release from PEG-PLGA NPs. Future work should compare the efficacy of free CLN and CLN-PEG-PLGA NPs in advanced *in vitro* and *in vivo* models of BV to enhance understanding of its potential for the treatment of pregnant and non-pregnant patients with BV.

### **5.3 Significance, Innovation, and Impact of the Research**

Pregnancy complications present significant challenges for both the mother and the developing fetus, as treatment options are limited due to safety and ethical concerns. Conditions such as preeclampsia, fetal growth restriction (FGR), and placenta accreta are examples of pregnancy-induced conditions that lack effective treatments. As pregnancy progresses, these conditions worsen, leading to adverse effects on maternal and fetal health. Consequently, emergency delivery via cesarean section is often required, resulting in additional complications associated with premature birth for the newborns. It is crucial to develop therapeutic advancements that can effectively treat pregnancy-related conditions without harming the developing baby, addressing the urgent need for improved maternal and fetal health during pregnancy.

In recent years, various NP-based carrier systems have been engineered to target a wide range of diseases, including cancers<sup>191</sup>. It is widely recognized that the behavior of nanocarriers in the body following systemic delivery depends on factors such as size, shape, and surface chemistry. While researchers have utilized this knowledge to develop powerful systems for treating diseases like cervical cancer, endometriosis, and HIV, the exploration of nanomedicine for pregnancy complications has been limited. The unique state of pregnancy introduces additional variables that affect NP distribution and design, including the dynamic physiology of the maternal reproductive system, the transport of nutrients and drugs through the placenta, and the development of the fetus. Understanding the impact of these factors on NP distribution

is crucial for the development of effective treatments that can support full-term pregnancies and improve maternal and fetal health.

This thesis demonstrates the potential of nanomedicines in overcoming biological barriers for targeted delivery of therapeutics to specific reproductive organs through systemic and vaginal administration. Additionally, it provides proof-of-concept that NP-based drug carriers can treat diseases affecting reproductive organs. These significant advancements in the maternal-fetal health field pave the way for future progress in the development of these and other nanotechnologies for the treatment of pregnancy conditions.

The innovation of this thesis arises from developing a fundamental understanding of the use of nanocarrier systems to treat maternal conditions during pregnancy. Through this work, we determined (i) how gestational age affects NP distribution following systemic and vaginal administration and (ii) how PEG-PLGA-NP drug carriers with different L:G ratios could be utilized to treat a vaginal bacterial infection, BV. Understanding how NPs distribute in the pregnant murine model after different administration methods and understanding how NP drug carriers limit bacterial growth is critical to informing how NP-based treatment systems might traffic and function in human subjects. Knowledge of NP safety in pregnant murine models is also critical to understanding the potential safety/toxicity in human subjects. Overall, this thesis has provided an important foundation on which future research can build to optimize treatments for maternal/fetal health conditions.

Prior to this thesis, gestational age had not been explored as a contributing factor towards NP distribution. PEGylated NPs were optimal carriers to study this important question, as they are commonly utilized in nanomedicine applications. In this work, we established that gestational age impacts the distribution of systemically administered, but not vaginally administered, PEGylated NPs. Future studies should confirm these results and expand them to include additional gestational ages (only two gestational ages were included in our experiments for each delivery method). The results obtained from this work contributed towards the field by defining how and when each administration method could be utilized to treat maternal conditions during pregnancy.

In previous work in non-maternal/fetal health applications, drug-loaded NPs have shown great success in increasing drug retention and efficacy at desired target sites. In this thesis, we encapsulated clindamycin in PEG-PLGA NPs of three L:G ratios, 50:50, 75:25, and 85:15, to analyze how the tunable polymer degradation and drug release profile affected *G. vaginalis* growth in vitro. By testing the three L:G ratios and its impact on *G. vaginalis* growth inhibition, we were able to determine short-term bacterial growth inhibition is not impacted by NP L:G ratio. Despite there being minimal differences of growth inhibition between the NP and free CLN treatments, this work displayed proof of concept that NPs can successfully deliver CLN to disrupt *G. vaginalis* growth in the short-term. The results from this study advanced upon the methods by which BV is currently treated and could guide the development of future novel treatments to manage BV in pregnant patients.

## **5.4 Future Directions**

This work introduces NP delivery systems that can overcome biological barriers for targeted delivery of therapeutics to specific reproductive organs through systemic and vaginal administration. Furthermore, it provides proof-of-concept that NP-based drug carriers can inhibit bacterial growth and potentially be used in treating diseases that affect reproductive organs during pregnancy. Although this work presents strategies to use nanomedicine to advance treatments in the field of maternal-fetal health, there are many more experiments that need to be performed before such systems can be implemented in the clinic. The future studies outlined in this research would contribute valuable knowledge to the field and could inform the development of NP-based systems for maternal-fetal health treatments.

### **5.4.1 Understanding Long-Term Effects of NP Delivery on Fetal Growth and Maternal Safety**

The use NPs for maternal-fetal health applications are a new application in the field of nanomedicine that needs to be explored further. Considering NPs have been shown to have minimal off-target effects *in vivo* and in the clinic, one would hope there would be minimal effects on maternal and fetal safety during pregnancy. In this work, NPs were shown to have little to no effect on maternal, placental, and fetal weight changes over a 24-hour period. However, there needs to be additional studies to investigate potential NP effects on maternal health and fetal outcomes over a long-term period. One initial study to be conducted would be to observe maternal weight

gain through delivery. In our study, the mice were sacrificed 24-hours after NP administration. However, if the mice were allowed to carry to term, one could evaluate maternal weight changes of NP injected mice compared to saline injected mice. This would inform researchers of potential NP effects on labor and delivery success. If the pregnant dams can successfully deliver all their pups without any obvious birth defects, such as underdevelopment and low weight, this would tell researchers the placentas remain efficient throughout the pregnancy despite NP injections. The evaluation of the long-term effects of NPs following early NP injections (E9.5) and late NP injections (E14.5 or E17.5) in this manner would be very beneficial in informing future treatment strategies because free drug treatments are typically administered at the start of the third trimester (or E14.5) in humans. If NP injections at E9.5 in pregnant dams result in minimal effects following NP injections, this would largely improve current treatment and management strategies for many conditions during pregnancy by allowing for earlier intervention.

Another area of research that needs to be explored in future work is the long-term development of pups following delivery. In our work, the embryos were not delivered, and therefore, behavioral analyses of the pups were not conducted. Behavioral studies, such as the Open Field Test<sup>192-194</sup> and the Morris Water Maze<sup>195,196</sup>, are conducted on murine pups following birth and aim to investigate various aspects of their development, cognition, and behavior. The Open Field Test allows researchers to observe the exploratory behavior and locomotor activity of the pups. It can provide insights into their physical development, motor skills, and overall

activity levels. The Morris Water Maze is particularly useful for assessing spatial learning and memory, which are important cognitive abilities for pups as they grow and develop. This test can indicate how well they are able to navigate and remember the location of a hidden platform, reflecting their cognitive development and spatial awareness. Both tests provide valuable information about the growth and development of murine pups from a behavioral perspective. To evaluate the development of the pups to ensure the safety of NPs, both tests should be conducted one per week starting at week 2 (when pups no longer require nursing) until the pups reach maturity at 2 months.

The fundamental knowledge presented in this thesis is essential for the initial development of nanomedicines that are applicable for maternal-fetal health conditions. With the additional experiments presented above, researchers would be able to determine the long-term effects of NP injections on pup development and growth. Overall, this could inform researchers how to use either the systemic or vaginal routes of administration to improve NP delivery and treatment success without sacrificing maternal or fetal health.

#### **5.4.2 Demonstrating the Need for NP Carriers for Treating BV**

In this work, we developed a fundamental understanding of the synthesis of CLN-PEG-PLGA NPs that were able to successfully inhibit *G. vaginalis* growth. However, our NPs did not outperform the free CLN treatment when applied to bacteria cultured in suspension or adhered to a surface. Due to the 12-hour time frame

of the study, the CLN-PEG-PLGA NPs were not highlighted for their sustained drug release that would be expected to outperform the effects of free CLN on *G. vaginalis* in the *in vivo* setting. To improve the study and properly show the benefits of a nanocarrier, an improved *in vitro* model should be developed to prolong the experimental time and/or to investigate the efficacy of multiple rounds of treatment. In the model used in our study, *G. vaginalis* was cultured on an agar petri dish. This is a simplistic model that can be used to understand how *G. vaginalis* grows in isolation. However, in physiologic conditions, *G. vaginalis* grows in abundance on the surface of the vaginal epithelium in the presence of other bacteria types, and mucus is also produced in abundance as a protective layer against foreign pathogens. An improved model of BV would include culturing *G. vaginalis* alone or in combination with other bacteria on vaginal epithelial cells<sup>173</sup>, then treating the samples in the presence of a thick mucus layer with the CLN-PEG-PLGA NPs (50:50), because this is the most used L:G ratio and there were no significant differences in drug efficacy observed between NPs with different L:G ratios in our study.

While *G. vaginalis* is a key bacterium associated with BV, there are several other bacterial species that can be present in this condition that could be incorporated in an improved *in vitro* model in future studies. These include *Atopobium vaginae*, *Prevotella* spp., *Mobiluncus* spp., *Mycoplasma hominis*, and various anaerobic bacteria such as *Peptostreptococcus* spp. and *Bacteroides* spp. These bacteria contribute to the dysbiosis of the vaginal ecosystem, leading to the characteristic symptoms of BV. Future work should incorporate multiple bacterial species, such as

*G. vaginalis*, *Atopobium vaginae*, and *Prevotella bivia* because they are the most abundant, to understand how BV as a condition can be treated, as opposed to one bacterium that was used in the current model. Understanding how the diverse bacterial species involved in BV can impact drug efficacy is crucial for developing effective NP treatments to restore the vaginal microbiota to a healthy state.

Another way to improve the *in vitro* model is to incorporate a clearance method to represent the constant removal of mucus from the vagina through the form of discharge. The model presented in this work does not include a clearance mechanism, but the model would greatly benefit from this because the clearing of freely delivered drug is a substantial issue when vaginally delivering antibiotics. In an *in vitro* model, one clearance strategy that could be used is consistent PBS washes. Each wash could be collected, and the absorbance could be measured to quantify how much drug or NP is lost with each clearing. Additionally, *G. vaginalis* cells that are collected in each wash could be stained using a live-dead assay to determine the efficacy of free CLN and CLN-PEG-PLGA NPs in the presence of consistent washes. While one would expect the CLN-PEG-PLGA NPs to outperform the free CLN, the knowledge from this study could inform researchers how NP design is upheld when clearance mechanisms are incorporated into a vaginal model.

Lastly, another aspect of the *in vitro* model that can be improved in future work is the dosing strategy. The treatment of BV often involves administering vaginal medications in multiple doses over several days. This approach is aimed at effectively eradicating the overgrowth of harmful bacteria and restoring a healthy balance in the

vaginal microbiota. This extended treatment regimen helps to ensure that the infection is fully cleared and reduces the risk of recurrence, promoting long-term vaginal health. In our work, only a single dose of NPs was administered, and the effects were evaluated for 12 hours. However, a repeated dosing strategy over a longer time frame, such 5-7 days (the typical length of traditional antibiotic treatments), would inform researchers how frequently NPs must be administered to outperform currently utilized vaginal creams.

### **5.4.3 Traditional Considerations**

For NPs to be used in maternal-fetal applications, there are many factors must be considered and researched extensively before NP-based treatments can be administered in the clinic. The physiologic differences between animal models and humans are vast and it is imperative that researchers investigate how these differences can impact human maternal and fetal health in the short-term and long-term with the use of NP treatment strategies during pregnancy.

The barrier CVM was introduced in this work, but the additional barrier of the cervical mucus plug (CMP) was not incorporated. In humans, the CMP is developed early pregnancy, typically around 6 to 12 weeks' gestation. As the pregnancy progresses, the cervix undergoes changes under the influence of hormonal shifts. These changes lead to the production of thick, sticky mucus that accumulates in the cervical canal, eventually forming the mucus plug. Unlike humans, mice do not have a

CMP. Therefore, the vaginal administration model used in this work does not reflect all the barriers that are present in the human pregnancy model. In Chapter 3, we observed Cy5-PEG-PLGA NPs could distribute to the placenta and embryo, yet due to the missing CMP in the mouse model, these results may not be applicable to the vaginal delivery of NPs in humans. This major difference between humans and mice would largely affect researchers' understanding of the vaginal administration route during pregnancy.

Another major difference between humans and mice during pregnancy is the placental organization, depth of trophoblast invasion, and trophoblast differentiation. The labyrinth in the murine placenta is comparable to the chorionic villous in humans and facilitates nutrient exchange between maternal blood and the fetus. Trophoblast invasion depth is slightly less in mice compared to humans and primarily occurs during mid-gestation to provide protective measures for the fetus. Unlike humans where arterial remodeling of the uterine arteries occurs in the 2<sup>nd</sup> trimester, blood flow to the placenta takes place in mice during the third trimester (E15-E16) in mice. In terms of NP delivery, these differences could impact the distribution of NPs to the reproductive organs following systemic delivery. Additionally, the placenta originates from the fetus, and the role of fetal sex should be considered as differential responses of sex in fetal development and disease are well established<sup>197–200</sup>. In terms of NP delivery, these differences could impact the distribution of NPs to the reproductive organs and efficacy following systemic delivery.

Lastly, fetal development is a huge safety consideration that researchers must adhere to tight guidelines for due to ethical concerns regarding pregnancy related treatments. In this thesis murine models were the only animal models. Throughout this thesis, the safety of the fetus is consistently considered because the interruption of fetal development would have extensive effects on clinical translation. Although NPs had minimal short-term effects on the fetus, it is important to recognize fetal development in mice primarily occurs after delivery, whereas human embryo development occurs during pregnancy. Further, the pregnancy term in humans is 9 months compared to the 21 days of gestation in mice<sup>188</sup>. Considering the vast difference in pregnancy term between humans and mice, researchers should pay close attention to fetal heart rate, fetal movements, muscle tone, breathing movements, amniotic fluid, and blood flow in the umbilical cord, placenta, and fetal vessels. These methods are commonly used to assess fetal health during pregnancy and should be closely monitored before, during, and after administering NP treatments.

Overall, extending the research to the ideas discussed in this section will provide insight and knowledge to the use of NPs in maternal-fetal health applications. The work presented in this thesis gives promise to the field and provides essential information to expand the use of NP-based systems to applications in reproductive health. In conclusion, the incorporation of this work with future work will yield new and effective treatment methods for pregnancy-related conditions that will substantially improve the quality of life for many mothers and children.

## REFERENCES

1. NNI. What Is Nanotechnology? National Nanotechnology Initiative. *United States National Nanotechnology Initiative* (2021).
2. Astruc, D. Introduction to nanomedicine. *Molecules* **21**, (2016).
3. Hoyert, D. L. Maternal mortality rates in the United States, 2020. *National Center Health Statistics* vol. 4 1–5 (2021).
4. Nour, N. M. An introduction to maternal mortality. *Reviews in obstetrics & gynecology* vol. 1 77–81 (2008).
5. Declercq, E. & Zephyrin, L. Maternal Mortality in the United States: A Primer | Commonwealth Fund. *Commonwealth Fund* (2020).
6. Guisbiers, G., Mejía-Rosales, S. & Leonard Deepak, F. Nanomaterial properties: Size and shape dependencies. *J. Nanomater.* **2012**, (2012).
7. Huang, H., Feng, W., Chen, Y. & Shi, J. Inorganic nanoparticles in clinical trials and translations. *Nano Today* vol. 35 (2020).
8. Ventola, C. L. The nanomedicine revolution: Part 2: Current and future clinical applications. *P T* **37**, 582–591 (2012).
9. Kwok, P. & Chan, H.-K. Nanotechnology Versus other Techniques in Improving Drug Dissolution. *Current Pharmaceutical Design* vol. 20 474–482 (2014).
10. Albanese, A., Tang, P. S. & Chan, W. C. W. The Effect of Nanoparticle Size, Shape, and Surface Chemistry on Biological Systems. *Annu. Rev. Biomed. Eng.* **14**, 1–16 (2012).
11. Gratton, S. E. A. *et al.* The effect of particle design on cellular internalization pathways. *Proc. Natl. Acad. Sci. U. S. A.* **105**, 11613–11618 (2008).
12. Behzadia, S. *et al.* Cellular Uptake of Nanoparticles: Journey Inside the cell. *Chem. Soc. Rev.* **46**, 4218–4244 (2017).
13. Qiu, Y. *et al.* Surface chemistry and aspect ratio mediated cellular uptake of Au nanorods. *Biomaterials* vol. 31 7606–7619 (2010).
14. Tranquilli, A. L. *et al.* The classification, diagnosis and management of the hypertensive disorders of pregnancy: A revised statement from the ISSHP. *Pregnancy Hypertens. An Int. J. Women's Cardiovasc. Heal.* **4**, 97–104 (2014).
15. McCarthy, F. P. & Kenny, L. C. Hypertension in pregnancy. *Obstet. Gynecol. Reprod. Med.* **22**, 141–147 (2012).
16. Maynard, S. E. *et al.* Excess Placental Soluble fms-like Hypertension , and Proteinuria in. *J. Clin. Invest.* **111**, 649–58 (2003).
17. Li, Z. *et al.* Recombinant vascular endothelial growth factor 121 attenuates hypertension and improves kidney damage in a rat model of preeclampsia.

- Hypertension* **50**, 686–692 (2007).
18. Chen, D., Wang, H., Huang, H. & Dong, M. Vascular endothelial growth factor attenuates N $\omega$ -Nitro-L-arginine methyl ester-induced preeclampsia-like manifestations in rats. *Clin. Exp. Hypertens.* **30**, 606–615 (2008).
  19. Gilbert, J. S. *et al.* Recombinant vascular endothelial growth factor 121 infusion lowers blood pressure and improves renal function in rats with placental ischemia-induced hypertension. *Hypertension* **55**, 380–385 (2010).
  20. Bergmann, A. *et al.* Reduction of circulating soluble Flt-1 alleviates preeclampsia-like symptoms in a mouse model. *J. Cell. Mol. Med.* **14**, 1857–1867 (2010).
  21. Woods, A. K. *et al.* Adenoviral delivery of VEGF121 early in pregnancy prevents spontaneous development of preeclampsia in BPH/5 mice. *Hypertension* **57**, 94–102 (2011).
  22. Logue, O. C., Mahdi, F., Chapman, H., George, E. M. & Bidwell, G. L. A Maternally Sequestered, Biopolymer-Stabilized Vascular Endothelial Growth Factor (VEGF) Chimera for Treatment of Preeclampsia. *J. Am. Hear. Assoc.* **6**, (2017).
  23. Kuna, M., Waller, J. P., Logue, O. C. & Bidwell, G. L. Polymer size affects biodistribution and placental accumulation of the drug delivery biopolymer elastin-like polypeptide in a rodent pregnancy model. *Placenta* **72–73**, 20–27 (2018).
  24. Yu, J., Jia, J., Guo, X., Chen, R. & Feng, L. Modulating circulating sFlt1 in an animal model of preeclampsia using PAMAM nanoparticles for siRNA delivery. *Placenta* **58**, 1–8 (2017).
  25. Alexander, B. T. *et al.* Reduced uterine perfusion pressure during pregnancy in the rat is associated with increases in arterial pressure and changes in renal nitric oxide. *Hypertens. (Dallas, Tex. 1979)* **37**, 1191–5 (2001).
  26. Menjoge, A. R. *et al.* Transport and Biodistribution of Dendrimers Across Human Fetal Membranes: Implications for Intravaginal Administration of Dendrimers. *Biomaterials* **31**, 5007–5021 (2010).
  27. Turanov, A. A. *et al.* RNAi modulation of placental sFLT1 for the treatment of preeclampsia. *Nat. Biotechnol.* **36**, 1164–1173 (2018).
  28. Li, L. *et al.* Trophoblast-Targeted Nanomedicine Modulates Placental sFLT1 for Preeclampsia Treatment. *Front. Bioeng. Biotechnol.* **8**, (2020).
  29. Suhag, A. & Berghella, V. Intrauterine Growth Restriction (IUGR): Etiology and Diagnosis. doi:10.1007/s13669-013-0041-z.
  30. BARKER, D. J. P. Adult Consequences of Fetal Growth Restriction. *Clin. Obstet. Gynecol.* **49**, (2006).
  31. Ferretti, C., Bruni, L., Dangles-Marie, V., Pecking, A. P. & Bellet, D. Molecular circuits shared by placental and cancer cells, and their implications in the proliferative, invasive and migratory capacities of trophoblasts. *Human Reproduction Update* vol. 13 121–141 (2007).
  32. Constância, M. *et al.* Placental-specific IGF-II is a major modulator of placental

- and fetal growth. *Nature* **417**, 945–948 (2002).
33. Forbes, K., Westwood, M., Baker, P. N. & Aplin, J. D. Insulin-like growth factor I and II regulate the life cycle of trophoblast in the developing human placenta. 1313–1322 (2023) doi:10.1152/ajpcell.00035.2008.
  34. King, A. *et al.* Tumor-homing peptides as tools for targeted delivery of payloads to placenta. *Adv. Sci.* (2016).
  35. Fowden, A. L. & Forhead, A. J. Endocrine mechanisms of intrauterine programming. *Reproduction* **127**, 515–526 (2004).
  36. Ellah, N. A. *et al.* Development of Non-Viral, Trophoblast-Specific Gene Delivery for Placental Therapy. *PLoS One* **10**, e0140879 (2015).
  37. Beards, F., Jones, L. E., Charnock, J., Forbes, K. & Harris, L. K. Placental homing peptide-microRNA inhibitor conjugates for targeted enhancement of intrinsic placental growth signaling. *Theranostics* **7**, 2940–2955 (2017).
  38. Cureton, N. *et al.* Selective targeting of a novel vasodilator to the uterine vasculature to treat impaired uteroplacental perfusion in pregnancy. *Theranostics* **7**, 3715–3731 (2017).
  39. Lyall, F., Greer, I. A., Young, A. & Myatt, L. Nitric oxide concentrations are increased in the fetoplacental circulation in intrauterine growth restriction. *Placenta* vol. 17 165–168 (1996).
  40. Myatt, L., Eis, A. L. W., Brockman, D. E. & Greer, I. A. *Endothelial nitric oxide synthase in placental villous tissue from normal, pre-eclamptic and intrauterine growth restricted pregnancies\**. *Human Reproduction* vol. 12 (1997).
  41. Medicine, I. of M. (US) R. on E. H. S. R. and. Preterm Birth and Its Consequences. in *National Library of Medicine* (2003).
  42. Goldenberg, R. L., Culhane, J. F., Iams, J. D. & Romero, R. Epidemiology and causes of preterm birth. *Lancet* (2008) doi:10.1016/S0140-6736(08)60074-4.
  43. Refuerzo, J. S. *et al.* Uterus-targeted liposomes for preterm labor management: Studies in pregnant mice. *Sci. Rep.* **6**, 1–12 (2016).
  44. Paul, J. W. *et al.* Drug delivery to the human and mouse uterus using immunoliposomes targeted to the oxytocin receptor. in *American Journal of Obstetrics and Gynecology* vol. 216 283.e1-283.e14 (Mosby Inc., 2017).
  45. Hoang, T. *et al.* Development of a muco-inert progesterone nanosuspension for safer and more effective prevention of preterm birth. *J. Control. Release* **295**, 74–86 (2019).
  46. Seelbach-Goebel, B. Antibiotic therapy for premature rupture of membranes and preterm labor and effect on fetal outcome. *Geburtshilfe Frauenheilkd.* **73**, 1218–1227 (2013).
  47. Kemp, M. W. *et al.* Maternal intravenous administration of azithromycin results in significant fetal uptake in a sheep model of second trimester pregnancy. *Antimicrob. Agents Chemother.* **58**, 6581–6591 (2014).
  48. Menon, R. & Fortunato, S. J. Infection and the role of inflammation in preterm premature rupture of the membranes. *Best Pract. Res. Clin. Obstet. Gynaecol.*

- 21**, 467–478 (2007).
49. Poma, P. A. & Chicago, I. PREMATURE RUPTURE OF MEMBRANES approximately 10% of deliveries, and results in the loss of the natural protection of the fetus and intrauterine. 27–32 (1990).
  50. Farquhar, C. Endometriosis. *BMJ* **334**, 325–341 (2019).
  51. Parasar, P., Ozcan, P. & Terry, K. L. Endometriosis: Epidemiology, Diagnosis and Clinical Management. *Curr. Obstet. Gynecol. Rep.* **6**, 34–41 (2017).
  52. Alimi, Y., Iwanaga, J., Loukas, M. & Tubbs, R. S. The Clinical Anatomy of Endometriosis: A Review. *Cureus* **10**, (2018).
  53. Igarashi, M., Iizuka, M. & Abe, Y. Novel vaginal danazol ring therapy for pelvic endometriosis , in particular deeply infiltrating endometriosis. **13**, 1952–1956 (1998).
  54. Gabbe, S. G. & Graves, C. R. Management of diabetes mellitus complicating pregnancy. *Obstet. Gynecol.* **102**, 857–868 (2003).
  55. Lauenborg, J. *et al.* Audit on stillbirths in women with pregestational type 1 diabetes. *Diabetes Care* vol. 26 1385–1389 (2003).
  56. Evers, I. M., De Valk, H. W. & Visser, G. H. A. Risk of complications of pregnancy in women with type 1 diabetes: Nationwide prospective study in the Netherlands. *Br. Med. J.* **328**, 915–918 (2004).
  57. Kampmann, U. Gestational diabetes: A clinical update. *World J. Diabetes* **6**, 1065 (2015).
  58. ADA. Diagnosis and classification of diabetes mellitus. American Diabetes Association. *Diabetes Care* vol. 36 S67–S74 (2013).
  59. Buchanan, T. A. & Xiang, A. H. Gestational diabetes mellitus. *J Clin Invest* **115**, 485 (2005).
  60. Petitt, D. J., Bennett, P. H., Knowler, W. C., Baird, H. R. & Aleck, K. A. Gestational diabetes mellitus and impaired glucose tolerance during pregnancy. Long-term effects on obesity and glucose tolerance in the offspring. *Diabetes* vol. 34 119–122 (1985).
  61. Rizzo, T. A., Metzger, B. E., Dooley, S. L. & Cho, N. H. Early Malnutrition and Child Neurobehavioral Development\_ Insights from the Study of Children of Diabetic Mothers. 26–38 (1997).
  62. Rodriguez, B. S. Q. & Mahdy, H. Gestational Diabetes. in *StatPearls (Internet)* (2020).
  63. Wang, C. & Yang, H.-X. Diagnosis, prevention and management of gestational diabetes mellitus. *Chronic Dis. Transl. Med.* **2**, 199–203 (2016).
  64. Parast, V. M. & Paknahad, Z. Antioxidant Status and Risk of Gestational Diabetes Mellitus: a Case-Control Study. *Clin. Nutr. Res.* **6**, 81 (2017).
  65. Vafaei-Pour, Z., Shokrzadeh, M., Jahani, M. & Shaki, F. Embryo-protective effects of cerium oxide nanoparticles against gestational diabetes in mice. *Iran. J. Pharm. Res.* **17**, 964–975 (2018).
  66. Karthick, V. *et al.* Effect of biologically synthesized gold nanoparticles on alloxan-induced diabetic rats-An in vivo approach. *Colloids and Surfaces B:*

- Biointerfaces* vol. 122 505–511 (2014).
67. Zhao, Y. *et al.* A comparison between sphere and rod nanoparticles regarding their in vivo biological behavior and pharmacokinetics. *Sci. Rep.* **7**, (2017).
  68. Basarkar, A. & Singh, J. Poly (lactide-co-glycolide)-polymethacrylate nanoparticles for intramuscular delivery of plasmid encoding interleukin-10 to prevent autoimmune diabetes in mice. *Pharmaceutical Research* vol. 26 72–81 (2009).
  69. Damgé, C., Socha, M., Ubrich, N. & Maincent, P. Poly ( $\epsilon$ -caprolactone) eudragit nanoparticles for oral delivery of aspart-insulin in the treatment of diabetes - *Journal of Pharmaceutical Sciences* - 2010.pdf. 879–889 (2010).
  70. Zhang, C. *et al.* pH-sensitive MOF integrated with glucose oxidase for glucose-responsive insulin delivery. *J. Control. Release* **320**, 159–167 (2020).
  71. Li, C. *et al.* Glucose and H<sub>2</sub>O<sub>2</sub> dual-sensitive nanogels for enhanced glucose-responsive insulin delivery - *Nanoscale* (RSC Publishing). (2019).
  72. Volpatti, L. R. *et al.* Glucose-Responsive Nanoparticles for Rapid and Extended Self-Regulated Insulin Delivery. *ACS Nano* **14**, 488–497 (2020).
  73. Wang, J. *et al.* Charge-switchable polymeric complex for glucose-responsive insulin delivery in mice and pigs. *Science Advances* vol. 5 (2019).
  74. McIntyre, H. D. *et al.* Gestational diabetes mellitus | *Nature Reviews Disease Primers*. (2019).
  75. Hutcheon, J. A., Lisonkova, S. & Joseph, K. S. Epidemiology of pre-eclampsia and the other hypertensive disorders of pregnancy - *ScienceDirect*. 391–403 (2011).
  76. Sibai, B. M. Chronic hypertension in pregnancy. *Obstetrics & Gynecology* 369–377 (2002) doi:10.1161/CIRCULATIONAHA.113.003904.
  77. McCarthy, F. P. & Kenny, L. C. Hypertension in pregnancy. *Obstetrics, gynecology and reproductive medicine* 141–147 (2012) doi:10.1055/s-0028-1123979.
  78. Dokras, A. *et al.* Severe fetoplacental abnormalities precede the onset of hypertension and proteinuria in a mouse model of preeclampsia. *Biol. Reprod.* **75**, 899–907 (2006).
  79. Davison, R. L. *et al.* Discovery of a spontaneous genetic mouse model of preeclampsia. *Hypertension* **39**, 337–342 (2002).
  80. Lynch, A. M. *et al.* The interrelationship of complement-activation fragments and angiogenesis-related factors in early pregnancy and their association with pre-eclampsia. *BJOG: An International Journal of Obstetrics and Gynaecology* vol. 117 456–462 (2010).
  81. Lynch, A. M. & Salmon, J. E. Dysregulated Complement Activation as a Common Pathway of Injury in Preeclampsia and Other Pregnancy Complications. *Placenta* vol. 31 561–567 (2010).
  82. Girardi, G., Yarilin, D., Thurman, J. M., Holers, V. M. & Salmon, J. E. Complement activation induces dysregulation of angiogenic factors and causes

- fetal rejection and growth restriction. *J. Exp. Med.* **203**, 2165–2175 (2006).
83. Gelber, S. E. *et al.* Prevention of Defective Placentation and Pregnancy Loss by Blocking Innate Immune Pathways in a Syngeneic Model of Placental Insufficiency. *J. Immunol.* **195**, 1129–1138 (2015).
  84. Wang, W. *et al.* Autoantibody-mediated complement c3a receptor activation contributes to the pathogenesis of preeclampsia. *Hypertension* **60**, 712–721 (2012).
  85. Qing, X. *et al.* Targeted inhibition of complement activation prevents features of preeclampsia in mice. *Kidney Int.* **79**, 331–339 (2011).
  86. Kumar, N. *et al.* Bacterial vaginosis: Etiology and modalities of treatment - A brief note. *Journal of Pharmacy and Bioallied Sciences* vol. 3 496–503 (2011).
  87. Hay, P. Bacterial vaginosis. *Med. (United Kingdom)* **42**, 359–363 (2014).
  88. Hillier, S. L. *et al.* Association between Bacterial Vaginosis and Preterm Delivery of a Low-Birth-Weight Infant. *New England Journal of Medicine* vol. 333 1737–1742 (1995).
  89. Darwish, A., Elnshar, E. M., Hamadeh, S. M. & Makarem, M. H. Treatment options for bacterial vaginosis in patients at high risk of preterm labor and premature rupture of membranes. *Journal of Obstetrics and Gynaecology Research* vol. 33 781–787 (2007).
  90. Gratacós, E. *et al.* Spontaneous recovery of bacterial vaginosis during pregnancy is not associated with an improved perinatal outcome. *Acta Obstetrica et Gynecologica Scandinavica* vol. 77 37–40 (1998).
  91. Kurki, T., Sivonen, A., Renkonen, O. V., Savia, E. & Ylikorkala, O. Bacterial vaginosis in early pregnancy and pregnancy outcome. *Obstetrics and Gynecology* vol. 80 173–177 (1992).
  92. Dingens, A. S., Fairfortune, T. S., Reed, S. & Mitchell, C. Bacterial vaginosis and adverse outcomes among full-term infants: A cohort study. *BMC Pregnancy Childbirth* **16**, 1–8 (2016).
  93. Bradshaw, C. S. & Sobel, J. D. Current Treatment of Bacterial Vaginosis- Limitations and Need for Innovation. *J. Infect. Dis.* **214**, S14–S20 (2016).
  94. Zhou, Y. *et al.* Therapeutic effects of probiotic *Clostridium butyricum* on bacterial vaginosis in mice. *J. Appl. Microbiol.* **127**, 565–575 (2019).
  95. Machado, A. & Cerca, N. Influence of biofilm formation by *Gardnerella vaginalis* and other anaerobes on bacterial vaginosis. *J. Infect. Dis.* **212**, 1856–1861 (2015).
  96. Haute, D. Van & Berlin, J. M. Challenges in realizing selectivity for nanoparticle biodistribution and clearance: lessons from gold nanoparticles. *Ther. Deliv.* **8**, 763–774 (2017).
  97. Doane, T. & Burda, C. Nanoparticle mediated non-covalent drug delivery. *Advanced Drug Delivery Reviews* vol. 65 607–621 (2013).
  98. Perrault, S. D. & Chan, W. C. W. Synthesis and surface modification of highly monodispersed, spherical gold nanoparticles of 50–200 nm. *Journal of the American Chemical Society* vol. 131 17042–17043 (2009).

99. Poley, M. *et al.* Chemotherapeutic Nanoparticles Accumulate in the Female Reproductive System during Ovulation Affecting Fertility and Anticancer Activity. (2020).
100. Katz, D. F. & Dunmire, E. N. Cervical mucus. *Adv. Drug Deliv. Rev.* **11**, 385–401 (1993).
101. MOGHISSI, K., NEUHAUS, O. W. & STEVENSON, C. S. Composition and properties of human cervical mucus. I. Electrophoretic separation and identification of proteins. *J. Clin. Invest.* **39**, 1358–1363 (1960).
102. Katz, D. F., Yuan, A. & Gao, Y. Vaginal drug distribution modeling. *Adv. Drug Deliv. Rev.* **92**, 2–13 (2015).
103. Eggert-Kruse, W. Antimicrobial activity of human cervical mucus. *Hum. Reprod.* **15**, 778–784 (2000).
104. Ensign, L. M., Cone, R. & Hanes, J. Nanoparticle-based drug delivery to the vagina: a review. *J. Control. Release* **190**, 500–14 (2014).
105. Kutteh, W. H. & Franklin, R. D. Quantification of immunoglobulins and cytokines in human cervical mucus during each trimester of pregnancy. *Am. J. Obstet. Gynecol.* **184**, 865–874 (2001).
106. Hein, M., Valore, E. V., Helmig, R. B., Uldbjerg, N. & Ganz, T. Antimicrobial factors in the cervical mucus plug. *Am. J. Obstet. Gynecol.* **187**, 137–144 (2002).
107. Becher, N., Waldorf, K. A., Hein, M. & Uldbjerg, N. The cervical mucus plug: Structured review of the literature. *Acta Obstet. Gynecol. Scand.* **88**, 502–513 (2009).
108. Becher, N., Hein, M., Danielsen, C. C. & Uldberg, N. Matrix metalloproteinases in the cervical mucus plug in relation to gestational age, plug compartment, and preterm labor. *Reprod. Biol. Endocrinol.* **8**, 1–9 (2010).
109. Lai, S. K., Wang, Y.-Y., Hida, K., Cone, R. & Hanes, J. Nanoparticles reveal that human cervicovaginal mucus is riddled with pores larger than viruses. *Proc. Natl. Acad. Sci.* **107**, 598–603 (2010).
110. Maisel, K. *et al.* Nanoparticles coated with high molecular weight PEG penetrate mucus and provide uniform vaginal and colorectal distribution in vivo. *Nanomedicine* **11**, 1337–1343 (2016).
111. Khutoryanskiy, V. V. Beyond PEGylation: Alternative surface-modification of nanoparticles with mucus-inert biomaterials. *Adv. Drug Deliv. Rev.* **124**, 140–149 (2018).
112. Goel, A. & Rana, S. Angiogenic factors in preeclampsia: potential for diagnosis and treatment. *Curr. Opin. Nephrol. Hypertens.* **22**, 643–50 (2013).
113. Redman, C. W. & Sargent, I. L. Latest Advances in Understanding Preeclampsia. *Science (80-. )*. **308**, 1592–1594 (2005).
114. Huppertz, B., Weiss, G. & Moser, G. Trophoblast invasion and oxygenation of the placenta: measurements versus presumptions. *J. Reprod. Immunol.* **101102**, 74–79 (2014).
115. Osol, G. & Mandala, M. Maternal Uterine Vascular Remodeling During

- Pregnancy George. *Physiology* **24**, 58–71 (2009).
116. Chernausk, S. D. Update: Consequences of abnormal fetal growth. *J. Clin. Endocrinol. Metab.* **97**, 689–695 (2012).
  117. Woods, L., Perez-Garcia, V. & Hemberger, M. Regulation of Placental Development and Its Impact on Fetal Growth—New Insights From Mouse Models. *Front. Endocrinol. (Lausanne)*. **9**, 1–18 (2018).
  118. Bartels, H. C., Postle, J. D., Downey, P. & Brennan, D. J. Placenta Accreta Spectrum: A Review of Pathology, Molecular Biology, and Biomarkers. *Dis. Markers* **2018**, 1507674 (2018).
  119. Goh, W. A. & Zalud, I. Placenta accreta: Diagnosis, management and the molecular biology of the morbidly adherent placenta. *J. Matern. Neonatal Med.* **29**, 1795–1800 (2016).
  120. Irvin-Choy, N. S., Nelson, K. M., Gleghorn, J. P. & Day, E. S. Design of nanomaterials for applications in maternal/fetal medicine. *J. Mater. Chem. B* **8**, 6548–6561 (2020).
  121. Ci, L. Q. *et al.* Enhanced delivery of imatinib into vaginal mucosa via a new positively charged nanocrystal-loaded in situ hydrogel formulation for treatment of cervical cancer. *Pharmaceutics* **11**, (2019).
  122. Chen, J. *et al.* Nanotechnology in the management of cervical cancer. *Rev. Med. Virol.* **25**, 72–83 (2015).
  123. Friend, D. R. Drug delivery for the treatment of endometriosis and uterine fibroids. *Drug Deliv. Transl. Res.* **7**, 829–839 (2017).
  124. Chaudhury, K. *et al.* Mitigation of endometriosis using regenerative cerium oxide nanoparticles. *Nanomedicine Nanotechnology, Biol. Med.* **9**, 439–448 (2013).
  125. Cunha-Reis, C. *et al.* Nanoparticles-in-film for the combined vaginal delivery of anti-HIV microbicide drugs. *J. Control. Release* **243**, 43–53 (2016).
  126. Chaowanachan, T., Krogstad, E., Ball, C. & Woodrow, K. A. Drug Synergy of Tenofovir and Nanoparticle-Based Antiretrovirals for HIV Prophylaxis. *PLoS One* **8**, (2013).
  127. Nelson, K. M., Irvin-Choy, N. D., Hoffman, M. K., Gleghorn, J. P. & Day, E. S. Diseases and conditions that impact maternal and fetal health and the potential for nanomedicine therapies. *Adv. Drug Deliv. Rev.* (2020) doi:10.1016/j.addr.2020.09.013.
  128. Myers, K. M. *et al.* The mechanical role of the cervix in pregnancy. *J. Biomech.* **48**, 1511–1523 (2015).
  129. Timmons, B., Akins, M. & Mahendroo, M. Cervical Remodeling during Pregnancy and Parturition. *Trends Endocrinol. Metab.* **21**, 353–361 (2010).
  130. Chang, K. L. & Zhang, L. Steroid Hormones and Uterine Vascular Adaptation to Pregnancy. *Reprod Sci* **15**, 336–348 (2008).
  131. Griffiths, S. K. & Campbell, J. P. Placental structure, function and drug transfer. *Contin. Educ. Anaesthesia, Crit. Care Pain* **15**, 84–89 (2015).
  132. Ali, H., Kalashnikova, I., White, M. A., Sherman, M. & Rytting, E. Preparation,

- characterization, and transport of dexamethasone-loaded polymeric nanoparticles across a human placental in vitro model. *Int. J. Pharm.* **454**, 149–157 (2013).
133. Naidu, K. & Fredlund, K. L. Gestational age assessment. *StatPearls (Internet)* (2019) doi:10.5005/jp/books/10040\_11.
  134. Yang, H. *et al.* Effects of nanoparticle size and gestational age on maternal biodistribution and toxicity of gold nanoparticles in pregnant mice. *Toxicol. Lett.* **230**, 10–18 (2014).
  135. Semmler-Behnke, M. *et al.* Size dependent translocation and fetal accumulation of gold nanoparticles from maternal blood in the rat. *Part. Fibre Toxicol.* **11**, 1–12 (2014).
  136. Ho, D. *et al.* Maternal-placental-fetal biodistribution of multimodal polymeric nanoparticles in a pregnant rat model in mid and late gestation. *Sci. Rep.* **7**, 1–11 (2017).
  137. Huang, J. P. *et al.* Nanoparticles can cross mouse placenta and induce trophoblast apoptosis. *Placenta* **36**, 1433–1441 (2015).
  138. Georgiades, P., Fergusson-Smith, A. C. & Burton, G. J. Comparative developmental anatomy of the murine and human definitive placentae. *Placenta* **23**, 3–19 (2002).
  139. Frens. Controlled Nucleation for the Regulation of the Particle Size in Monodisperse Gold Suspensions. *Nat. Phys. Sci.* **241**, (1973).
  140. Oldenburg, S. J., Averitt, R. D., Westcott, S. L. & Halas, N. J. Nanoengineering of optical resonances. *Chem. Phys. Lett.* **288**, 243–247 (1998).
  141. Duff, D. G., Baiker, A. & Edwards, P. P. A New Hydrosol of Gold Clusters. 1. Formation and Particle Size Variation. *Langmuir* **9**, 2301–2309 (1993).
  142. Melamed, J. R., Kreuzberger, N. L., Goyal, R. & Day, E. S. Spherical Nucleic Acid Architecture Can Improve the Efficacy of Polycation-Mediated siRNA Delivery. *Mol. Ther. - Nucleic Acids* **12**, 207–219 (2018).
  143. Riley, R. S. & Day, E. S. Frizzled7 Antibody-Functionalized Nanoshells Enable Multivalent Binding for Wnt Signaling Inhibition in Triple Negative Breast Cancer Cells. *Small* **13**, 1–10 (2017).
  144. Raz, T. *et al.* The Hemodynamic Basis for Positional- and Inter-Fetal Dependent Effects in Dual Arterial Supply of Mouse Pregnancies. *PLoS One* **7**, 1–15 (2012).
  145. Fushima, T. *et al.* Reduced uterine perfusion pressure (RUPP) model of preeclampsia in Mice. *PLoS One* **11**, 1–12 (2016).
  146. Beck, S. L. Effects of position in the uterus on fetal mortality and on response to trypan blue. *J. Embryol. Exp. Morphol.* **17**, 617–624 (1967).
  147. Avni, R., Raz, T., Biton, I. E., Kalchenko, V. & Garbow, J. R. Europe PMC Funders Group Unique in utero identification of fetuses in multi-fetal mouse pregnancies by placental bi-directional arterial spin labeling ( BD-ASL ) MRI. **68**, 560–570 (2013).
  148. Hayward, C. E. *et al.* Placental adaptation: What can we learn from

- Birthweight:placental weight ratio? *Front. Physiol.* **7**, 1–13 (2016).
149. Coan, P. M. *et al.* Adaptations in placental nutrient transfer capacity to meet fetal growth demands depend on placental size in mice. *J. Physiol.* **586**, 4567–4576 (2008).
  150. Yang, H. *et al.* Effects of gestational age and surface modification on materno-fetal transfer of nanoparticles in murine pregnancy. *Sci. Rep.* **2**, 1–8 (2012).
  151. Zhang, B., Liang, R., Zheng, M., Cai, L. & Fan, X. Surface-functionalized nanoparticles as efficient tools in targeted therapy of pregnancy complications. *Int. J. Mol. Sci.* **20**, 1–16 (2019).
  152. Rattanapinyopituk, K. *et al.* Demonstration of the clathrin- and caveolin-mediated endocytosis at the maternal-fetal barrier in mouse placenta after intravenous administration of gold nanoparticles. *J. Vet. Med. Sci.* **76**, 377–387 (2014).
  153. Myllynen, P. K. *et al.* Kinetics of gold nanoparticles in the human placenta. *Reprod. Toxicol.* **26**, 130–137 (2008).
  154. Buerki-Thurnherr, T., Von Mandach, U. & Wick, P. Knocking at the door of the unborn child: Engineered nanoparticles at the human placental barrier. *Swiss Med. Wkly.* **142**, 1–20 (2012).
  155. Aengenheister, L. *et al.* An advanced human in vitro co-culture model for translocation studies across the placental barrier. *Sci. Rep.* **8**, 5388 (2018).
  156. Menezes, V., Malek, A. & Keelan, J. Nanoparticulate Drug Delivery in Pregnancy: Placental Passage and Fetal Exposure. *Curr. Pharm. Biotechnol.* **12**, 731–742 (2011).
  157. Wadsack, C. *et al.* Selective Cholesteryl Ester Uptake from High Density Lipoprotein by Human First Trimester and Term Villous Trophoblast Cells. *Placenta* **24**, 131–143 (2003).
  158. Ericsson, A., Hamark, B., Powell, T. L. & Jansson, T. Glucose transporter isoform 4 is expressed in the syncytiotrophoblast of first trimester human placenta. *Hum. Reprod.* **20**, 521–530 (2005).
  159. Katz, D. F. & Dunmire, E. N. Cervical mucus. Problems and opportunities for drug delivery via the vagina and cervix. *Adv. Drug Deliv. Rev.* **11**, 385–401 (1993).
  160. Cunha-Reis, C. *et al.* Nanoparticles-in-film for the combined vaginal delivery of anti-HIV microbicide drugs. *J. Control. Release* **243**, 43–53 (2016).
  161. Chaudhury, K. *et al.* Mitigation of endometriosis using regenerative cerium oxide nanoparticles. *Nanomedicine Nanotechnology, Biol. Med.* **9**, 439–448 (2013).
  162. Hoshyar, N., Gray, S., Han, H. & Bao, G. The effect of nanoparticle size on in vivo pharmacokinetics and cellular interaction. *Nanomedicine* vol. 11 673–692 (2016).
  163. Alexis, F., Pridgen, E., Molnar, L. K. & Farokhzad, O. C. Factors affecting the clearance and biodistribution of polymeric nanoparticles. *Mol. Pharm.* **5**, 505–515 (2008).

164. Chenthamara, D. *et al.* Therapeutic efficacy of nanoparticles and routes of administration. *Biomater. Res.* **23**, 1–29 (2019).
165. Figueroa-Espada, C. G., Mitchell, M. J., Riley, R. S. & Hofbauer, S. Exploiting the placenta for nanoparticle-mediated drug delivery during pregnancy. *Adv. Drug Deliv. Rev.* **160**, 244–261 (2020).
166. Young, R. E. *et al.* Lipid Nanoparticle Composition Drives mRNA Delivery to the Placenta. *bioRxiv : the preprint server for biology* (2022) doi:10.1101/2022.12.22.521490.
167. Irvin-Choy, N. S., Nelson, K. M., Dang, M. N., Gleghorn, J. P. & Day, E. S. Gold nanoparticle biodistribution in pregnant mice following intravenous administration varies with gestational age. *Nanomedicine Nanotechnology, Biol. Med.* **36**, 22–24 (2021).
168. Owens, D. E. & Peppas, N. A. Opsonization, biodistribution, and pharmacokinetics of polymeric nanoparticles. *International Journal of Pharmaceutics* vol. 307 93–102 (2006).
169. Blanco, E., Shen, H., Ferrari, M. & Author, N. B. Principles of nanoparticle design for overcoming biological barriers to drug delivery. *Nat. Biotechnol.* **33**, 941–951 (2016).
170. Cu, Y., Booth, C. J. & Saltzman, M. W. In vivo distribution of surface modified PLGA nanoparticles following intravaginal delivery. *J. Control. Release* **156**, 258–264 (2011).
171. Zierden, H. C. *et al.* Avoiding a sticky situation: bypassing the mucus barrier for improved local drug delivery. *Trends Mol. Med.* **27**, 436–450 (2022).
172. Ensign, L. M. *et al.* Ex vivo characterization of particle transport in mucus secretions coating freshly excised mucosal tissues. *Mol Pharm* **10**, 2176–2182 (2013).
173. Edwards, V. L. *et al.* Three-dimensional models of the cervicovaginal epithelia to study host-microbiome interactions and sexually transmitted infections. *Pathog. Dis.* **80**, 1–13 (2022).
174. Harris, J. C., Sterin, E. H. & Day, E. S. Membrane-Wrapped Nanoparticles for Enhanced Chemotherapy of Acute Myeloid Leukemia. *ACS Biomater. Sci. Eng.* **8**, 4439–4448 (2022).
175. Valcourt, D. M., Dang, M. N., Scully, M. A. & Day, E. S. Nanoparticle-Mediated Co-Delivery of Notch-1 Antibodies and ABT-737 as a Potent Treatment Strategy for Triple-Negative Breast Cancer. *ACS Nano* **14**, 3378–3388 (2020).
176. Khanal, S. *et al.* pH-Responsive PLGA Nanoparticle for Controlled Payload Delivery of Diclofenac Sodium. *J. Funct. Biomater.* **7**, 21 (2016).
177. Cu, Y., Booth, C. J. & Saltzman, M. W. In vivo distribution of surface modified PLGA nanoparticles following intravaginal delivery. *J. Control. Release* **156**, 258–264 (2011).
178. Sugiyama, M. *et al.* Vaginal mucus in mice: developmental and gene expression features of epithelial mucous cells during pregnancy†. *Biol. Reprod.*

- 105**, 1272–1282 (2021).
179. Schwebke, J. R., Muzny, C. A. & Josey, W. E. Role of Gardnerella vaginalis in the pathogenesis of bacterial vaginosis: A conceptual model. *J. Infect. Dis.* **210**, 338–343 (2014).
  180. Lamont, R. F., Jones, B. M., Mandal, D., Hay, P. E. & Sheehan, M. The efficacy of vaginal clindamycin for the treatment of abnormal genital tract flora in pregnancy. *Infect. Dis. Obstet. Gynecol.* **11**, 181–189 (2003).
  181. Brocklehurst, P., Gordon, A., Heatley, E. & Milan, S. J. Antibiotics for treating bacterial vaginosis in pregnancy. *Cochrane Database Syst. Rev.* **2013**, (2013).
  182. Wilson, J. Managing recurrent bacterial vaginosis. *Sex. Transm. Infect.* **80**, 8–11 (2004).
  183. Oleen-Burkey, M. K. A., Hillier, S. L., Oleen-Burkey, M. K. A. & Hillier, S. L. Pregnancy Complications Associated With Bacterial Vaginosis and Their Estimated Costs. *Infect. Dis. Obstet. Gynecol.* **3**, 149–157 (1995).
  184. Subtil, D. *et al.* Early clindamycin for bacterial vaginosis in pregnancy (PREMEVA): a multicentre, double-blind, randomised controlled trial. *Lancet* **392**, 2171–2179 (2018).
  185. Hines, D. J. & Kaplan, D. L. Poly(lactic-co-glycolic) acid-controlled-release systems: Experimental and modeling insights. *Crit. Rev. Ther. Drug Carrier Syst.* **30**, 257–276 (2013).
  186. Yang, M. *et al.* Biodegradable polymer nanoparticles that rapidly penetrate the human mucus barrier. *Proc. Natl. Acad. Sci.* **106**, 19268–19273 (2009).
  187. Swider, E. *et al.* Customizing poly(lactic-co-glycolic acid) particles for biomedical applications. *Acta Biomater.* **73**, 38–51 (2018).
  188. Chernokal, B., Gonyea, C. R. & Gleghorn, J. P. Lung Development in a Dish: Models to Interrogate the Cellular Niche and the Role of Mechanical Forces in Development. *Adv. Exp. Med. Biol.* **1413**, 29–48 (2023).
  189. Henry, C. E. *et al.* Anti-PEG antibodies alter the mobility and biodistribution of densely PEGylated nanoparticles in mucus. *Acta Biomater.* **43**, 61–70 (2016).
  190. Suk, J. S., Xu, Q., Kim, N., Hanes, J. & Ensign, L. M. PEGylation as a strategy for improving nanoparticle-based drug and gene delivery. *Adv. Drug Deliv. Rev.* **1**, 28–51 (2016).
  191. Sharifi, M. *et al.* An Updated Review on EPR-Based Solid Tumor Targeting Nanocarriers for Cancer Treatment. *Cancers (Basel)*. **14**, 1–17 (2022).
  192. de Figueiredo Cerqueira, M. M. *et al.* Comparative analysis between Open Field and Elevated Plus Maze tests as a method for evaluating anxiety-like behavior in mice. *Heliyon* **9**, e14522 (2023).
  193. Seibenhener, M. L. & Wooten, M. C. Use of the open field maze to measure locomotor and anxiety-like behavior in mice. *J. Vis. Exp.* 1–6 (2015) doi:10.3791/52434.
  194. Eltokhi, A., Kurpiers, B. & Pitzer, C. Behavioral tests assessing neuropsychiatric phenotypes in adolescent mice reveal strain- and sex-specific effects. *Sci. Rep.* **10**, 1–15 (2020).

195. Vorhees, C. V & Williams, M. T. Morris water maze: procedures for assessing spatial and related forms of learning and memory. *Nat Prot* **1**, 848–858 (2006).
196. Bromley-Brits, K., Deng, Y. & Song, W. Morris Water Maze test for learning and memory deficits in Alzheimer’s disease model mice. *J. Vis. Exp.* 2–6 (2011) doi:10.3791/2920.
197. Zhang, Y., Dong, X., Shirazi, J., Gleghorn, J. P. & Lingappan, K. Pulmonary endothelial cells exhibit sexual dimorphism in their response to hyperoxia. *Am. J. Physiol. - Hear. Circ. Physiol.* **315**, H1287–H1292 (2018).
198. Zhang, Y. *et al.* Microrna-30a as a candidate underlying sex-specific differences in neonatal hyperoxic lung injury: Implications for bpd. *Am. J. Physiol. - Lung Cell. Mol. Physiol.* **316**, L144–L156 (2019).
199. Lingappan, K., Hayward-Piatkovskyi, B. & Gleghorn, J. P. Neonatal Lung Disease: Mechanisms Driving Sex Differences. *Physiol. Heal. Dis.* **26**, 784–790 (2021).
200. Hayward-Piatkovskyi, B., Gonyea, C. R., Pyle, S. C., Lingappan, K. & Gleghorn, J. P. Sex-related external factors influence pulmonary vascular angiogenesis in a sex-dependent manner. *Am. J. Physiol. - Hear. Circ. Physiol.* **324**, H26–H32 (2023).

## Appendix

### PERMISSIONS FOR USE

#### A.1 Nanomedicine: Nanotechnology, Biology, and Medicine Journal Permissions

##### Details on gold open access articles

##### User rights

All articles published gold open access will be immediately and permanently free for everyone to read and download. We offer authors a choice of [user licenses](#), which define the permitted reuse of articles. We are continuously working with our author communities to select the best choice of license options, currently being defined for this journal as follows:

***Creative Commons Attribution (CC BY)***: lets others distribute and copy the article, to create extracts, abstracts, and other revised versions, adaptations or derivative works of or from an article (such as a translation), to include in a collective work (such as an anthology), to text or data mine the article, even for commercial purposes, as long as they credit the author(s), do not represent the author as endorsing their adaptation of the article, and do not modify the article in such a way as to damage the author's honor or reputation.

***Creative Commons Attribution-NonCommercial-NoDerivs (CC BY-NC-ND)***: for non-commercial purposes, lets others distribute and copy the article, and to include in a collective work (such as an anthology), as long as they credit the author(s) and provided they do not alter or modify the article.

## A.2 Drug Delivery Translational Research Journal Permissions

### Creative Commons licences

---

Open access articles in Springer Nature journals are published under Creative Commons licences. These provide an industry-standard framework to support easy re-use of open access material. Under Creative Commons licences, authors retain copyright of their articles.

*Drug Delivery and Translational Research* articles are published open access under a [CC BY licence](#) (Creative Commons Attribution 4.0 International licence). The CC BY licence is the most open licence available and considered the industry 'gold standard' for open access; it is also preferred by many funders. This licence allows readers to copy and redistribute the material in any medium or format, and to alter, transform, or build upon the material, including for commercial use, providing the original author is credited.

In instances where authors are not allowed to retain copyright to their own article (where the author is a US Government employee for example), authors should contact the Open Research Support team ([ORSupport@springernature.com](mailto:ORSupport@springernature.com)) before submitting their article so we can advise as to whether their non-standard copyright request can be accommodated.

Authors are advised to check their funder's requirements before selecting open access, to ensure compliance. Learn more about [funder compliance](#).